



UNIVERSITÉ DE LILLE

Faculté des Sciences et Technologies

École doctorale : Sciences de l'ingénierie et des systèmes (ENGSYS)

Spécialité : Électronique et Communications

Département : Électronique et Microélectronique

Thèse de doctorat

Présentée par : **Selina Cheggour**

Titre

**Solutions massives MIMO 5G économes en énergie et intelligentes
basées sur l'apprentissage automatique pour les communications
véhiculaires**

Soutenance publique : **26 septembre 2025**

Membres du jury

Président	Abdelhamid Mellouk, Ph.D., HDR – Professeur des universités, Université Paris-Est Créteil (UPEC)
Directeur de thèse	Eric Simon, Ph.D., HDR – Maître de conférences, Université de Lille
Co-directrice de thèse	Valeria Loscri, Ph.D., HDR – Directrice de recherche, Inria Lille – Centre Inria de l'Université de Lille
Rapporteure	Lina Mroueh, Ph.D., HDR – Maître de conférences, Institut Supérieur d'Électronique de Paris (ISEP)
Rapporteur	Abderrezak Rachedi, Ph.D., HDR – Professeur des universités, Université Gustave Eiffel



UNIVERSITY OF LILLE

Faculty of Science and Technology

Doctoral School: Science of Engineering and Systems (ENGSYS)

Specialty: Electronics and Communications

Department: Electronics and Microelectronics

Ph.D. Thesis

Presented by: **Selina Cheggour**

Title

**Energy-efficient and intelligent 5G massive MIMO solutions
based on machine learning for vehicular communications**

Public defence: **September 26, 2025**

Jury

Chair	Abdelhamid Mellouk, Ph.D., HDR – Full Professor, Université Paris-Est Créteil (UPEC)
Thesis Director	Eric Simon, Ph.D., HDR – Associate Professor, University of Lille
Co-Director	Valeria Loscri, Ph.D., HDR – Research Director, Inria Lille - Centre Inria de l'Université de Lille
Reviewer	Lina Mroueh, Ph.D., HDR – Associate Professor, Institut Supérieur d'Électronique de Paris (ISEP)
Reviewer	Abderrezak Rachedi, Ph.D., HDR – Full Professor, Université Gustave Eiffel

© 2025
Selina Cheggour
ALL RIGHTS RESERVED

RÉSUMÉ

L'évolution vers un monde hyper-connecté, stimulée par la prolifération des dispositifs intelligents et des services sensibles à la latence, transforme profondément les attentes en matière d'architecture et de performance des réseaux sans fil. Au cœur de cette transformation se trouve le Cell-Free Massive MIMO centré utilisateur (UC-CFmMIMO), un paradigme qui abolit les frontières cellulaires rigides pour offrir une connectivité fluide, à haute capacité et ultra-fiable. Contrairement aux systèmes cellulaires conventionnels, l'UC-CFmMIMO coordonne des points d'accès distribués pour desservir conjointement les utilisateurs de manière flexible et adaptative, ce qui le rend particulièrement adapté aux applications à forte mobilité telles que les communications véhiculaires, le transport autonome et les systèmes de transport intelligents (ITS). L'importance de cette architecture se reflète dans son inclusion dans la feuille de route de la Release 19 du 3GPP, dont l'achèvement est prévu pour décembre 2025, marquant une étape clé dans la transition de la 5G-Advanced vers les réseaux de sixième génération (6G).

Face à la croissance continue des besoins en faible latence, haut débit et équité d'accès, en particulier dans des conditions de mobilité et de rareté spectrale, de nouveaux principes de conception sont nécessaires pour répondre à ces exigences. Cette thèse aborde ces impératifs à travers une ligne de recherche progressive visant à construire une base pratique et sécurisée pour le déploiement de l'UC-CFmMIMO dans des scénarios véhiculaires réalistes. Le travail débute par la remise en question des hypothèses de propagation idéalisées souvent rencontrées dans la littérature. À la place, il introduit un cadre de modélisation de canal sélectif en fréquence réaliste basé sur le modèle WINNER II et la plateforme QuaDRiGa, conçus pour être conformes aux spécifications 3GPP et largement utilisés pour simuler la propagation sans fil dans des scénarios véhiculaires standardisés. Ces modèles capturent les caractéristiques essentielles de l'étalement Doppler, de la diversité spatiale et des dynamiques de sous-bandes, offrant une représentation fidèle des canaux sans fil urbains dans les environnements véhiculaires. Cette base est cruciale non seulement pour l'évaluation,

mais aussi pour garantir que tout mécanisme d'optimisation proposé soit adapté aux complexités opérationnelles des environnements riches en mobilité.

Une fois cette base de canal réaliste établie, la recherche se concentre sur la conception de stratégies d'allocation des ressources fréquentielles capables de fonctionner efficacement sous les contraintes imposées par les environnements à forte mobilité. La phase suivante introduit des mécanismes d'allocation heuristiques innovants qui vont au-delà des schémas orthogonaux classiques. Deux métriques clés de la couche physique, le nombre de condition du canal et la corrélation inter-utilisateur des canaux, sont proposées comme critères centraux pour guider l'allocation des sous-bandes dans des scénarios multi-utilisateurs. Ces métriques sont utilisées pour alimenter des heuristiques légères basées sur la recherche, capables d'autoriser le partage de sous-bandes sans compromettre le contrôle de l'interférence. Cette approche se révèle particulièrement efficace dans les environnements véhiculaires, où les ressources spectrales sont limitées et les densités d'utilisateurs fortement dynamiques.

S'appuyant sur ces premiers résultats heuristiques, la thèse introduit un cadre d'optimisation multi-objectifs plus rigoureux. Ce cadre formule la tâche d'allocation comme un problème de maximisation d'utilité prenant en compte simultanément l'efficacité spectrale, l'équité et l'interférence. Chacun de ces objectifs est mathématiquement formulé dans un vecteur pondéré exploré via un ensemble de métaheuristiques évolutives, incluant le recuit simulé, les algorithmes génétiques et l'optimisation par colonie de fourmis. Le cadre obtenu est non seulement adaptable à différentes tailles et configurations de réseau, mais il présente également des améliorations significatives des performances système, notamment en termes de débit et d'équité, mesurées via l'analyse de l'indice de Gini. Cette phase démontre que des outils d'optimisation classiques, lorsqu'ils sont adaptés avec soin, peuvent encore produire des solutions efficaces et scalables pour les environnements sans fil de nouvelle génération.

Afin d'améliorer davantage l'adaptabilité dans des environnements dynamiques et de dépasser les limites des fonctions objectifs définies manuellement, la recherche évolue vers une formulation basée sur l'apprentissage. Cette dernière phase d'optimisation introduit un cadre hybride d'allocation des ressources intégrant l'apprentissage par

renforcement Actor-Critic Deep Deterministic Policy Gradient avec l'optimiseur Aquila, une métaheuristique inspirée de la nature récemment proposée. Le système résultant entraîne un agent autonome à prendre des décisions d'allocation fréquentielle en réponse directe aux observations de l'environnement, sans supervision humaine ni fonctions objectifs prédéfinies. Cette méthode hybride surpasse ses composants individuels ainsi que les bases de référence classiques, notamment en vitesse de convergence, adaptabilité à la mobilité des utilisateurs et réactivité face aux fluctuations du réseau.

Bien que ces avancées améliorent considérablement les performances et la scalabilité, le recours croissant aux modèles d'apprentissage automatique introduit de nouvelles vulnérabilités. Reconnaissant cet enjeu émergent, la dernière contribution de la thèse examine la robustesse des systèmes CFmMIMO assistés par IA face aux manipulations adversariales. Un cadre d'attaque en boîte noire est proposé, dans lequel un adversaire externe, sans accès aux modèles internes du système, entraîne un réseau de neurones substitut sur des données captées localement et génère des perturbations à l'aide de la méthode du gradient rapide (Fast Gradient Sign Method). Ces entrées adversariales sont soigneusement conçues pour contourner la détection d'anomalies et sont injectées dans la liaison montante via une contamination des pilotes. L'étude révèle que même de petites perturbations furtives peuvent perturber la prédiction du gain de canal et entraîner des allocations spectrales incorrectes en cascade. Les résultats soulignent l'urgence de développer des défenses contextuellement conscientes pour les mécanismes d'apprentissage de la couche physique, en particulier dans les réseaux véhiculaires à forte mobilité où la fiabilité est essentielle.

Ensemble, ces contributions forment une progression cohérente qui aborde à la fois la conception et la résilience des stratégies d'allocation de ressources dans les systèmes UC-CFmMIMO. La thèse s'aligne non seulement sur les objectifs de la Release 19 du 3GPP, mais anticipe également les exigences futures des réseaux 6G en proposant des solutions scalables, intelligentes et sécurisées pour les communications sans fil dans des environnements de plus en plus mobiles et critiques. En établissant un cadre robuste pour l'allocation adaptative des ressources et la robustesse aux attaques adversariales,

ce travail trace une voie fondamentale pour le déploiement de réseaux véhiculaires de nouvelle génération à la fois performants, fiables et prêts pour l'avenir.

Mots-clés : UC-CFmMIMO, 6G, réseaux véhiculaires, allocation des ressources fréquentielles, optimisation multi-objectifs, métaheuristiques, apprentissage par renforcement, apprentissage automatique adversarial, WINNER II, QuaDRiGa, efficacité spectrale, équité, sécurité des communications sans fil.

ABSTRACT

The evolution toward a hyper-connected world, fueled by the surge in intelligent devices and latency-sensitive services, is reshaping the architectural and performance expectations of wireless networks. At the forefront of this transformation is User-Centric Cell-Free Massive MIMO (UC-CFmMIMO), a paradigm that dissolves rigid cell boundaries to deliver seamless, high-capacity, and ultra-reliable connectivity. Unlike conventional cellular systems, UC-CFmMIMO orchestrates distributed access points to jointly serve users in a flexible and adaptive manner, making it particularly attractive for high-mobility applications such as vehicular communications, autonomous transportation, and intelligent transportation systems (ITS). The importance of this architecture is reflected in its inclusion in the 3GPP Release 19 roadmap, which is slated for completion by December 2025, marking a critical step in defining the 5G-Advanced transition toward sixth-generation (6G) networks.

As the demand for low-latency, high-throughput, and fair access continues to grow, particularly under mobility and spectrum scarcity constraints, new design principles are urgently needed to fulfill these requirements. This thesis addresses these imperatives through a progressive line of research aimed at building a practical and secure foundation for UC-CFmMIMO deployment in realistic vehicular scenarios. The work begins by tackling the limitations of overly idealized propagation assumptions found in prior literature. Instead, it introduces a realistic frequency-selective channel modeling framework based on the WINNER II model and the QuaDRiGa platform, which is designed to be compliant with 3GPP specifications and widely used for simulating wireless propagation in standardized vehicular scenarios. These models capture the essential characteristics of Doppler spread, spatial diversity, and subband dynamics, offering a faithful representation of urban vehicular wireless channels. This foundation is crucial not only for evaluation, but also for ensuring that any proposed optimization mechanism is tailored to the operational intricacies of mobility-rich environments.

With a realistic channel foundation in place, the research advances toward designing frequency resource allocation strategies that can effectively operate under the con-

straints imposed by high-mobility environments. The next phase introduces novel heuristic allocation mechanisms that go beyond classical orthogonal schemes. Two key physical-layer metrics, channel condition number and inter-user channel correlation, are proposed as core criteria to guide subband allocation in multi-user scenarios. These metrics are used to inform lightweight search-based heuristics capable of enabling subband sharing without compromising interference control. The approach proves particularly effective in vehicular settings, where spectral resources are scarce and user densities are highly dynamic.

Building upon these early heuristic gains, the thesis introduces a more principled multi-objective optimization framework. This framework formulates the allocation task as a utility maximization problem that jointly considers spectral efficiency, fairness, and interference. Each of these objectives is mathematically encoded into a weighted vector formulation, which is explored using a set of evolutionary metaheuristics including Simulated Annealing, Genetic Algorithms, and Ant Colony Optimization. The resulting framework is not only adaptable to various network sizes and configurations but also exhibits significant improvements in system-level performance metrics such as throughput and fairness, quantified through Gini index analysis. This phase demonstrates how classical optimization tools, when carefully adapted, can still yield scalable and efficient solutions in next-generation wireless environments.

To further enhance adaptability in dynamic environments and move beyond the limitations of handcrafted objective functions, the research transitions to a learning-based formulation. This final optimization phase introduces a hybrid resource allocation framework that integrates Actor-Critic Deep Deterministic Policy Gradient reinforcement learning with the Aquila Optimizer, a recent nature-inspired metaheuristic. The resulting system trains an autonomous agent to make responsive frequency allocation decisions directly from environmental observations, without the need for manual supervision or predefined objective functions. This hybrid method outperforms both its standalone components and traditional baselines, particularly in convergence speed, adaptability to user mobility, and responsiveness to network fluctuations.

While these advances significantly improve performance and scalability, the increasing reliance on machine learning models introduces new vulnerabilities. Recognizing

this emerging threat landscape, the final contribution of the thesis investigates the robustness of AI-assisted CFmMIMO systems against adversarial manipulation. A black-box attack framework is proposed in which an external adversary, without access to the system’s internal models, trains a surrogate neural network on locally captured data and crafts perturbations using the Fast Gradient Sign Method. These adversarial inputs are carefully shaped to evade anomaly detection and are injected into the uplink via pilot contamination. The study reveals that even small, stealthy perturbations can disrupt channel gain prediction and lead to cascading misallocations of spectral resources. The results underscore the urgency of developing context-aware defenses for learning-based physical layer mechanisms, especially in high-mobility vehicular networks where reliability is critical.

Together, these contributions form a coherent progression that addresses both the design and resilience of resource allocation strategies in UC-CFmMIMO systems. The thesis not only aligns with the goals of 3GPP Release 19 but also anticipates future demands of 6G networks by offering scalable, intelligent, and secure solutions for wireless communication in increasingly mobile and mission-critical environments. By establishing a robust framework for adaptive resource allocation and adversarial robustness, this work lays a foundational path for the deployment of next-generation vehicular networks that are not only high-performing, but also trustworthy and future-ready.

Keywords: UC-CFmMIMO, 6G, vehicular networks, frequency resource allocation, multi-objective optimization, metaheuristics, reinforcement learning, adversarial machine learning, WINNER II, QuaDRiGa, spectral efficiency, fairness, wireless security.

ACKNOWLEDGMENTS

I would like to express my deepest gratitude to the University of Lille for its financial support throughout my doctoral studies. This generous funding made it possible for me to fully dedicate myself to my research and professional development during these formative years.

I also extend my sincere thanks to Inria Lille Nord Europe for providing an exceptional research environment. The access to office space, computing resources, and a dynamic scientific ecosystem created ideal conditions for productive and inspired work on my PhD.

A special and heartfelt acknowledgment goes to my thesis co-director, **Dr. Valeria Loscri**, whose guidance, encouragement, and trust have been instrumental throughout this journey. Beyond her scientific expertise and dedication, I am deeply grateful for the many opportunities she offered me, from participating in international training schools to engaging in collaborative projects, as well as for her generous human support. Her mentorship has shaped both my academic path and personal growth in ways I will always carry forward.

DEDICATION

To my parents, whose unconditional love and sacrifices are the foundation of everything I have achieved.

To my sisters and my brother, for their constant support, encouragement, and belief in me.

To my paternal aunts, for their kindness and unwavering presence throughout my journey.

And to my dear friends, who stood by me with patience, laughter, and strength.

TABLE OF CONTENTS

Résumé	v
ABSTRACT	ix
	Page
LIST OF TABLES	xix
LIST OF FIGURES	xx
LIST OF SYMBOLS	xxiv
CHAPTER	
1. INTRODUCTION	1
1.1 Research Motivation	1
1.1.1 Problem Description	4
1.1.2 Research Objectives and Contributions	7
1.1.3 Structure of the Thesis	11
2. FUNDAMENTALS OF CELL-FREE MASSIVE MIMO	13
2.1 5G NR Protocol Stack and Functional Layer Roles	14
2.1.1 5G NR Protocol Stack Architecture	14
2.1.2 User Plane vs. Control Plane Separation	15
2.1.3 Physical Layer Functional Overview	17
2.2 Evolution of 5G and the Road Towards 6G	20
2.2.1 Standardization Progress in 3GPP Releases	20
2.2.2 Motivation for Cell-Free Massive MIMO	22
2.2.3 Cell-Free Massive MIMO Systems Basics	24
2.3 General Physical Layer Architecture in Cell-Free Massive MIMO	28
2.3.1 Uplink Physical Layer Chain	29

2.3.2	Downlink Physical Layer Chain	31
2.4	System Model	32
2.5	Practical Challenges of UC-CFmMIMO	37
2.6	Literature Review	41
3.	HEURISTIC APPROACHES TO FREQUENCY RESOURCE ALLOCA- TION IN UC CF MASSIVE MIMO	44
3.1	Introduction	44
3.2	Channel Model	47
3.2.1	WINNER II Channel Model Overview	47
3.2.1.1	Key Components of the Model	48
3.2.2	Channel Generation Process	49
3.2.2.1	Network Layout and Link Conditions	49
3.2.2.2	Three-Dimensional Antenna Array Model	50
3.2.2.3	Computation of the Channel Matrix	51
3.2.2.4	Interpretation of the Channel Data	53
3.3	Simulation Setup And Data Generation	55
3.3.1	Overview of the Simulation Environment	55
3.3.2	Deployment Configurations and Parameterization	56
3.3.3	Channel Realization and Frequency-Domain Representation	58
3.3.4	Mobility and Doppler Considerations	59
3.4	Proposed Resource Allocation Algorithms	59
3.4.1	Condition Number (CN)-Based Algorithm	60
3.4.2	Channel Correlation (CC)-Based Algorithm	61
3.4.3	Baseline: Best Subband First (BFS) Algorithm	62
3.4.4	Shared Algorithmic Structure	62

3.4.5	Computational Complexity Analysis	63
3.5	Numerical Results	65
3.6	Conclusion and Future Scope of Work	71
4.	METAHEURISTIC SOLUTIONS FOR FREQUENCY RESOURCE ALLOCATION IN UC CF MASSIVE MIMO	73
4.1	Introduction	73
4.2	Channel Model	77
4.3	Simulation Setup And Data Generation	80
4.4	Problem Formulation	84
4.5	Proposed Resource Allocation Algorithms	86
4.5.1	Simulated Annealing-Based Optimization	87
4.5.2	Genetic Algorithm-Based Optimization	89
4.5.3	Ant Colony Optimization-Based Strategy	89
4.5.4	Computational Complexity	90
4.6	Numerical Results	91
4.7	Conclusion and Future Scope of Work	96
5.	REINFORCEMENT LEARNING-BASED APPROACHES TO FREQUENCY RESOURCE ALLOCATION IN UC CF MASSIVE MIMO	98
5.1	Introduction	98
5.2	Channel Model	101
5.3	Simulation Setup and Data Generation	103
5.4	Proposed Resource Allocation Algorithms	105
5.4.1	Metaheuristic Optimization using Aquila Optimizer (AO)	106
5.4.2	Reinforcement Learning-Based Resource Allocation	109
5.4.3	Hybrid Optimization Framework: AO-Assisted Actor-Critic Learning	112

5.4.4	Architecture and Training Dynamics of the DDPG Framework	115
5.4.5	Hyperparameter Tuning and Optimization of the DDPG Agent	117
5.4.6	Computational Complexity Analysis	120
5.5	Numerical Results	122
5.6	Conclusion and Future Scope of Work	127
6.	ADVERSARIAL MACHINE LEARNING IN UC-CFMMIMO: VULNER- ABILITIES IN FREQUENCY-DOMAIN CHANNEL PREDICTION . . .	130
6.1	Introduction	130
6.2	Channel Model	133
6.3	Threat Model	135
6.3.1	Protocol-Level Vulnerability of Pilot Signals in 3GPP Networks	136
6.3.2	Adversarial Model	138
6.3.3	Adversary’s Goal	140
6.3.4	Adversary’s Capability, Limitations, and the 3GPP Security Perspective	142
6.4	Adversarial Attack Strategy	144
6.5	Experiments	148
6.5.1	Evaluation Framework and Predictive Models	149
6.5.2	Adversarial Robustness	152
6.5.3	Impact on Resource Allocation Consistency	155
6.6	Conclusion and Future Scope of Work	157
7.	CONCLUSIONS AND FUTURE RESEARCH DIRECTIONS	160
7.1	Conclusions	160
7.2	Future Research Directions	162
	BIBLIOGRAPHY	164
	APPENDICES	

A.	Code Examples	188
A.1	WINNER II channel model simulation	188
A.2	SUMO Vehicle Trajectory Extraction	193
A.3	Actor-Critic Agent for Deep Reinforcement Learning	195

LIST OF TABLES

Table		Page
3.1	WINNER II Simulation Parameters	57
3.2	Complexity Comparison of Resource Allocation Algorithms	63
5.1	QuaDRiGa Simulation Parameters.	105
5.2	Hyperparameter Ranges Used in Random Search.	118
5.3	Asymptotic Computational Complexity of the Proposed Methods	122
6.1	Clean performance of predictive models on the validation set	151
6.2	Detection accuracy of different classifiers on mixed (50% clean, 50% adversarial) test data. Attacks were generated using FGSM based on the LSTM substitute model.	154

LIST OF FIGURES

Figure	Page	
2.1	Separation of the user-plane and control-plane protocol stacks in 5G NR, showing the functional roles of each layer in both UE and gNB [2].	16
2.2	Time-frequency structure in 5G NR: numerology (μ), slot duration, and supported bandwidths.	18
2.3	Chronological evolution of 3GPP 5G Releases and their main focus areas from Release 15 to 19.	21
2.4	Illustrations of the different layers in a cell-free network. Each user equipment (in this case, a vehicle) connects to a subset of the APs, which is illustrated by the shaded regions. Each AP is connected to one CPU via fronthaul. The CPUs are interconnected either directly or via the core network.	25
2.5	Comparison between centralized and distributed processing in cell-free massive MIMO systems, highlighting the functional responsibilities at the CPU and AP levels (adapted from [53]).	26
2.6	Uplink and downlink physical layer chains in a cell-free massive MIMO architecture with centralized processing and O-RAN Split 7-2x. The schematic highlights LDPC coding, OFDM waveform processing, DMRS-based channel estimation, and the role of fronthaul in distributing signal and control flow between APs and the CPU.	31
2.7	Illustration of a user-centric CFmMIMO system model, where each UE dynamically connects to a subset of distributed APs based on clustering and wireless channel conditions. The coordination enables flexible, frequency-dependent transmission decisions.	33
3.1	3D system setup representation. APs are shown as circles, UEs as crosses, and links as straight lines. Only the links from one AP to all UEs are shown for visual clarity.	56
3.2	Simulated channel gains across frequency for 10 AP-UE links.	59
3.3	Comparison of average data rates as a function of varying β_{\min} using the CC algorithm for $L = 100, N = 4$ and $L = 400, N = 1$	66
3.4	UPE and allocation success under subband variation for the setup $L = 400, N = 1$	67

3.5	KDE of free subbands in the CC algorithm for two simulated scenarios with $\beta_{\min} = 0.4$	68
3.6	KDE of free subbands in the CN algorithm for the two deployment setups.	68
3.7	CDF of spectral efficiency in setup 1 ($L = 100, N = 4$) for $\beta_{\min} = 0.05$ and $\beta_{\min} = 0.4$	69
3.8	CDF of spectral efficiency in setup 2 ($L = 400, N = 1$) for $\beta_{\min} = 0.05$ and $\beta_{\min} = 0.4$	70
4.1	Manhattan city simulation scenario, SUMO view.	81
4.2	4 UE positions and trajectories over mobility steps. The starting positions are indicated by filled circles, and arrows illustrate the direction of movement and the evolution of the vehicles' positions. . .	82
4.3	Frequency response of measured channel gains across 10 AP-UE links. Each curve represents the wireless channel gain for a specific AP-UE link in the first user pair, where $h_{1,1}$ corresponds to AP 1 and user 1, $h_{1,2}$ to AP 1 and user 2, and so on.	83
4.4	PDP of the channel gains for the 10 AP-UE links.	84
4.5	Convergence of fitness values across algorithms: Comparison for a single user distribution with 20 available frequency resources.	92
4.6	Convergence of fitness values across algorithms: Performance comparison over five distinct user distributions with 20 available frequency resources.	92
4.7	Convergence of SE performance across user distributions and varying subband resources.	93
4.8	Percentage of free available bandwidth.	94
4.9	Gini Fairness.	95
4.10	Convergence behavior of SA for different user densities ($K = 40, K = 80$).	95
5.1	Channel frequency responses of the 10 AP-UE pair links.	104
5.2	Illustration of the four hunting strategies in the Aquila Optimizer. Each phase models a distinct movement pattern balancing exploration and exploitation.	108

5.3	Deep Deterministic Policy Gradient (DDPG) agent for frequency subband allocation in UC-CFmMIMO systems. The actor network generates continuous allocation scores from observed CFRs, while the critic network estimates the value of state-action pairs for policy optimization.	111
5.4	Hybrid AO-enhanced reinforcement learning architecture integrating Aquila-based exploration with DDPG’s actor-critic framework. . . .	113
5.5	Architecture of Actor and Critic deep neural networks (DNNs). . .	115
5.6	Evolution of actor loss for six hyperparameter configurations. Trial 5 exhibits the most consistent convergence.	118
5.7	Critic loss curves across training trials. Trial 5 achieves the lowest final error with minimal variance.	119
5.8	Objective value convergence comparison for AO, AC-RL, and HYM approaches.	123
5.9	Spectral efficiency (SE) evolution across iterations for the three algorithms.	124
5.10	Gini index evolution over iterations for AO, AC-RL, and HYM. . .	125
5.11	SE comparison across increasing user densities (40, 60, and 80 UEs).	126
5.12	SE variation with different subband allocations (40, 80, and 120 subbands).	126
6.1	Overview of the two attack phases in the proposed threat model. .	140
6.2	Overview of the adversarial attack based on FGSM.	145
6.3	Temporal prediction of frequency-domain channel gain using LSTM on a representative AP-UE pair. The model accurately tracks gain evolution, validating its predictive capacity.	151
6.4	Effect of perturbation strength and corruption percentage on R^2 . The left panel shows model-wise degradation at 50% corruption. The right panel shows LSTM degradation across varying corruption ratios.	152
6.5	Comparison of predicted frequency-domain gain under clean and adversarial conditions for the same user and antenna. The adversarial case shows greater deviation and a higher MSE, despite visually subtle differences.	153

6.6	Detection accuracy behavior under varying perturbation parameters using a Random Forest classifier.	154
6.7	Jaccard similarity between subband-user allocations under clean and adversarial CSI.	156

LIST OF SYMBOLS

Algorithmic and Optimization Variables

α	Weighting coefficient for spectral efficiency in utility function
β	Weighting coefficient for fairness in utility function
δ	Weighting coefficient for interference minimization in utility function
\mathbf{x}	Candidate solution in optimization space
\mathcal{A}	Set of allocation actions or strategies
\mathcal{P}	Set of available subbands
\mathcal{S}	Search space of possible frequency allocations
\mathcal{U}	Utility function to be maximized
CC	Channel correlation coefficient between users
CN	Condition number of the channel matrix
F	Fitness function used in metaheuristic optimization
$f(\mathbf{x})$	Objective value for solution \mathbf{x}
UPE	User Packing Efficiency metric

Channel and Communication Parameters

$\beta_{k,l}$	Large-scale fading coefficient between UE k and AP l
Δf	Subcarrier spacing
γ_k	Signal-to-noise ratio (SNR) for user k
λ	Wavelength corresponding to f_c
\mathbf{H}	Channel matrix between all UEs and APs
τ_p	Length of pilot sequence
B	System bandwidth
f_c	Carrier frequency
$h_{k,l,n}$	Channel coefficient between AP l and UE k on subband n
K	Number of user equipments (UEs)

- L Number of access points (APs)
- N Number of available subbands
- T_s OFDM symbol duration

Machine Learning and Reinforcement Learning Symbols

- ϵ Perturbation magnitude in FGSM attack
- \hat{Q} Target Q-value used for critic update
- \mathcal{A} Action space
- \mathcal{D} Experience replay buffer
- \mathcal{L}_{adv} Adversarial loss function
- \mathcal{R} Reward function
- \mathcal{S} State space
- ∇_{θ} Gradient with respect to parameter θ
- π Policy function in reinforcement learning
- FGSM Fast Gradient Sign Method used for adversarial example generation
- θ Parameter vector of the neural network (e.g., actor or critic)
- L Loss function used in training
- $Q(s, a)$ Action-value function estimating return of taking action a in state s
- $V(s)$ State-value function estimating return from state s

System Model Parameters and Indices

- \mathbf{g}_k Effective channel gain vector for user k
- \mathbf{R}_k Covariance matrix of the channel for user k
- \mathbf{W} Precoding matrix
- \mathbf{y}_k Received signal at user k
- \mathbf{z} Additive noise vector
- \mathcal{K} Set of all UEs
- \mathcal{L} Set of all APs
- \mathcal{N} Set of all subbands

$d_{k,l}$	Distance between user k and access point l
k	Index of user equipment (UE), $k = 1, \dots, K$
l	Index of access point (AP), $l = 1, \dots, L$
n	Index of frequency subband, $n = 1, \dots, N$
P_t	Transmit power
t	Time slot index
v_k	Velocity of user k

Chapter 1

INTRODUCTION

1.1 Research Motivation

The transition from fifth-generation (5G) to sixth-generation (6G) wireless networks is being driven by an unprecedented demand for capabilities that support complex, data-intensive, and low-latency applications. Although 5G networks introduced significant advancements, including expanded spectrum use, improved air interfaces, and the deployment of massive MIMO (mMIMO) systems, several inherent limitations persist. Issues such as inter-cell interference, particularly at cell edges, and resource contention continue to constrain network performance. These limitations restrict the full potential of advanced applications like the industrial Internet of Things (IoT), brain-computer interfaces, autonomous systems, and the tactile Internet, all of which depend on ultra-reliable, low-latency communication. Such challenges clearly indicate the need for innovative 6G architectures and resource management techniques that can efficiently support next-generation applications.

In addressing these demands, user centric cell-free massive MIMO (UC-CFmMIMO) presents a transformative architecture. By eliminating traditional cell boundaries and employing distributed antennas across extensive areas, UC-CFmMIMO offers a “cell-less” approach that enables seamless handover and spatial diversity. The cooperative nature of UC-CFmMIMO reduces inter-cell interference, improves spectral efficiency, and provides more consistent quality of service (QoS) for users. These features are particularly valuable in dynamic environments like vehicular networks, where continuous and low-latency connectivity is essential for Intelligent Transportation Systems

(ITS) and emerging vehicle-to-everything (V2X) applications, including autonomous driving. However, these benefits come with challenges in the form of frequency management, scalability, and adaptation to high-mobility conditions. UC-CFmMIMO's success in vehicular networks hinges on its ability to allocate frequency resources efficiently while maintaining connectivity despite rapid changes in user locations and environmental factors.

The increasing number of user equipment (UE) in high-demand environments, such as urban roadways and highways, further compounds the challenge of efficient spectrum allocation. For vehicular networks, the Federal Communication Commission (FCC) allocated 75 MHz of licensed spectrum within the 5.9 GHz band (5.850–5.925 GHz), standardized under IEEE 802.11p for vehicular communication [100, 108]. This allocation, though supportive of high-speed, short-range communications, is already under considerable pressure due to high usage demand. Regulatory limitations and significant costs associated with expanding this spectrum make it impractical to simply increase bandwidth to meet demand. As such, there is a critical need for wireless transmission techniques that maximize the efficiency of existing spectrum resources without compromising QoS.

One promising strategy in this context is multi-UE subband sharing, where multiple users share a given frequency resource simultaneously. This approach optimizes spectral efficiency by allowing more users to transmit and receive data within the same subband, achieving higher data rates and efficient resource utilization over multipath radio channels. Multi-UE subband sharing has already proven valuable in existing wireless systems but faces new challenges when implemented within UC-CFmMIMO, especially in the context of high-mobility vehicular networks. For UC-CFmMIMO to effectively meet the demands of future 6G networks, innovations are needed to refine

and adapt multi-UE subband sharing to environments with high user mobility and frequent channel variations.

Furthermore, the dynamic and unpredictable nature of vehicular networks brings challenges related to resource allocation stability and interference management. Vehicles move rapidly through coverage zones, creating Doppler effects that shift signal frequencies and introduce additional interference factors [25, 137]. This high-mobility environment demands adaptive and efficient resource allocation strategies that can respond to shifting channel conditions while ensuring fairness, throughput, and connectivity. Standard methods of resource allocation that rely on static or orthogonal subcarrier assignments are insufficient here, as they cannot fully leverage the spectrum's potential in dense, high-mobility scenarios [26]. By innovating resource allocation strategies that can manage multi-user allocation within shared subbands, UC-CFmMIMO systems can achieve greater spectral efficiency, supporting a higher density of UEs without requiring additional spectrum.

In parallel with these spectrum and mobility challenges, the anticipated integration of native Artificial Intelligence (AI) and Machine Learning (ML) into 6G wireless networks introduces additional sources of vulnerability that must be carefully considered. While AI-driven mechanisms promise unprecedented adaptability in functions such as resource allocation, channel prediction, and interference management, they also expose the network to new types of weaknesses, particularly in terms of security and system integrity. Unlike conventional optimization techniques, ML models are susceptible to adversarial manipulations, where subtle and often imperceptible perturbations can destabilize decision processes at the physical layer. In vehicular contexts, characterized by fast-changing conditions and tight latency constraints, these vulnerabilities pose a heightened threat, as the accuracy and reliability of AI-based operations become even more critical to maintain seamless and safe communications.

Recognizing and addressing the potential fragility of AI-enhanced components is thus an essential dimension of future 6G system design, as overlooking these emerging vulnerabilities could compromise the very performance gains that next-generation architectures aim to achieve.

This research is motivated by the need to develop UC-CFmMIMO resource allocation methods that enable more efficient spectrum usage while adapting to dynamic mobility and interference challenges. In vehicular networks, where low latency, high reliability, and operational integrity are essential, optimizing UC-CFmMIMO to allocate shared subbands among multiple UEs offers a pathway to achieving consistent high-performance outcomes. As 6G networks take shape, this study aims to lay the groundwork for practical, scalable, and adaptive frequency allocation schemes that not only enhance UC-CFmMIMO's potential to support the ITS ecosystem and next-generation V2X communication applications but also account for the emerging vulnerabilities of AI-driven components, ultimately advancing the robustness and capabilities of 6G vehicular networks.

1.1.1 Problem Description

Deploying UC-CFmMIMO systems in high-mobility environments like vehicular networks introduces unique challenges, many of which stem from the highly dynamic and frequency-selective nature of the wireless channels. Unlike in static settings, vehicular networks experience significant variations in channel conditions across different frequency bands due to multipath propagation and Doppler shifts, leading to frequency-selective fading. This selective fading means that signal quality varies across subbands, creating a need for resource allocation methods that can dynamically adapt to these frequency dependencies to ensure efficient spectrum usage and QoS.

Addressing these frequency-selective conditions requires effective frequency allocation strategies, and heuristic algorithms are often well-suited for solving allocation problems when the search space is manageable. For scenarios where the number of access points (APs), UE, and subbands is limited, heuristic methods can efficiently navigate the search space and find near-optimal solutions within a reasonable time-frame. Heuristic algorithms, through their straightforward search-based approach, are highly applicable for discrete, smaller-scale problems in UC-CFmMIMO, where they can deliver effective results with relatively low computational overhead.

However, as the feasible region of possible allocations expands, such as in large vehicular networks with high user density, the search space grows exponentially, and the time required for these algorithms to converge to optimal or near-optimal solutions increases significantly. In such cases, heuristic algorithms may become less efficient, and exploring broader areas of the solution space can prove challenging. To address these scenarios, metaheuristic approaches, such as genetic algorithms and simulated annealing, provide powerful alternatives. Metaheuristics incorporate strategies for exploring the search space more effectively, employing techniques like iterative improvement and randomization to avoid local optima and increase the chances of finding globally optimal solutions. These methods offer a practical solution for UC-CFmMIMO frequency allocation problems in larger-scale settings, balancing computational efficiency with solution quality.

While metaheuristics offer improved scalability and adaptability compared to simple heuristics, they may still face limitations in highly dynamic and time-sensitive environments. In vehicular networks, where the network topology and channel conditions can shift rapidly due to high-speed movement, even metaheuristic methods can struggle to keep pace with the rate of change in optimal allocation configurations. Here, reinforcement learning (RL) presents an attractive approach for optimizing

UC-CFmMIMO resource allocation. By framing the allocation problem as a dynamic decision-making process, an RL agent can learn from its interactions with the environment, continuously improving its allocation policy based on observed outcomes.

Reinforcement learning is particularly beneficial in environments with high variability, as it enables an agent to continuously adapt to changing network conditions, Doppler-induced frequency shifts, and fluctuating interference levels. Unlike traditional optimization algorithms, which may need to restart or reconfigure with each environmental change, an RL agent can refine its policy on the fly, potentially providing more responsive and robust allocation strategies. While heuristic and metaheuristic algorithms remain valuable in scenarios with more stable or predictable channel conditions, RL introduces the capacity to handle more complex and unpredictable settings, enhancing UC-CFmMIMO's ability to meet the demands of 6G vehicular networks.

However, the incorporation of AI-native approaches such as reinforcement learning into UC-CFmMIMO resource management also introduces a new category of system vulnerabilities. Unlike purely algorithmic methods, ML-driven components are inherently sensitive to the quality and integrity of their input data, making them susceptible to adversarial manipulations and intentional perturbations. In the context of vehicular networks, where decisions are made under high-mobility and time-critical conditions, the impact of even subtle disruptions in AI-based predictions, such as compromised channel state information, can propagate rapidly, degrading allocation performance and undermining system reliability. As 6G networks increasingly embed machine learning models into core physical-layer processes, recognizing these emerging cybersecurity risks becomes a crucial part of the problem landscape, adding an additional layer of complexity to the already challenging task of designing scalable, adaptive, and robust UC-CFmMIMO resource allocation strategies.

In summary, UC-CFmMIMO deployment in vehicular networks requires a combination of approaches to address the challenges of frequency-selective fading, large search spaces, and adaptability to rapidly changing conditions. Heuristic algorithms are effective for smaller-scale, less dynamic settings; metaheuristics expand this capability to larger and more complex search spaces; and reinforcement learning offers a promising extension for highly dynamic environments. Together, these techniques provide a layered approach to optimize UC-CFmMIMO frequency allocation across various scenarios. However, as future 6G vehicular networks increasingly rely on AI-driven resource management, it is equally important to account for the emerging system vulnerabilities these methods introduce, ensuring that performance gains are not undermined by new security risks and that overall network robustness is preserved.

1.1.2 Research Objectives and Contributions

The primary objective of this thesis is to develop practical and efficient frequency resource allocation schemes for UC-CFmMIMO systems that address the unique demands of high-mobility environments such as vehicular networks. The proposed methods aim to improve network resource utilization while guaranteeing that users' minimum rate requirements are met, maintaining fairness among users, and enhancing overall resource utilization simultaneously. The framework underlying these contributions operates at the physical layer (PHY), enabling responsive adaptability to challenging conditions while supporting high-performance requirements. The key contributions of this research are as follows:

- **Frequency-Dependent Channel Generation:** To accurately reflect the complex propagation environment of urban vehicular networks, we generate frequency-dependent channels using the WINNER II MATLAB toolbox. By

incorporating frequency selectivity into the channel model, this approach simulates realistic urban propagation scenarios and enhances the accuracy of UC-CFmMIMO channel modeling. This frequency-dependent modeling is crucial for capturing the impact of frequency-selective fading, which varies across subbands, thereby providing a more reliable foundation for testing and optimizing UC-CFmMIMO resource allocation strategies.

- **Novel Frequency Allocation Algorithms:** To improve frequency resource allocation efficiency under various network demands, we introduce two innovative frequency allocation algorithms based on the condition number (CN) and channel correlation (CC). The CN-based heuristic algorithm leverages a search-based strategy to minimize interference by focusing on subbands that exhibit favorable channel conditions, effectively reducing signal degradation. Meanwhile, the CC-based algorithm utilizes channel correlation as a guiding criterion to enhance spectral utilization, enabling efficient multi-user allocation within shared subbands. Together, these algorithms contribute to more effective allocation and management of frequency resources within UC-CFmMIMO systems, particularly in high-density vehicular networks where user demands vary dynamically.
- **Integration of Realistic Mobility and Channel Simulations:** To enhance the realism and applicability of the UC-CFmMIMO performance evaluations, this research integrates the Simulation of Urban Mobility (SUMO) platform for generating accurate urban vehicular mobility patterns and the Quadriga channel simulator for detailed channel modeling. SUMO provides realistic, time-evolving vehicle positions and speeds based on real traffic data, capturing the dynamic nature of urban road networks. These mobility traces are then combined with Quadriga’s geometry-based stochastic channel models, of-

fering high-fidelity multipath and frequency-selective channel representations tailored to vehicular environments. This integration ensures that the developed resource allocation strategies are validated against realistic, large-scale mobility and channel dynamics, improving the practical relevance and robustness of the proposed solutions.

- **Multi-Objective Utility-Based Resource Allocation:** Building on these allocation algorithms, we develop a utility-based multi-objective optimization framework that maximizes spectral efficiency, maintains user fairness, and minimizes interference across the network. This framework leverages a weighted utility vector to address various performance metrics simultaneously, providing a balanced approach that optimizes throughput, connectivity, and resource usage while adhering to system constraints. By ensuring that users meet their minimum rate requirements, the framework supports diverse QoS demands across the network, helping to maintain an equitable distribution of resources and improving network reliability and efficiency in high-mobility settings.
- **Metaheuristic Optimization with Simulated Annealing (SA), Genetic Algorithm (GA), and Ant Colony Optimization (ACO):** To handle the extensive and complex search space inherent in UC-CFmMIMO resource allocation, this research incorporates metaheuristic optimization techniques, specifically simulated annealing (SA), genetic algorithm (GA), and ant colony optimization (ACO). These metaheuristics are used to navigate the high-dimensional search space, where conventional heuristics may struggle to find optimal solutions efficiently. By exploring combinations of potential resource allocations, SA, GA, and ACO help improve the likelihood of achieving near-optimal configurations for multi-user subband sharing, thus supporting the network's spectral efficiency and QoS objectives. This approach is particularly useful in larger

networks or when the computational complexity escalates due to high-density user distributions.

- **Reinforcement Learning for Frequency Allocation:** Reinforcement learning is introduced as an advanced method for enabling adaptive, unsupervised frequency allocation. By employing an autonomous agent within the UC-CFmMIMO system, the RL framework allows the network to dynamically adjust its allocation policy in response to changing channel conditions and user mobility. This capability makes RL well-suited for highly dynamic environments, as the agent can learn from ongoing feedback, continuously improving resource allocation to maintain user QoS across diverse conditions. As the agent’s experience grows, it learns to balance multiple objectives, such as maximizing spectral efficiency and minimizing interference, without the need for explicit supervision, paving the way for UC-CFmMIMO to support advanced 6G applications with high adaptability.
- **Adversarial Vulnerability Analysis of AI-Driven Channel Gain Prediction:** This research investigates, for the first time in the context of UC-CFmMIMO vehicular networks, the adversarial vulnerabilities inherent in integrating machine learning models, specifically Long Short-Term Memory (LSTM)-based channel gain predictors, into physical-layer resource allocation. A black-box adversarial framework is developed, using a surrogate LSTM model trained on passively collected RF data to craft FGSM-based perturbations that degrade channel gain predictions without requiring access to the internal parameters of the target system. By injecting these perturbations through uplink pilot contamination, the study demonstrates how subtle input manipulations can cascade into severe resource misallocations, undermining subband-user scheduling and overall system reliability. This contribution provides critical insights into the

systemic fragility of AI-native UC-CFmMIMO networks and highlights the necessity of incorporating security-aware design principles alongside performance optimization.

These contributions collectively establish a robust foundation for UC-CFmMIMO to deliver high-throughput, low-latency, and reliable communication in high-mobility scenarios. By addressing the requirements for efficient resource allocation, adaptive responsiveness, and fairness across users, this research advances UC-CFmMIMO's capabilities to support Intelligent Transportation Systems (ITS) and other critical applications, contributing to the broader development of next-generation 6G vehicular networks.

1.1.3 Structure of the Thesis

This dissertation is thoughtfully organized to guide the reader through a logical progression of research, moving from foundational principles to advanced solutions and emerging challenges in UC-CFmMIMO systems for 6G vehicular networks.

Chapter 1 introduces the study, outlining the motivations, research challenges, and the significance of developing efficient and robust UC-CFmMIMO systems, along with a summary of the key research objectives and contributions.

Chapter 2 presents the fundamental background, reviewing the 5G NR protocol stack, physical-layer architectures, and the evolution toward 6G networks, with a detailed overview of UC-CFmMIMO principles, practical challenges, and a comprehensive literature review identifying gaps in existing resource allocation methods.

Chapter 3 focuses on heuristic approaches to frequency resource allocation, describing the system model, WINNER II-based frequency-selective channel generation, and

the design of novel heuristic algorithms, including condition number (CN)-based and channel correlation (CC)-based strategies, supported by detailed simulation setups and numerical evaluations.

Chapter 4 expands the methodological landscape by introducing metaheuristic optimization solutions, such as simulated annealing (SA), genetic algorithms (GA), and ant colony optimization (ACO), providing a comparative analysis of their performance in optimizing frequency allocation under large-scale and complex vehicular scenarios.

Chapter 5 explores reinforcement learning (RL)-based approaches, presenting an advanced framework where autonomous agents adaptively manage frequency resources in response to changing conditions, including hybrid resource allocation strategies that integrate metaheuristics (such as the Aquila optimizer) with actor-critic learning, supported by in-depth analysis of the architecture, training dynamics, and hyperparameter tuning of the RL agents.

Chapter 6 introduces a novel research dimension on adversarial machine learning in UC-CFmMIMO systems, analyzing the vulnerabilities of LSTM-based channel gain predictors to black-box adversarial attacks. This chapter details the threat models, attack strategies, evaluation frameworks, and the impact of adversarial perturbations on resource allocation consistency, broadening the research scope to encompass critical cybersecurity challenges.

Chapter 7 concludes the dissertation by summarizing the major findings, reflecting on the implications of the proposed solutions, and outlining future research directions, particularly regarding the secure, scalable, and adaptive design of UC-CFmMIMO systems in next-generation vehicular networks.

Chapter 2

FUNDAMENTALS OF CELL-FREE MASSIVE MIMO

The rapid evolution of mobile networks, culminating in the standardization and global deployment of 5G New Radio (5G NR), has introduced unprecedented flexibility and capacity at the physical layer. Despite these advances, conventional cellular architectures continue to face critical challenges in meeting the demands of ubiquitous connectivity, especially at cell edges and in dense deployments. To overcome these limitations, a new paradigm known as Cell-Free Massive MIMO (CFmMIMO) has emerged, aiming to provide uniformly high service quality through dense, distributed, and cooperative deployment of access points.

This chapter begins by revisiting the foundational elements of the 5G NR physical layer, as defined in the 3GPP specifications, with an emphasis on the transmission chain, reference signaling, resource allocation, and scheduling procedures. This foundation serves as a baseline for identifying the architectural and functional shifts introduced by the cell-free approach.

We then explore the principles of Cell-Free Massive MIMO, examining how the traditional notions of cells, handovers, and centralized antennas are replaced by user-centric cooperation across multiple access points. The differences between centralized and distributed processing strategies are highlighted in terms of control and data plane partitioning, latency, and scalability.

Finally, we conclude the chapter by presenting a general system model for CFmMIMO and summarizing relevant literature, setting the stage for the technical developments and contributions of this dissertation.

2.1 5G NR Protocol Stack and Functional Layer Roles

2.1.1 5G NR Protocol Stack Architecture

As the cornerstone of modern wireless networks, the 5G New Radio (NR) protocol stack embodies a sophisticated layering of functional blocks designed to support the performance ambitions of next-generation communication systems. Building on the foundation established by LTE, the NR stack refines and extends key principles to accommodate highly diverse service requirements, including ultra-reliable low-latency communication (URLLC), enhanced mobile broadband (eMBB), and massive machine-type communication (mMTC). At its core, the protocol stack provides a systematic framework for translating user and signaling data into robust, adaptable radio transmissions, ensuring seamless end-to-end delivery between the User Equipment (UE) and the gNB (Next Generation Node B).

Functionally, the NR stack is organized into a set of interdependent layers, each contributing a distinct class of operations. The uppermost layer, the Service Data Adaptation Protocol (SDAP), manages the mapping of application-layer quality-of-service (QoS) flows to radio bearers. Beneath it, the Packet Data Convergence Protocol (PDCP) handles header compression, ciphering, and integrity protection while preserving packet sequence and reordering. The Radio Link Control (RLC) layer further refines delivery reliability through segmentation, retransmission, and flow control, adapting to fluctuating radio conditions. The Medium Access Control (MAC) layer governs resource scheduling and multiplexing across logical channels and coordinates hybrid ARQ operations. At the foundation of the stack lies the Physical Layer (PHY), responsible for encoding, modulation, waveform mapping, and transmission over the air interface using OFDM-based techniques and advanced multi-antenna configurations [2].

Each of these layers is instantiated symmetrically at both the gNB and UE ends of the link, operating in parallel to maintain a reliable and efficient communication session. The structure and responsibilities of these layers remain consistent across deployment scenarios but are flexibly configured to adapt to varying service demands, spectrum allocations, and radio access technologies. The sophistication and modularity of this design make 5G NR both scalable and extensible, which is an essential trait as the system evolves toward 5G-Advanced and beyond.

2.1.2 User Plane vs. Control Plane Separation

A defining characteristic of the NR architecture is the explicit separation between the user and control planes, a design choice that enables clean functional isolation, enhanced flexibility, and fine-grained QoS enforcement. While both planes share the same lower-layer transport mechanisms, they diverge in purpose, composition, and treatment within the stack.

The user plane is tasked with the transport of application data, ranging from web traffic to real-time video streams, and originates at the UE's service layer before traversing through SDAP, PDCP, RLC, MAC, and ultimately the PHY for transmission. The SDAP layer, unique to the user plane, plays a pivotal role in associating each QoS Flow Identifier (QFI) with its corresponding Data Radio Bearer (DRB), enabling the enforcement of differentiated service guarantees as dictated by the 5G Core Network [7].

In contrast, the control plane carries the signaling necessary to initiate, configure, and maintain the radio link, including procedures for connection setup, mobility, and session management. At the apex of this stack resides the Radio Resource Control (RRC) protocol, which interfaces directly with the Access and Mobility Management

Function (AMF) in the core network. RRC messages are encapsulated within Signaling Radio Bearers (SRBs) and routed through the common lower layers, PDCP, RLC, MAC, and PHY, using configurations optimized for reliability and latency [6].

Although both planes leverage the same transmission pipeline below the PDCP layer, their operational behaviors and requirements differ substantially. Control-plane messages typically receive higher priority, are always integrity-protected, and often utilize acknowledged transmission modes in RLC to ensure delivery. User-plane traffic, on the other hand, may prioritize throughput or latency depending on service class, and can be configured for unacknowledged delivery if desired. These distinct requirements are reflected in bearer-specific configurations at each layer, allowing NR to satisfy diverse application needs without compromising architectural coherence.

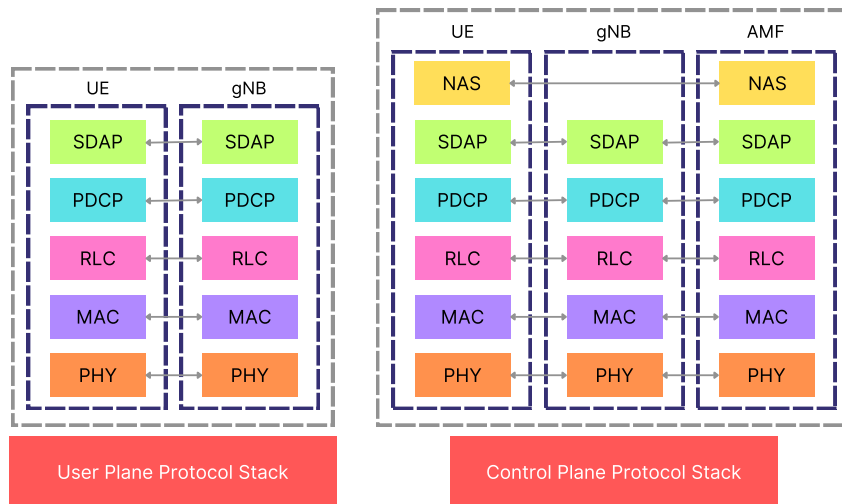


Figure 2.1: Separation of the user-plane and control-plane protocol stacks in 5G NR, showing the functional roles of each layer in both UE and gNB [2].

Figure 2.1 illustrates this structural bifurcation between user and control planes, highlighting the parallelism and layer-specific distinctions present across the UE and gNB. The architecture’s modularity ensures that both data delivery and signaling

procedures can operate concurrently and efficiently, enabling NR networks to deliver high service quality with robust control.

Scope of this Thesis.

The core of this dissertation is situated within the physical layer of the 5G NR protocol stack, with particular emphasis on aspects related to resource management, realistic channel state information (CSI) simulation, and distributed coordination mechanisms. Although the reference framework is grounded in the 5G NR architecture, the research is forward-facing and aligned with the evolution toward sixth-generation (6G) systems, which are anticipated to build upon and extend the foundational principles established by 5G. This work investigates how physical-layer functions such as channel modeling, downlink sounding, precoding schemes, and frequency resource allocation can be efficiently orchestrated to support dynamic user-AP associations and meet the scalability demands of cell-free massive MIMO systems under vehicular constraints. By addressing these challenges, the thesis contributes to the broader objective of shaping physical-layer strategies that will underpin the performance and reliability of next-generation 6G vehicular networks. The following section explores these foundational physical-layer procedures in greater detail, establishing the technical groundwork for the models and contributions developed in subsequent chapters.

2.1.3 Physical Layer Functional Overview

The physical layer (PHY) forms the foundation of the 5G NR protocol stack, handling all signal-level operations required to transmit and receive information over the air interface. Defined across multiple 3GPP specifications (including TS 38.201, TS 38.211, TS 38.212, TS 38.213, and TS 38.214), the PHY layer is responsible not only for waveform generation and channel coding but also for enabling channel estimation,

resource allocation, CSI reporting, and antenna domain processing such as precoding and combining [2].

In 5G NR, the PHY adopts an orthogonal frequency-division multiplexing (OFDM) waveform structure, with support for scalable numerologies that allow subcarrier spacings of 15, 30, 60, 120, and 240 kHz. The time domain is organized into frames (10 ms), subframes (1 ms), and slots (variable in duration depending on the numerology), as illustrated in Figure 2.2 [2].

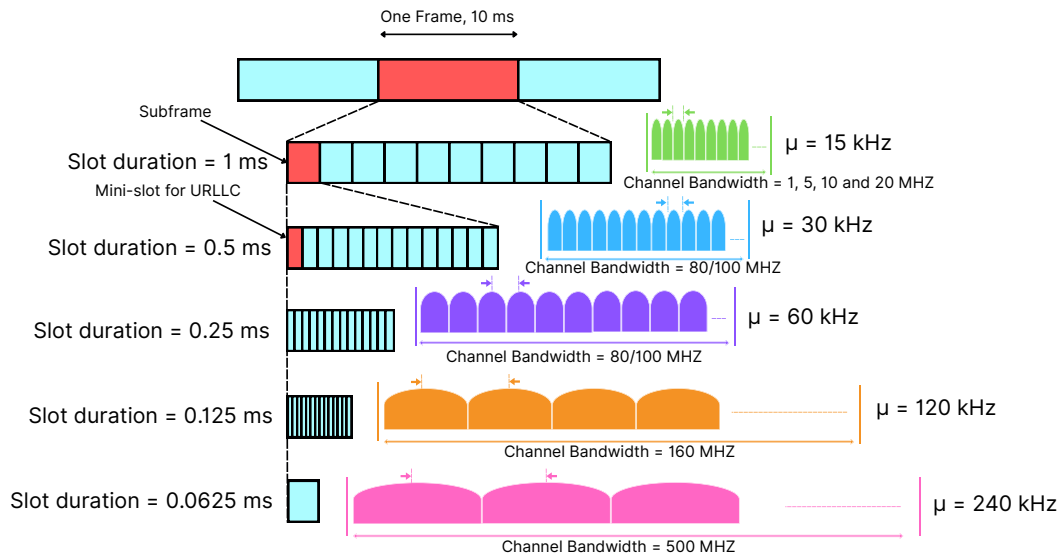


Figure 2.2: Time-frequency structure in 5G NR: numerology (μ), slot duration, and supported bandwidths.

Each slot typically contains 14 OFDM symbols, and frequency resources are structured into resource blocks (RBs), each composed of 12 subcarriers. This flexible time-frequency design enables fine-tuned adaptation to different deployment scenarios, ranging from high-throughput urban cells to latency-sensitive vehicular networks.

From a transmitter perspective, whether at the gNB for downlink or the UE for uplink, the PHY layer processes higher-layer data through a sequence of operations.

These include cyclic redundancy check (CRC) attachment, channel coding (LDPC for data, polar codes for control), rate matching, scrambling, modulation mapping (e.g., QPSK, 16-QAM, 64-QAM, 256-QAM), and layer mapping for MIMO. The resulting modulated symbols are then mapped onto physical resource elements and OFDM-modulated for transmission [2].

At the receiver end, the PHY performs inverse operations, including downconversion, synchronization, FFT processing, channel estimation using reference signals (e.g., DMRS and SRS), equalization (e.g., MMSE), demodulation, and decoding. CRC checks are performed to validate block integrity before passing the data up to MAC.

A key capability of the 5G NR PHY layer is its support for massive MIMO and advanced beamforming techniques. The transmitter may apply spatial precoding to direct signal energy toward intended users, based on the available channel state information. This spatial domain processing is closely linked to the structure and usage of reference signals and the CSI reporting process.

CSI acquisition is a central component of PHY-layer operation. In time division duplex (TDD) systems, uplink sounding reference signals (SRS) transmitted by UEs allow the gNB (or access points in a cell-free setup) to estimate the uplink channel. Under channel reciprocity assumptions, these estimates are then reused for downlink precoding. In frequency division duplex (FDD) systems, downlink CSI reference signals (CSI-RS) are employed, and the UE transmits quantized CSI reports via the uplink. The 3GPP specification supports both Type-I and Type-II CSI reporting, which differ in terms of signaling overhead and feedback resolution [6].

In addition to CSI, the PHY layer also manages time-frequency resource allocation. Scheduling decisions made at the MAC layer are translated into specific RB and symbol-level allocations at PHY. These define exactly where within a slot or mini-

slot user data or control information is to be mapped and transmitted. This fine granularity allows the system to adapt dynamically to channel conditions, traffic loads, and latency constraints.

In the context of this dissertation, which addresses cell-free massive MIMO systems under mobility constraints, the PHY layer plays a pivotal role in enabling distributed and cooperative signal processing. The assignment of pilot sequences, configuration of sounding signals, mapping of time-frequency resources, and distributed precoding strategies are all rooted in physical-layer procedures. A deep understanding of these elements, particularly under vehicular scenarios, is essential for achieving scalable and reliable operation in dense, user-centric architectures.

2.2 Evolution of 5G and the Road Towards 6G

2.2.1 Standardization Progress in 3GPP Releases

The 3GPP has orchestrated a series of pivotal releases (15 through 19) that chronologically chart the evolution of 5G and lay the groundwork for 6G. Each release is associated with a formal completion date and a set of technical goals, gradually expanding the capabilities of the network beyond enhanced mobile broadband towards ultra-reliable, low-latency, and beyond. Below, in Figure 2.3, we outline Releases 15–19, highlighting their finalization timelines, key technical scope, and contributions to 5G evolution and early 6G enablers.



Figure 2.3: Chronological evolution of 3GPP 5G Releases and their main focus areas from Release 15 to 19.

Release 15 (2018) – 5G NR Foundation (eMBB Focus): Release 15 marked the first complete set of 5G standards, introducing the 5G New Radio (NR) and the Next Generation Core (5GC) network architecture [51]. It supported both Non-Standalone (NSA) and Standalone (SA) deployment modes, with a primary focus on enhanced Mobile Broadband (eMBB). Key innovations included a flexible NR physical layer with scalable numerologies, high-frequency operation up to millimeter waves, and cloud-native service-based architecture in the 5GC.

Release 16 (2020) – 5G Expansion for URLLC and Industry: Finalized in 2020, Release 16 extended 5G capabilities to ultra-reliable low-latency communication (URLLC), industrial automation, and V2X applications. It introduced NR Sidelink for direct communication between devices, NR operation in unlicensed spectrum (NR-U), enhanced positioning, and improved network slicing [141]. This release addressed new verticals such as smart manufacturing, transport, and mission-critical services.

Release 17 (2022) – 5G Enhancement for New Use Cases: Completed in 2022, Release 17 further broadened 5G’s applicability. It introduced Reduced Capability (RedCap) devices for mid-range IoT, initiated Non-Terrestrial Networks (NTN) integration with satellite support, and improved MIMO coordination with multi-TRP enhancements [114]. Other additions included expanded mmWave frequencies, improved power efficiency, and better support for positioning and extended reality (XR).

Release 18 (2024) – Launch of 5G-Advanced: Release 18 represents the first phase of 5G-Advanced, completed in 2024. It initiated the integration of Artificial Intelligence (AI) and Machine Learning (ML) into network operations, improved MIMO beamforming, and enhanced XR support with reduced latency and jitter. RedCap enhancements and initial AI-native RAN functionalities were also included [114].

Release 19 (Expected 2025) – 5G-Advanced Evolution and Bridge to 6G: Release 19, expected to finalize in 2025, focuses on deepening AI/ML integration, optimizing energy efficiency, supporting larger MIMO arrays, and extending support for ambient IoT and NTN enhancements [58]. This release aims to complete the 5G-Advanced vision while preparing foundational technologies for the eventual transition to 6G.

Open Research Directions: Despite extensive standardization, several areas remain open for exploration. Cell-free massive MIMO, for example, has not yet been standardized. Although techniques such as multi-TRP and CoMP appear in current releases, they fall short of the fully distributed cooperative processing envisioned in cell-free systems [132, 183]. Achieving scalable and robust performance under this paradigm requires further advances in fronthaul coordination, pilot design, synchronization, and real-time signal processing. These gaps motivate ongoing research into physical-layer resource management and distributed architectures, especially in high-mobility and dense deployment scenarios.

2.2.2 Motivation for Cell-Free Massive MIMO

As the wireless community looks beyond 5G-Advanced and into the realm of 6G, one of the most promising architectural shifts is the transition from cell-centric to user-centric designs. Traditional cellular networks, even with advanced techniques like

coordinated multipoint (CoMP) and multi-TRP, are still fundamentally constrained by the presence of inter-cell interference and the need for users to be associated with specific base stations. This structure creates performance disparities across the coverage area, especially at cell edges or in dense urban and vehicular environments.

Cell-free massive MIMO (CF-mMIMO) proposes a radically different approach. Instead of dividing the service area into fixed cells, CF-mMIMO envisions a large number of geographically distributed access points (APs), all jointly serving users in a cooperative and dynamic manner. Each user is served by a subset of APs based on large-scale fading characteristics, without being tied to a single cell. The result is a network that eliminates cell boundaries, reduces interference through coherent joint transmission and reception, and offers more uniform quality of service [132].

This architecture offers several critical advantages that align well with emerging 6G requirements. First, by exploiting macro-diversity and spatial multiplexing across a wide area, CF-mMIMO can significantly enhance spectral and energy efficiency. Second, the user-centric nature of the design leads to more stable link quality and better support for mobility, particularly in scenarios involving vehicular users. Third, by dynamically updating the set of serving access points rather than relying on rigid cell boundaries, CF-mMIMO largely eliminates traditional cell-based handovers. Instead, the system implements cluster-level reassociation or soft handovers to manage changes in user location, which reduces control signalling overhead and simplifies mobility management as network density increases [181][183].

While some of the foundational ideas of CF-mMIMO overlap with concepts like CoMP, distributed MIMO, or multi-TRP in 5G-Advanced, CF-mMIMO goes further by advocating a fully cooperative, fully distributed system with local processing at the AP level and global coordination through a central unit or a decentralized mechanism. The feasibility of such systems depends on efficient pilot allocation, scalable fronthaul

design, synchronization strategies, and advanced physical-layer resource management, topics that are still open in current standards [91].

Given these open issues and the promising performance benefits, CF-mMIMO is a highly active area of research. It offers a compelling solution to several 5G limitations, while also acting as a candidate architecture for future 6G networks. This thesis builds upon this context, focusing on how resource allocation and coordination can be optimized in cell-free systems under realistic physical-layer constraints and high-mobility conditions.

In the following section, we delve deeper into the architecture of cell-free massive MIMO systems, highlighting both centralized and distributed implementations. This will be followed by a comparative discussion on how such architectures relate to and diverge from the conventional 5G NR framework. Finally, a system model will be introduced to formalize the assumptions and configurations under which this dissertation's analyses and contributions are developed.

2.2.3 Cell-Free Massive MIMO Systems Basics

Cell-free massive MIMO systems are characterized by a fundamentally different architectural philosophy from traditional cellular networks. Rather than dividing the service area into discrete cells, the network consists of a large number of access points (APs), distributed over a wide geographical area, which collaboratively serve all users without pre-defined cell boundaries, as illustrated in Figure 2.4. This user-centric paradigm enables uniform service quality and efficient spatial diversity exploitation.

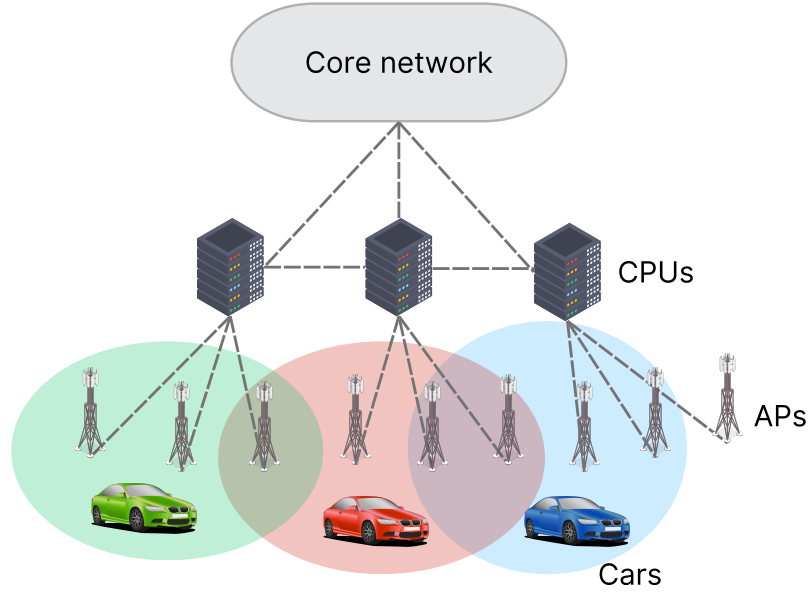


Figure 2.4: Illustrations of the different layers in a cell-free network. Each user equipment (in this case, a vehicle) connects to a subset of the APs, which is illustrated by the shaded regions. Each AP is connected to one CPU via fronthaul. The CPUs are interconnected either directly or via the core network.

At the core of the cell-free massive MIMO architecture lies a coordination framework that governs signal processing, resource allocation, and access point (AP) cooperation across the network. Depending on the deployment, this coordination is either managed through a centralized processing unit (CPU), which aggregates global channel state information and supervises physical-layer operations, or through distributed units (DUs) at the APs, which handle selected processing tasks locally and exchange only essential information with the higher-level management layer. The choice between centralized and distributed coordination shapes not only the division of computational responsibilities but also determines key system properties, including scalability, fronthaul load, and achievable performance.

Within this context, two principal architectural models have been established in the cell-free framework, as illustrated in Figure 2.5:

- Centralized Processing:** In this configuration, the APs primarily function as radio heads, forwarding received baseband signals (uplink) or transmitting precoded signals (downlink) under the full supervision of the CPU. The CPU performs all critical physical-layer operations, including channel estimation, combining, decoding, and precoding. This approach offers performance advantages by leveraging global channel knowledge but imposes stringent demands on the fronthaul network, requiring high-capacity, low-latency links to support real-time coordination.
- Distributed Processing:** In this configuration, a portion or all of the physical-layer tasks, such as local channel estimation, combining, or precoding, are delegated to the APs themselves. Only processed or compressed information, such as quantized symbols or soft estimates, is exchanged with the coordinating layer. While this architecture alleviates fronthaul load and enhances scalability, it may introduce performance trade-offs due to limited availability of global channel state information and reduced coordination granularity.

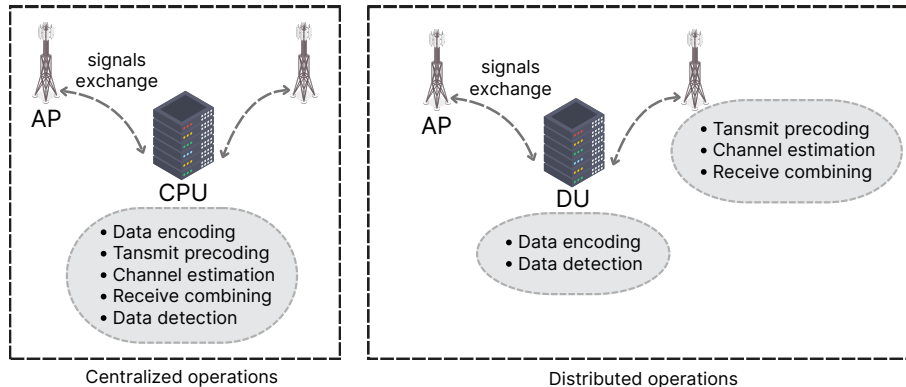


Figure 2.5: Comparison between centralized and distributed processing in cell-free massive MIMO systems, highlighting the functional responsibilities at the CPU and AP levels (adapted from [53]).

In both architectures, users transmit or receive signals over shared time-frequency resources. Pilot sequences are transmitted in the uplink to enable channel estimation either locally at APs or globally at the CPU, depending on the processing scheme. Downlink transmission may involve joint precoding across multiple APs, aiming to coherently serve users based on their channel states. Power control and user-AP association strategies are critical to ensuring fairness and spectral efficiency in such distributed environments.

From a protocol perspective, the CF-mMIMO architecture retains the conventional layered communication model but introduces architectural reallocation of functions. While the physical (PHY) and medium access control (MAC) layers remain, their implementation may be split across APs and CPU. For instance, in centralized setups, the MAC and scheduling reside entirely at the CPU, whereas in distributed schemes, hybrid MAC may be implemented across the network.

Compared to CoMP or multi-TRP implementations in 5G NR, cell-free architectures do not limit user service to predefined cooperating sets or fixed sectors. Instead, user-AP associations are dynamic and flexible, typically based on large-scale fading conditions. This flexibility allows the system to serve users more uniformly, especially in mobility scenarios or areas with variable user density.

The architectural design of CF-mMIMO systems has a direct impact on the system model and analytical framework used in performance evaluation and optimization. This motivates a deeper look into how cell-free architectures are implemented at the physical layer, particularly in relation to the 5G NR standard. The next section outlines the general physical layer architecture in cell-free systems, mapping out the end-to-end uplink and downlink chains, key signal processing components, and the differences introduced by distributed AP coordination. This forms the technical basis for the system model used throughout this thesis.

2.3 General Physical Layer Architecture in Cell-Free Massive MIMO

The physical layer in cell-free massive MIMO systems is composed of conventional NR transmission components repurposed for highly distributed cooperative operation. While retaining compatibility with the 5G NR protocol stack, the fundamental difference lies in how physical-layer functions are coordinated across multiple access points (APs), requiring distributed signal processing, channel state information (CSI) management, and synchronization across the network.

Cell-free deployments operate without traditional cell boundaries, and the physical layer must therefore support coherent joint transmission and reception across geographically separated APs. This design amplifies the need for precise uplink pilot processing, downlink beamforming, and low-latency fronthaul support, all while adhering to the physical-layer standards defined in the 3GPP 38-series specifications [11, 34].

The transmission chain in cell-free massive MIMO systems closely mirrors that of 5G NR, but with significant structural adaptations. In the uplink, UEs transmit modulated data over the PUSCH after LDPC encoding, rate matching, and OFDM waveform generation using either CP-OFDM or DFT-s-OFDM [11]. Demodulation reference signals (DMRS) are embedded to facilitate channel estimation at the APs [10]. Each AP performs baseband signal processing and forwards either raw or processed data to a central processing unit (CPU), where signal combining is performed, either via Maximum Ratio Combining (MRC), MMSE, or large-scale fading decoding (LSFD) [39].

In the downlink, the CPU (or distributed APs) encodes data for each user, maps it to modulation symbols, and performs spatial precoding. These precoded signals

are transmitted over the PDSCH using synchronized OFDM waveforms from multiple APs [46]. The UEs demodulate and decode the combined signal using DMRS-assisted channel estimation [10]. The use of reciprocity-based precoding in TDD systems, leveraging sounding reference signals (SRS) from the uplink, allows efficient downlink channel inference without explicit feedback [91].

Compared to traditional cellular MIMO systems, which centralize physical-layer coordination at individual base stations, cell-free architectures distribute these responsibilities across many APs. The result is improved macro-diversity, reduced interference, and more uniform performance across the network [132]. However, this benefit comes with additional challenges in fronthaul bandwidth, synchronization, and real-time CSI exchange.

The following sections dissect the uplink and downlink physical-layer chains in greater detail, clarifying how each processing step aligns with 5G NR standards while highlighting the distinctions introduced by cell-free operation under both centralized and distributed processing regimes. Particular emphasis is placed on the downlink chain, where this dissertation is positioned. Specifically, our work addresses frequency-domain resource allocation in the downlink configuration, with a focus on realistic CSI acquisition and coordination constraints imposed by cell-free operation in mobile environments. This contextualizes the detailed system model and methodology developed in the subsequent chapters.

2.3.1 Uplink Physical Layer Chain

In the uplink, user equipments (UEs) transmit data on the Physical Uplink Shared Channel (PUSCH). Each transmission begins with the generation of a CRC, followed by channel coding using LDPC as specified in TS 38.212 [11]. The resulting codewords

undergo rate matching and bit scrambling before modulation (e.g., QPSK, 16-QAM, 64-QAM). These modulated symbols are then mapped to time-frequency resources and transformed into a time-domain waveform using DFT-s-OFDM or CP-OFDM, depending on the configuration.

To enable channel estimation at the receiving APs, DMRS (Demodulation Reference Signals) are embedded within the PUSCH [10]. Additionally, sounding reference signals (SRS) may be transmitted separately for broader uplink channel measurements and reciprocity-based downlink estimation.

Upon reception, each AP performs downconversion, FFT, DMRS extraction, and local channel estimation. In centralized processing architectures, these baseband signals or channel estimates are forwarded to the CPU, where multi-AP signal combining is performed using schemes like MRC, MMSE, or LSFD [39]. In distributed setups, APs may conduct local equalization and forward soft bits (e.g., LLRs) to the CPU, reducing fronthaul load at the cost of centralized precision [46], as shown in Figure 2.6.

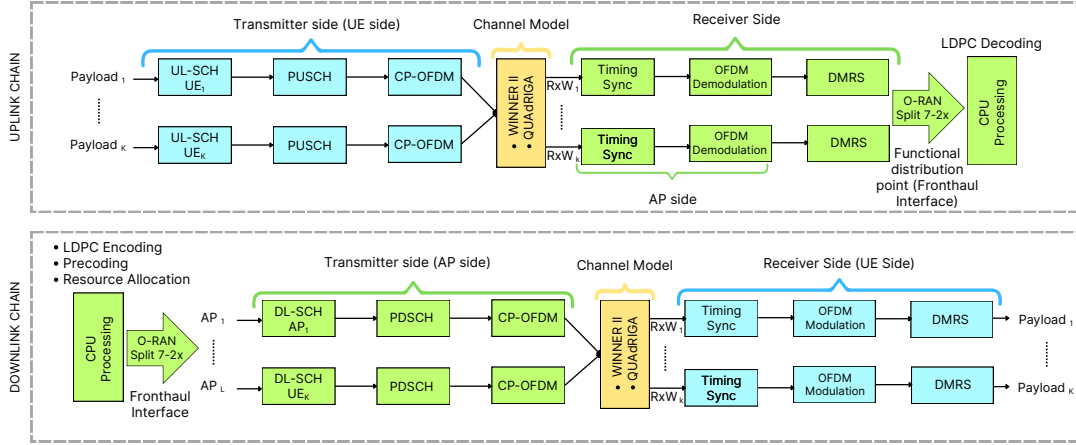


Figure 2.6: Uplink and downlink physical layer chains in a cell-free massive MIMO architecture with centralized processing and O-RAN Split 7-2x. The schematic highlights LDPC coding, OFDM waveform processing, DMRS-based channel estimation, and the role of fronthaul in distributing signal and control flow between APs and the CPU.

2.3.2 Downlink Physical Layer Chain

In the downlink (also illustrated in Figure 2.6), data originates at the CPU or distributed processing nodes, where it is encoded using LDPC, scrambled, modulated, and mapped to spatial layers. Channel estimates obtained from uplink pilots (in TDD) are used to generate precoding weights, typically via MRT or Zero-Forcing approaches [46, 91].

These precoded signals are mapped to physical resource blocks (PRBs) and OFDM modulated at the APs. In synchronized deployments, the APs transmit jointly and coherently, enabling the target UE to receive a superimposed signal from multiple geographically separated APs.

At the UE side, reception involves synchronization, FFT processing, DMRS-based channel estimation, equalization, demodulation, and LDPC decoding, followed by CRC verification [11]. This cooperative transmission structure boosts signal uniformity and reliability across the service area.

Our work is situated within this downlink chain, focusing on how frequency-domain resource blocks are dynamically assigned across distributed APs under CSI and fronthaul limitations. The goal is to ensure efficient spectrum utilization while maintaining coherent transmission and system scalability.

2.4 System Model

This section presents a foundational system model for user-centric cell-free massive MIMO (UC-CFmMIMO) networks, forming the basis for the analyses and applications discussed in later chapters. The UC-CFmMIMO approach emphasizes the allocation of resources around each user equipment (UE) by dynamically grouping access points (APs) to meet the real-time connectivity and quality of service (QoS) demands of each user, as illustrated in Figure 2.7. To ensure robust spatial diversity and connectivity, a UC-CFmMIMO network typically features a large-scale deployment of APs, L , which greatly exceeds the number of UEs, K , across the network. This configuration ensures that the system can maintain high performance even in dense or high-mobility environments.

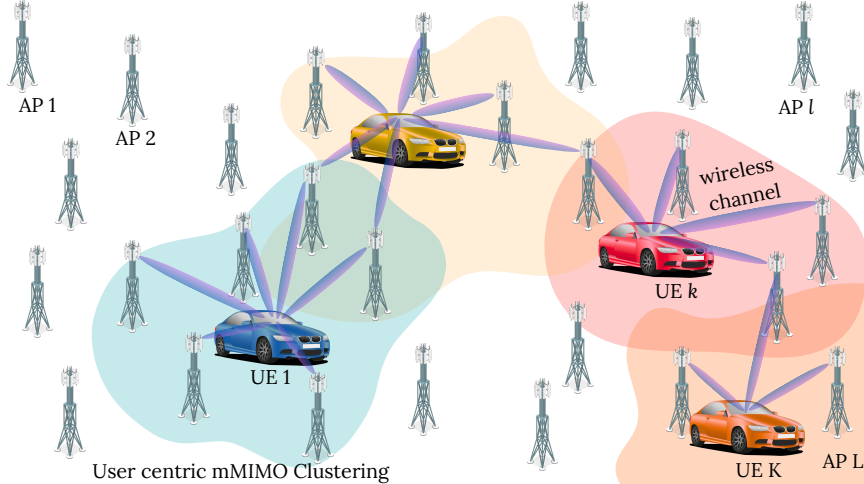


Figure 2.7: Illustration of a user-centric CFmMIMO system model, where each UE dynamically connects to a subset of distributed APs based on clustering and wireless channel conditions. The coordination enables flexible, frequency-dependent transmission decisions.

In this model, we consider a CFmMIMO network comprising K single-antenna UEs that are randomly distributed over a defined coverage area of R square meters. These UEs are served by L APs, each equipped with N antennas, that are also randomly deployed across the area. By utilizing a high density of APs, the network ensures that each UE maintains reliable service and experiences consistent signal quality regardless of its position within the network area. To achieve effective and flexible resource allocation, the total available bandwidth, denoted B_W , is divided into S subbands, where each subband occupies a portion of the available spectrum. This structure allows the network to adapt its frequency resources dynamically based on real-time network demands.

The system's operation depends heavily on the frequency-dependent characteristics of the wireless channel. In real-world scenarios, wireless channels vary in their response across different frequencies, an effect known as frequency-selective fading. This phenomenon is particularly relevant in CFmMIMO systems, where signals transmitted over different subbands experience distinct propagation conditions due to multipath

effects, environmental factors, and Doppler shifts, especially in high-mobility contexts. In our studies, the frequency-dependent nature of the channel has been incorporated to simulate realistic propagation environments, allowing for an in-depth examination of how different subbands affect signal quality and user experience. This channel dependence on frequency is crucial for designing effective resource allocation and interference management strategies in CFmMIMO systems.

In this model, the downlink channel between AP l and UE k on subband s is represented by the $1 \times N$ channel vector $\mathbf{h}_{k,l,s}$, which captures the channel gain and phase shift associated with that specific link and subband. To represent the combined downlink channel effect of all APs serving UE k over subband s , we define the $1 \times NL$ collective channel vector as $\mathbf{h}_{k,s} = [\mathbf{h}_{k,1,s}, \mathbf{h}_{k,2,s}, \dots, \mathbf{h}_{k,L,s}]$. This collective channel vector serves as the basis for modeling the downlink signal from all APs to each UE, allowing the system to adaptively adjust its transmission strategy based on the specific channel conditions experienced by each UE.

A central processing unit (CPU) is responsible for coordinating the APs across the network. The CPU manages downlink transmissions and processes data received from each AP via fronthaul links, operating under the assumption that perfect channel state information (CSI) is available for each UE. The CSI, obtained through standard channel estimation techniques, enables the CPU to perform centralized processing and optimize data precoding and transmission strategies across the network. This centralized access to CSI is critical for ensuring that each UE experiences a high-quality downlink connection, as it allows the CPU to manage interference and allocate resources efficiently.

At this early stage of resource allocation, AP resources are allocated to users based on criteria such as proximity and channel quality, ensuring that each UE is served by the most relevant APs. This initial allocation framework is implemented through a

dynamic cooperation clustering process [52], where only a subset of APs is selected to serve each UE according to network conditions [89]. This AP selection mechanism, which is distinct from the frequency resource allocation strategies addressed in later chapters, is represented by the $N \times N$ matrix $\mathbf{D}_{k,l}$, where $\mathbf{D}_{k,l} = \mathbf{I}_N$ if AP l serves UE k and $\mathbf{D}_{k,l} = \mathbf{0}_{N \times N}$ otherwise. By focusing on AP assignment as a preliminary step, this clustering framework establishes a foundational association between APs and UEs, preparing the network for subsequent frequency allocation and signal processing decisions.

In this downlink model, the received signal y_k at UE k on subband s is given by:

$$y_k = \sum_{l=1}^L \mathbf{h}_{k,l,s} \mathbf{x}_{l,s} + n_{k,s}, \quad (2.1)$$

where $n_{k,s} \sim \mathcal{N}(0, \sigma^2)$ represents the receiver noise, and $\mathbf{x}_{l,s}$ is the $N \times 1$ signal vector transmitted by AP l on subband s , defined as:

$$\mathbf{x}_{l,s} = \sum_{i \in \mathcal{K}_s} \mathbf{D}_{i,l} \mathbf{w}_{i,l} a_i. \quad (2.2)$$

Here, a_i denotes the data signal for UE i with unit power, and $\mathbf{w}_{i,l}$ is the $N \times 1$ precoding vector applied by AP l for UE i . This setup enables the APs to serve multiple UEs on each subband by exploiting spatial and frequency diversity, resulting in improved signal quality. By substituting $\mathbf{x}_{l,s}$ into the expression for y_k , we obtain a network-wide perspective of the received signal at UE k on subband s :

$$y_k = \mathbf{h}_{k,s} \sum_{i \in \mathcal{K}_s} \mathbf{D}_i \mathbf{w}_i a_i + n_{k,s}, \quad (2.3)$$

where $\mathbf{D}_i = \mathbf{D}_{i,1} \oplus \mathbf{D}_{i,2} \oplus \cdots \oplus \mathbf{D}_{i,L}$ is an $NL \times NL$ block diagonal matrix that indicates the selected APs serving UE i , and $\mathbf{w}_i = [\mathbf{w}_{i,1}^T, \dots, \mathbf{w}_{i,L}^T]^T$ represents the collective $NL \times 1$ precoding vector for UE i . Here, $\mathbf{w}_{i,l}^T$ denotes the transpose of the vector $\mathbf{w}_{i,l}$.

The signal-to-interference-plus-noise ratio (SINR) for UE k on subband s is given by:

$$\text{SINR}_k = \frac{|\mathbf{h}_{k,s} \mathbf{D}_k \mathbf{w}_k|^2}{\sum_{i \in \mathcal{K}_s \setminus k} |\mathbf{h}_{k,s} \mathbf{D}_i \mathbf{w}_i|^2 + \sigma^2}. \quad (2.4)$$

The spectral efficiency (SE) for UE k is derived from this SINR as follows:

$$\text{SE}_k = \log_2(1 + \text{SINR}_k). \quad (2.5)$$

In user-centric CFmMIMO, interference management is a critical component. We limit interference calculations to those UEs sharing APs with UE k on the same subband [52]. The subset of interfering UEs, denoted \mathcal{C}_k , includes UEs that share APs with UE k , defined as:

$$\mathcal{C}_k = \{i : \mathbf{D}_i \mathbf{D}_k \neq \mathbf{0}_{N \times N}\}. \quad (2.6)$$

To mitigate interference from UEs in $\mathcal{C}_{k,s} = \mathcal{K}_s \cap \mathcal{C}_k$, we employ a zero-forcing (ZF) precoding technique, constructing the $|\mathcal{C}_{k,s}| \times NL$ channel matrix as $\mathbf{H}_{k,s} = [\mathbf{h}_{k,s}; \mathbf{h}_{i,s} : i \in \mathcal{C}_{k,s} \setminus \{k\}]$. The ZF precoding vector \mathbf{w}_k is determined by solving:

$$\mathbf{H}_{k,s} \mathbf{D}_k \mathbf{w}_k = [1, 0, \dots, 0]^T, \quad (2.7)$$

where $\mathbf{H}_{k,s}^H$ is the Hermitian (conjugate transpose) of the matrix $\mathbf{H}_{k,s}$. The solution for \mathbf{w}_k is given by the first column of:

$$\mathbf{D}_k \mathbf{H}_{k,s}^H (\mathbf{H}_{k,s} \mathbf{D}_k \mathbf{H}_{k,s}^H)^{-1}. \quad (2.8)$$

Finally, \mathbf{w}_k is scaled by transmit power ρ_k [40], given by an equal power allocation:

$$\rho_k = \frac{P_{\max}}{\tau_p}, \quad (2.9)$$

here, τ_p denotes the length of the uplink pilot sequence, which reflects the number of orthogonal pilots and determines the extent of pilot reuse in the system.

To evaluate system performance, we calculate the average data rate R_{avg} across all UEs:

$$R_{\text{avg}} = \frac{\sum_{k=1}^K R_k}{K}, \quad (2.10)$$

where $R_k = B_k \cdot \text{SE}_k$ denotes the data rate for UE k , representing the product of its allocated bandwidth B_k and spectral efficiency SE_k . This model provides a foundational framework for examining UC-CFmMIMO networks and developing resource allocation strategies in later chapters.

2.5 Practical Challenges of UC-CFmMIMO

User-centric cell-free massive MIMO (UC-CFmMIMO) systems promise high spectral efficiency, low latency, and macro-diversity through spatially distributed access points

(APs). However, realizing these benefits in practice demands addressing a variety of system-level challenges that stem from hardware limitations, real-time channel impairments, control and data plane orchestration, and resource allocation under complex constraints. This section outlines these core challenges and recent academic efforts to mitigate them [53, 101, 82, 149, 84, 77, 22].

Hardware Limitations and Fronthaul Constraints

UC-CFmMIMO networks require numerous distributed APs and centralized or semi-centralized processing units. Deploying high-performance hardware at each AP is impractical due to cost, energy consumption, and scalability issues. Low-resolution ADCs and DACs have been proposed to reduce fronthaul capacity and energy usage, albeit at the expense of signal quality [101]. Quantization noise and nonlinear distortion, especially from power amplifiers, must be accounted for in system models and signal processing designs [82, 149].

CSI Acquisition and Pilot Contamination

Reliable channel state information (CSI) is fundamental for effective transmission and resource allocation. However, acquiring accurate CSI is hindered by thermal noise, pilot contamination, and channel aging, particularly in high-mobility environments. The limited number of orthogonal pilots necessitates pilot reuse, leading to interference between users sharing pilots. Advanced pilot assignment schemes, such as graph coloring, greedy algorithms, and meta-heuristics, aim to minimize this contamination [84]. Additionally, low-resolution quantization affects the quality of CSI estimates, which must be addressed via quantization-aware estimators [149, 101].

Resource Allocation Complexity

Efficient resource management is vital in UC-CFmMIMO, particularly given the high density of UEs and APs. Key components include:

Power Control: Power must be judiciously allocated to balance fairness and energy efficiency. Max-min SINR and energy-efficient optimization approaches have shown effectiveness in both uplink and downlink scenarios [77, 53].

AP Clustering and Antenna Selection: Each user is served by a subset of APs. Dynamic AP selection strategies based on channel gain or service utility balance performance with computational complexity. Some studies propose binary antenna selection integrated with power control to reduce network energy consumption [149, 22].

Pilot Signal Allocation: Mitigating pilot contamination requires strategic pilot allocation. Graph-based methods and clustering-aware reuse schemes help isolate pilot-sharing users, thereby improving CSI accuracy [84, 53].

Frequency Resource Allocation: Wideband UC-CFmMIMO systems encounter frequency-selective fading, where each subband exhibits distinct channel behavior. Allocating subbands effectively under such variation is essential for maintaining throughput and reducing interference [53, 22, 82].

Coordination and Scalability

UC-CFmMIMO systems require coordination between distributed APs and central units. A fully centralized approach may achieve optimal performance but imposes heavy fronthaul and computational burdens. Distributed or hybrid coordination,

where local units make scheduling and beamforming decisions under guidance from a central controller, has been proposed as a scalable alternative [22, 53]. Beamforming strategies, such as partial or local zero-forcing, offer trade-offs between interference suppression and computational complexity [53, 149].

Scheduling, Synchronization, and Mobility

Dynamic scheduling allows time-frequency resource reuse and helps manage pilot collisions and AP contention. Algorithms such as proportional fair (PF) scheduling have been integrated into UC-CFmMIMO frameworks to maintain fairness and throughput [22]. Synchronization between APs in both timing and phase is critical for coherent joint transmission, especially in the downlink. High-mobility scenarios, including vehicular networks, require frequent updates in user-AP associations and robust handover protocols. Solutions include clustering stability, soft handoff design, and joint uplink-downlink optimization [82, 53].

Summary and Implications

Addressing these practical challenges is key to realizing the theoretical advantages of UC-CFmMIMO in real-world deployments. Frequency-domain resource allocation, in particular, has emerged as a core issue due to frequency-selective fading and multi-user interference. This dissertation focuses on designing efficient, scalable algorithms for frequency resource allocation in the downlink of UC-CFmMIMO systems, taking into account realistic channel behavior, mobility, and coordination constraints [53, 77, 82].

2.6 Literature Review

This section surveys key contributions to frequency resource allocation in cell-free massive MIMO (CF-mMIMO) systems, with emphasis on methods addressing frequency selectivity, realistic channel modeling, vehicular deployment conditions, and quality of service (QoS) optimization. As 5G networks adopt OFDM-based transmission, resource allocation becomes central to managing interference, maximizing spectral efficiency, and meeting user-centric performance demands.

In traditional cellular systems, water-filling algorithms have been widely applied to dynamically assign subcarriers and power based on channel state information (CSI) [187]. Proportional fairness methods [177] balance throughput and fairness, particularly in heterogeneous network environments. However, such approaches often struggle with computational scalability and responsiveness in ultra-dense deployments.

The distributed architecture of CF-mMIMO introduces additional complexity but also new opportunities for scalable resource control. Early contributions proposed heuristic pilot allocation based on spatial proximity and channel similarity, which reduces contamination with low computational overhead [132]. Similarly, location-aware frequency assignment has been explored to mitigate interference by prioritizing AP-UE proximity [31]. While these techniques are computationally efficient, they generally fail to provide optimal solutions under dynamic traffic and channel conditions.

To tackle the non-convexity of CF-mMIMO resource allocation, metaheuristic algorithms have gained popularity. Genetic algorithms (GA) have been used to jointly optimize AP-UE associations and power distribution [186], while particle swarm optimization (PSO) has shown effectiveness in OFDM subcarrier and power allocation tasks [46]. Ant colony optimization (ACO), simulated annealing (SA), and hybrid ap-

proaches further enhance solution diversity and convergence performance [167, 162]. For instance, [176] proposed a hybrid ACO-GA strategy for large-scale distributed antenna systems, achieving superior fairness and spectral efficiency. Nonetheless, metaheuristics typically require manual tuning and may face limitations under time-varying environments.

Reinforcement learning (RL) offers a dynamic alternative, where policies are learned via environmental interaction. Deep Q-Networks (DQN) have been used to adapt frequency and power assignments in non-stationary settings [83]. More advanced frameworks, such as multi-agent RL (MARL), enable distributed APs to collaboratively learn resource policies without centralized orchestration [179]. Hierarchical deep RL models have further improved energy efficiency and fairness in clustering and scheduling tasks [118]. Additionally, RL-based solutions have been applied to pilot allocation, dynamically avoiding contamination based on observed interference patterns [175]. Actor-critic-based models such as DDPG and soft actor-critic (SAC) have been recently employed for joint power control and beamforming [110]. Moreover, federated RL is emerging as a privacy-preserving alternative to central learning [139], with potential applications in multi-AP coordination.

From another perspective, deep learning has also been employed to approximate complex resource allocation mappings in CF-mMIMO. Convolutional and graph neural networks (GNNs) have been used to learn topology-aware transmission strategies [79, 97]. While data-driven methods can generalize well across scenarios, they typically require extensive offline training datasets, which may be impractical in high-mobility or real-time settings.

Hybrid strategies that integrate RL with heuristic or metaheuristic optimization have emerged to address the limitations of single-class solutions. Such methods balance exploration, convergence, and adaptability. For example, [157] proposed a DRL-

GA hybrid that dynamically tunes policy networks using genetic search, achieving robust results under channel variation. Likewise, [42] integrates DDPG with Aquila Optimizer to adapt frequency allocation under frequency-selective fading.

In light of this landscape, our work contributes new hybrid optimization strategies that integrate deep RL with metaheuristics to address frequency-selective subband allocation in vehicular CF-mMIMO systems. Leveraging realistic channel models (e.g., WINNER II and QuaDRiGa), we investigate scalable algorithms for joint user-subband assignment, interference minimization, and spectral efficiency enhancement. These contributions are detailed in the next section and span three complementary research studies [44, 41, 42].

Chapter 3

HEURISTIC APPROACHES TO FREQUENCY RESOURCE ALLOCATION IN UC CF MASSIVE MIMO

Publication Note

This chapter is based on the following peer-reviewed publication, accepted for presentation at the *IEEE International Symposium on Local and Metropolitan Area Networks (LANMAN)*, and presented in July 2025 [44].

3.1 Introduction

Heuristics are powerful tools for solving complex optimization problems, especially in scenarios where the problem size or constraints make exact solutions impractical. These approaches rely on intuitive, rule-based, or approximate methods to find near-optimal solutions within a reasonable timeframe. Their simplicity and adaptability make them particularly suitable for systems with dynamic and complex requirements, such as mobile networks. While user-centric cell-free massive MIMO (UC-CFmMIMO) systems are still in the early stages of research and have yet to be widely implemented, it is intuitive to consider heuristics as promising candidates for addressing the unique challenges of resource allocation in these systems. Their ability to efficiently handle large-scale, dynamic environments suggests potential for improving performance in UC-CFmMIMO networks.

To properly assess the efficacy of heuristic algorithms in such scenarios, it is critical to test them under realistic conditions. This involves generating high-quality, reliable data that captures the intricacies of signal propagation and user interactions in urban environments. For this purpose, we employ the WINNER II Matlab toolbox, a state-of-the-art simulation tool that leverages advanced mathematical models derived from empirical measurements. These models are tailored to represent frequency-dependent channel characteristics accurately, ensuring that our simulations reflect the complex behavior of real-world networks. By generating realistic and detailed data, we can provide a robust foundation for testing and evaluating the proposed heuristic algorithms.

In this chapter, we present innovative heuristic algorithms tailored to address the challenges of frequency resource allocation in UC-CFmMIMO systems. These algorithms focus on user pairing and subband allocation, aiming to optimize resource distribution while minimizing interference and ensuring fairness among users. By testing these heuristics on the high-fidelity data generated through the WINNER II toolbox, we explore their ability to effectively solve resource allocation problems under realistic conditions.

Furthermore, the chapter evaluates the power of the proposed heuristics to reduce critical performance bottlenecks, such as high condition numbers (CN) and channel correlation (CC), which are significant in densely populated and interference-prone environments. By addressing these issues, the algorithms enhance the effective utilization of frequency resources and improve the overall connectivity and spectral efficiency of the system. To benchmark their performance, a comparative analysis is conducted against traditional Best Subband (BS) allocation strategies, providing insights into the strengths and limitations of heuristic approaches in this emerging field.

This chapter makes several key contributions, summarized as follows:

- **Generation of frequency-dependent channels** with preprocessing using the WINNER II Matlab toolbox, ensuring simulations that closely mimic real-world signal propagation and environmental interactions.
- **Design of heuristic algorithms** for frequency resource allocation, focusing on user pairing and subband allocation strategies tailored for UC-CFmMIMO systems.
- **Performance enhancement** through the minimization of the condition number (CN) and reduction of channel correlation (CC), facilitating improved connectivity and resource utilization in high-density scenarios.
- **Comparative analysis** of the proposed algorithms against conventional methods, demonstrating the potential of heuristics in achieving superior performance in terms of fairness, efficiency, and scalability.

The remainder of this chapter is organized as follows. Section 3.2 introduces the channel model and provides an overview of the WINNER II Matlab toolbox, detailing how it works and the specific channel model it adopts. Section 3.3 describes the simulation setup and data generation process, highlighting the advanced methods employed to create realistic scenarios. In Section 3.4, we present the proposed resource allocation algorithms and their design principles, tailored for UC-CFmMIMO systems. Section 3.4.5 provides a comprehensive complexity analysis, evaluating the computational demands of the proposed heuristics. Section 3.5 discusses the numerical results obtained through extensive simulations, comparing the performance of the proposed methods against traditional strategies. Finally, Section 3.6 concludes the chapter with a summary of findings and a discussion on future research directions.

3.2 Channel Model

Wireless communication systems rely on accurate and reliable channel models to simulate real-world propagation conditions and evaluate the performance of transmission techniques. The *channel model* plays a crucial role in determining how signals propagate between transmitters and receivers in a given environment. In this work, we employ the **WINNER II channel model**, a sophisticated and widely accepted framework designed for system-level and link-level simulations.

The WINNER II model builds upon previous iterations of channel models, including the *3GPP/3GPP2 Spatial Channel Model (SCM)* and the *SCM(E) Extension models*, while introducing key enhancements to support **MIMO (Multiple Input Multiple Output) systems**, **3D-Antenna-Array modeling**, and various **propagation scenarios**.

This section introduces the underlying principles of the WINNER II model, explains the process of generating channels, details its features, and presents the resulting *Channel Impulse Response (CIR)* used for further analysis in this research.

3.2.1 WINNER II Channel Model Overview

The **WINNER II channel model** [37, 38] is a highly flexible and comprehensive framework designed for *radio channel characterization* in diverse propagation conditions. The primary goal of this model is to provide realistic *MIMO radio channel realizations* suitable for evaluating various wireless technologies, including **5G and beyond**.

3.2.1.1 Key Components of the Model

To achieve a highly accurate and adaptable radio channel model, WINNER II incorporates several essential components. These components are designed to handle the complexities of modern wireless communication, ensuring realistic simulation results that can be used for system design and evaluation. One of the most critical aspects of the model is its ability to simulate multiple propagation scenarios, ranging from indoor small-cell environments to large-scale urban and rural deployments. The model also supports diverse antenna configurations and propagation conditions, ensuring a comprehensive evaluation framework for wireless technologies.

One of the fundamental strengths of the WINNER II model is its ability to integrate 3D antenna array processing, which plays a crucial role in capturing spatial characteristics of the channel. Additionally, it supports deterministic modeling through predefined channel characteristics, making it highly effective for benchmarking purposes. The following components form the core structure of the WINNER II model:

- **3D-Antenna-Array (3D-AA) Model:** This model enables a complete 3D representation of antennas and their respective radiation patterns. It supports *polarization*, *directional filtering*, and *spatial displacement*, allowing for an accurate depiction of real-world antenna configurations.
- **Clustered Delay Line (CDL) Model Option:** This feature introduces a deterministic approach to channel modeling, where specific channel parameters such as angles of arrival, departure, and delay spreads are predefined based on measured data. The CDL model is particularly useful for benchmarking and standardized testing of wireless systems.

- **Multipath Clustering:** The model accounts for multiple propagation paths within a given scenario, capturing *spatial channel characteristics, delay spreads, and Doppler shifts*. These factors significantly affect the received signal’s strength and quality, making them essential considerations in wireless system performance evaluation.
- **Support for Various Scenarios:** The WINNER II model encompasses a broad range of predefined propagation environments, ensuring realistic simulation outcomes. It includes both *LOS (Line of Sight)* and *NLOS (Non-Line of Sight)* conditions, allowing researchers to examine system behavior under different transmission environments.

3.2.2 Channel Generation Process

The channel generation process in the **WINNER II model** involves multiple stages that collectively define the propagation characteristics of the wireless environment. These stages begin with the **network layout definition**, followed by the **antenna configuration and spatial modeling**, and conclude with the **generation of the channel matrix**, which serves as the basis for further simulation and analysis.

3.2.2.1 Network Layout and Link Conditions

Before simulating the channel, it is essential to define the **network layout**, which establishes the positions and configurations of both **Base Stations (BSs)** and **Mobile Stations (MSs)** within the simulated environment. The spatial distribution of these stations directly impacts the propagation characteristics and influences the overall performance of the modeled system.

The placement of BSs and MSs is carefully designed to align with the intended propagation scenario, whether it be an *urban macro-cell, micro-cell, rural area, or indoor environment*. Each scenario requires different assumptions regarding *antenna heights, transmission power, and environmental conditions*. Additionally, the movement of mobile stations is accounted for in dynamic simulations, ensuring that variations in the received signal due to mobility are accurately captured.

Another critical aspect of the layout definition is the classification of links as either **Line-of-Sight (LOS)** or **Non-Line-of-Sight (NLOS)**. LOS conditions imply a direct and unobstructed path between the transmitter and receiver, leading to stronger signal power and more predictable fading characteristics. Conversely, NLOS conditions introduce obstructions such as buildings, terrain, or other obstacles, leading to increased *multipath propagation, diffraction, and scattering effects*. Properly distinguishing between these two cases is essential for ensuring realistic modeling of wireless channels.

3.2.2.2 Three-Dimensional Antenna Array Model

To accurately capture spatial propagation characteristics, the **WINNER II model** employs a **3D-Antenna-Array (3D-AA) representation**. Unlike traditional *Uniform Linear Arrays (ULAs)*, which assume a *single-plane* radiation pattern, the **3D-AA model** extends the representation into three-dimensional space, enabling precise modeling of **beamforming, polarization effects, and direction-dependent filtering**.

Each antenna element is characterized by its **radiation pattern**, which defines how signals are transmitted and received at different angles. The model supports *arbitrary antenna array geometries*, allowing flexibility in *base station and mobile terminal*

antenna configurations. Furthermore, by incorporating *Effective Aperture Density Functions (EADF)*, the model efficiently captures **polarization-dependent signal variations**, ensuring that the impact of different polarization states on the received signal is accurately represented.

This 3D spatial modeling approach is particularly beneficial in **Massive MIMO (Multiple Input Multiple Output) systems**, where a large number of antennas operate simultaneously to enhance signal quality and system capacity. By incorporating *angular domain characteristics*, the WINNER II model provides a realistic representation of spatial correlation and angular spread effects, making it a suitable choice for evaluating advanced **beamforming and spatial diversity techniques**.

3.2.2.3 Computation of the Channel Matrix

Once the **network layout** and **antenna configurations** are established, the next step is the computation of the **MIMO channel matrix**. This process determines the **wireless channel response** and provides insights into signal propagation characteristics over time and space.

The first step in channel computation is **path loss estimation**, which quantifies the *attenuation of signal power* as it propagates through the medium. The **WINNER II model** includes a range of path loss models suited for different scenarios, taking into account *carrier frequency, antenna heights, environmental conditions, and separation distances*. These factors help in obtaining an accurate representation of received signal strength.

Following path loss estimation, the model proceeds with **multipath clustering**, which accounts for the presence of *multiple propagation paths* due to reflections, diffractions, and scatterers in the environment. Instead of treating each multipath

component separately, the WINNER II model groups them into **clusters**, where each cluster shares similar *delays, angles of arrival (AoA), and angles of departure (AoD)*. This clustering approach significantly improves computational efficiency while maintaining the realism of the modeled channel.

Once the **multipath components** have been established, the **channel impulse response (CIR)** is computed, encapsulating all relevant propagation effects. The CIR is stored in a *multidimensional channel matrix* H , which serves as the final output of the channel generation process. The structure of the **channel matrix** can be represented as:

$$H(U, S, N, T, K) \tag{3.1}$$

where:

- U represents the number of **receiver antenna elements**.
- S represents the number of **transmitter antenna elements**.
- N denotes the **number of multipath components**.
- T corresponds to the **number of time samples**.
- K accounts for the **number of active links**.

Each element in H is a **complex-valued coefficient** that represents the gain and phase shift applied to a signal traveling between a specific pair of transmit and receive antennas over a particular multipath component at a given time step.

By leveraging this structured **MIMO channel representation**, the WINNER II model provides a solid foundation for evaluating **wireless communication tech-**

nologies, supporting the analysis of **beamforming, spatial diversity, and interference mitigation techniques** in modern networks.

3.2.2.4 Interpretation of the Channel Data

The computed **Channel Impulse Response (CIR)** provides a comprehensive representation of the propagation effects in the wireless channel. Each element in the channel matrix H is a complex-valued coefficient that captures both the magnitude and phase variations introduced by multipath propagation. The formulation of H is governed by the superposition of **multiple propagation paths**, where each path contributes a delayed and phase-shifted version of the transmitted signal.

The general equation for computing the **MIMO channel matrix** H in the WINNER II model, based on your MATLAB implementation, is given by:

$$H(u, s, t, f, k) = \sum_{p=1}^{M_p} \alpha_p(u, s, t) e^{-2\pi j \tau_p f} \quad (3.2)$$

where: - $H(u, s, t, f, k)$ represents the channel coefficient between the u -th receiver antenna and the s -th transmitter antenna at time index t , frequency index f , and for link k . - M_p is the number of multipath components. - $\alpha_p(u, s, t)$ represents the complex channel coefficients for the p -th multipath component. - τ_p represents the delay associated with each propagation path. - f is the frequency over which the response is computed. - The exponential term accounts for **phase shifts** due to path delays.

From this equation, several key parameters can be extracted, each providing valuable insights into the channel behavior.

1. Delay Spreads: The delay spread represents the time dispersion introduced by multipath propagation. Since signals travel different distances due to reflections and scattering, each multipath component arrives at a different time τ_p . The channel coefficients α_p are weighted by an exponential phase term $e^{-2\pi j\tau_p f}$, capturing the time-domain shifts caused by these delays. A larger delay spread can lead to **Inter-Symbol Interference (ISI)**, affecting system performance in wideband communications.

2. Angles of Arrival (AoA) and Angles of Departure (AoD): The spatial distribution of multipath components is defined by their AoA and AoD. These angles determine how the signal propagates through the environment and interacts with obstacles before reaching the receiver. The phase rotations in the CIR coefficients depend on these angles, influencing the coherence of the received signal. This spatial information is essential for techniques such as beamforming and spatial diversity.

3. Doppler Shifts: Since the CIR is computed for different time instances, it captures the impact of mobility on the signal. When either the transmitter, receiver, or surrounding objects move, the frequency of the received signal is shifted, a phenomenon known as Doppler shift. This shift alters the phase of each multipath component dynamically, affecting the coherence time of the channel. In the given equation, Doppler effects are inherently captured in the time-evolving channel coefficient variations.

4. Power Delay Profiles (PDP): The **Power Delay Profile (PDP)** represents the power distribution across different path delays. Given the formulation:

$$P(\tau) = \sum_p |\alpha_p|^2 \tag{3.3}$$

where α_p are the complex channel coefficients, the PDP is computed by summing the power of each multipath component. Since α_p contains both real and imaginary parts, the total power contribution of each path is extracted by taking the squared magnitude.

By analyzing these parameters, one can extract meaningful insights about channel characteristics such as fading severity, coherence bandwidth, and time dispersion, all of which directly influence system performance. These insights aid in designing effective communication techniques like adaptive equalization, diversity schemes, and interference mitigation strategies, ensuring robust wireless communication in diverse environments.

3.3 Simulation Setup And Data Generation

To ensure that the forthcoming heuristic algorithms are tested under practical and diverse operating conditions, a comprehensive simulation framework was developed using the WINNER II Matlab toolbox. This toolbox is particularly suitable for modeling user-centric cell-free massive MIMO (UC-CFmMIMO) networks due to its advanced capability to simulate realistic propagation effects over frequency-dependent channels. In this section, we elaborate on the simulation setup, environment modeling, parameter configurations, and the overall data generation pipeline used to obtain the rich channel information necessary for algorithm design and performance analysis.

3.3.1 Overview of the Simulation Environment

The simulated environment emulates a dense urban deployment scenario, a configuration aligned with next-generation wireless networks aimed at supporting high user

mobility and massive connectivity. Both access points (APs) and user equipment (UEs), representing vehicles or mobile users, are randomly placed in a two-dimensional coverage area of 1 km^2 , with fixed height placements in the vertical (Z) dimension. Specifically, APs are placed at $h_{\text{AP}} = 12.5 \text{ m}$, typically corresponding to rooftop or lamppost-mounted infrastructure, while UEs are situated at ground level with a height of $h_{\text{UE}} = 1.5 \text{ m}$, simulating vehicular or pedestrian-mounted receivers.

Figure 3.1 illustrates a 3D representation of the deployment, where APs are shown as circles, UEs as crosses, and direct links between an AP and all UEs are visualized for clarity. The figure highlights the fully connected nature of the cell-free architecture, where every AP serves every user, thereby increasing spatial diversity and coverage reliability.

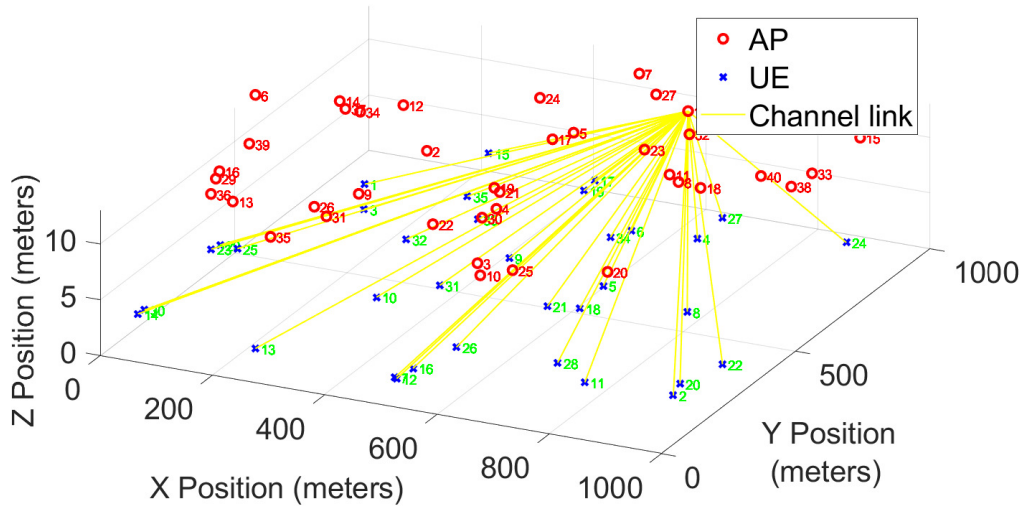


Figure 3.1: 3D system setup representation. APs are shown as circles, UEs as crosses, and links as straight lines. Only the links from one AP to all UEs are shown for visual clarity.

3.3.2 Deployment Configurations and Parameterization

Two main deployment configurations were evaluated, reflecting the trade-off between centralized processing and distributed antenna deployment:

- **Setup 1:** $L = 100$ APs, each equipped with $N = 4$ antennas (totaling 400 antenna elements).
- **Setup 2:** $L = 400$ APs, each with a single antenna ($N = 1$), enabling a highly distributed architecture with the same overall number of antennas.

Both configurations are consistent with the recommendations of UC-CFmMIMO deployments, where the total number of service antennas $L \times N$ is greater than the number of users $K = 40$. This over-provisioning ensures enhanced spatial degrees of freedom, enabling effective interference mitigation and beamforming in dense environments.

Table 3.1 provides a comprehensive summary of all key parameters used in the simulations, including antenna configurations, operating frequencies, channel resolution, and link dynamics.

Table 3.1: WINNER II Simulation Parameters

Parameter	Description	Value	Reference
f_c	Carrier frequency	5.9	[108]
B	System bandwidth	50	[140]
B_k	Subband bandwidth	180	[140]
S	Number of subbands	277	-
UCA	AP antenna type	Uniform Circular Array	[182]
ULA	UE antenna type	Uniform Linear Array	[188]
L	Number of APs	100 / 400	[135]
N	Antennas per AP	4 / 1	[147]
K	Number of UEs	40	[135]
N_{UE}	Antennas per UE	1	[135]
h_{AP}	AP height	12.5	[135]
h_{UE}	UE height	1.5	[135]
τ_p	Pilot sequence length	10	[135]
P_{max}	DL power per AP	200	[135]
V	UE average speed	2	[125]
Scenario	Propagation environment	Urban B1 (NLOS)	[130]

3.3.3 Channel Realization and Frequency-Domain Representation

The WINNER II toolbox was configured to produce wideband channel impulse responses over 277 frequency subbands, covering the range from 5.875 GHz to 5.925 GHz. Each subband comprises 12 subcarriers, consistent with 3GPP standards for subcarrier spacing. The simulation was conducted over 20 time samples to incorporate the effects of mobility and temporal variation.

At each time instant, a complete MIMO channel matrix $H(U, S, N, T, K)$ was generated, where:

- U and S denote the number of receive and transmit antennas,
- N is the number of multipath components,
- T is the number of time steps,
- K is the number of active links (AP-UE pairs).

The matrices were then transformed into the frequency domain via discrete Fourier transforms, yielding frequency-selective channel gains for each subband. These frequency-domain coefficients are later used as inputs to the proposed resource allocation algorithms.

Figure 3.2 presents an example of channel frequency responses for 10 AP-UE links. The distinct gain fluctuations across subbands demonstrate the highly selective nature of the wireless channel, reinforcing the need for intelligent and adaptive resource allocation strategies.

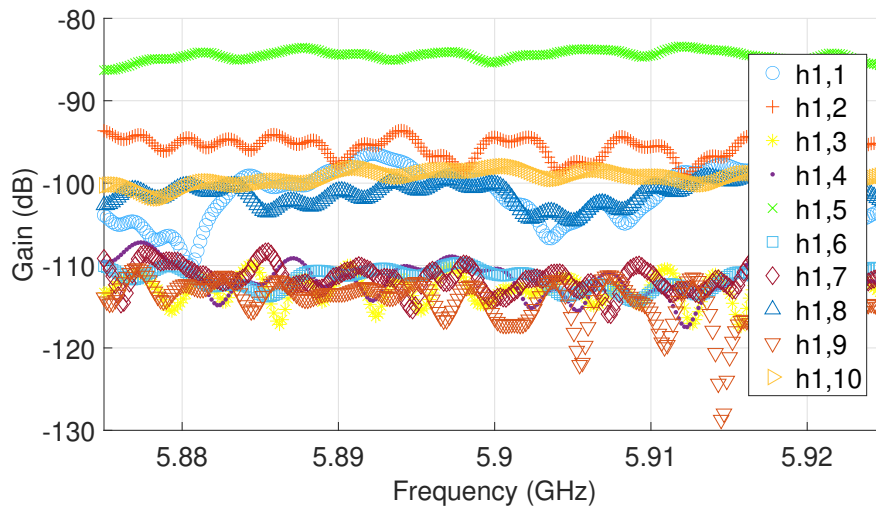


Figure 3.2: Simulated channel gains across frequency for 10 AP-UE links.

3.3.4 Mobility and Doppler Considerations

To model practical dynamics in urban scenarios, the simulation incorporated moderate UE mobility with a mean velocity of 2 m/s. This movement induced Doppler shifts and time-varying fading in the channel, which were reflected in the time-evolving channel coefficients. These temporal variations are important for validating the robustness and adaptability of the proposed heuristic solutions in realistic conditions.

3.4 Proposed Resource Allocation Algorithms

With the frequency-selective, high-fidelity channel matrices generated via the WINNER II simulation framework (as described in Section 3.3), we now turn our attention to the problem of frequency resource allocation. The objective is to efficiently assign users to subbands such that interference is minimized, fairness is preserved, and the spectral resources are utilized as effectively as possible under realistic propagation and mobility conditions.

This section introduces two heuristic resource allocation strategies tailored for user-centric cell-free massive MIMO (UC-CFmMIMO) networks. These algorithms leverage the rich spatial and frequency diversity present in the simulated environment to allocate subbands in a way that accommodates multiple users per subband, all while ensuring a guaranteed minimum spectral efficiency (SE) per user. Their design is motivated by the need to balance computational scalability with system performance, especially in dense, distributed deployments.

The two primary methods, Condition Number (CN)-based and Channel Correlation (CC)-based allocation, are adapted from prior work on cellular and multiuser massive MIMO systems [152, 20]. However, they are significantly restructured to operate efficiently in the cell-free, user-centric paradigm. Both methods are benchmarked against a simpler Best Subband First (BFS) baseline algorithm that prioritizes channel gain but allows only one user per subband.

Each approach is described in detail in the following subsections, including algorithmic rationale, mathematical modeling, and complexity considerations.

3.4.1 Condition Number (CN)-Based Algorithm

The CN-based heuristic exploits the condition number of the equivalent channel matrix as a proxy for system stability and spatial separability. The condition number $\kappa(\cdot)$ reflects the sensitivity of matrix inversion and signal estimation accuracy. In the context of MIMO systems, a lower condition number indicates better orthogonality among user channels, and thus more reliable detection and decoding.

The algorithm operates iteratively. At each step, a user is considered for allocation to the subband where its presence maintains or minimizes the condition number of the resulting multi-user channel matrix. If no subband satisfies this condition while

guaranteeing the minimum SE requirement η_{\min} , the user is assigned to the subband that yields the lowest degradation in terms of condition number. The mathematical formulation of the condition number used for evaluating a user k on subband s is given by:

$$\kappa(\mathbf{H}_{k,s}) = \|\mathbf{H}_{k,s}\| \cdot \|\mathbf{H}_{k,s}^{-1}\| \quad (3.4)$$

where $\mathbf{H}_{k,s}$ is the aggregated channel matrix of user k and the users already allocated to subband s . This evaluation is performed using the weighted channel vectors after applying the large-scale fading diagonal matrix \mathbf{D}_k .

While computationally more demanding due to matrix inversions, the CN-based algorithm ensures superior conditioning of the system matrix, which is especially beneficial in high-density deployments.

3.4.2 Channel Correlation (CC)-Based Algorithm

The CC-based heuristic emphasizes the spatial orthogonality among users sharing the same subband. Rather than computing full matrix condition numbers, this approach measures pairwise channel correlations to determine user compatibility. A new user is accepted into a subband if its channel vector is sufficiently uncorrelated with those already occupying the subband and if the minimum SE threshold is met.

The pairwise correlation between two users' channel vectors is quantified by:

$$\rho(\mathbf{h}_{k,s}, \mathbf{h}'_{k,s}) = \frac{|\langle \mathbf{h}_{k,s}, \mathbf{h}'_{k,s} \rangle|}{\|\mathbf{h}_{k,s}\| \cdot \|\mathbf{h}'_{k,s}\|} \quad (3.5)$$

A user is only accepted if $\rho \leq \beta_{\min}$, where β_{\min} is a predefined threshold, possibly updated dynamically to reflect system load. Compared to the CN method, the CC approach avoids costly matrix operations and offers a lower-complexity alternative suitable for large-scale dynamic networks.

3.4.3 Baseline: Best Subband First (BFS) Algorithm

To provide a comparative benchmark, a simplified BFS algorithm is also implemented. This method allocates subbands in a greedy fashion, assigning each user to its strongest available subband based on the norm of its channel gain. Importantly, only one user is allowed per subband, which eliminates intra-subband interference but results in underutilized spectral resources when the number of users is much smaller than the number of available subbands.

While BFS guarantees straightforward implementation and interference-free transmission, its lack of multiplexing across users makes it suboptimal in high-density scenarios or environments with stringent spectral efficiency requirements.

3.4.4 Shared Algorithmic Structure

Both CN and CC heuristics follow a shared allocation framework, which consists of:

1. Initializing user priorities based on differences in channel gain across subbands.
2. Iteratively assigning users to subbands, prioritizing low interference and sufficient SE.
3. Ensuring a minimum SE requirement $\eta_{\min} = 3.3$ bps/Hz, as recommended for vehicular communications [50].

The pseudocode for the combined CN/CC allocation strategy is summarized in Algorithm 3.1. The selection criteria within the loop differ depending on the algorithm used.

3.4.5 Computational Complexity Analysis

Understanding the computational demands of the proposed heuristics is crucial for evaluating their scalability in practical deployment scenarios with strict timing requirements. The CN-based algorithm involves matrix operations, particularly condition number evaluations, which require matrix inversion and norm computation. Consequently, its computational complexity is approximately $\mathcal{O}(KSN^3)$, where K is the number of users, S the number of subbands, and N the number of antennas per AP.

In contrast, the CC-based method bypasses matrix inversions by relying on pairwise inner products for correlation checks. Its complexity is therefore reduced to $\mathcal{O}(KS(K + N))$, offering a scalable solution even in large networks.

Both algorithms share a common initialization overhead of $\mathcal{O}(SKN)$ for building channel gain matrices and a sorting cost of $\mathcal{O}(K \log K)$ to determine allocation priorities. However, the runtime difference becomes significant as antenna counts increase, favoring the CC-based method for applications with strict timing constraints and limited computational budgets.

Table 3.2: *Complexity Comparison of Resource Allocation Algorithms*

Algorithm	Complexity
CN-Based Heuristic	$\mathcal{O}(KSN^3)$
CC-Based Heuristic	$\mathcal{O}(KS(K + N))$
BFS Baseline	$\mathcal{O}(K \log K + SK)$

Algorithm 3.1: Resource Allocation Algorithms: CN and CC

```

1: Input:  $L, N, K, S, \mathbf{D}_k, \mathcal{C}_k, \mathbf{h}_{k,s}, k = 1, \dots, K, s = 1, \dots, S$ 
2: Output: Assignment set  $\mathcal{A}_s, s = 1, \dots, S$ 
3: Initialize:
4:    $\eta_{\min} = 3.3$ ; // Minimum SE for vehicular communication
5:    $\eta_{\text{temp}} = 0$ ; // Temporary SE
6:    $\mathcal{A}_s = \emptyset, \mathcal{A}_s^{\text{temp}} = \emptyset$ ; // Resource matrices
7:    $\mathbf{G}(s, k) = \|\mathbf{h}_{k,s} \mathbf{D}_k\|$ ; //  $\mathbf{G}$ : Channel gain matrix
8:    $\alpha = 0$ ; // Flag to track if a UE is assigned to a free subband
9:    $\beta_{\min} = \text{initial value}$ ; // Initialize orthogonality threshold for CC
10:   $\gamma = 0$ ; // Initial correlation threshold
11:  Define  $\eta_{\text{fct}}$  as a function that computes the temporary SE for users in set  $\mathcal{A}_s^{\text{temp}}$ ;
12: Compute user priorities:
13: for  $k = 1 : K$  do
14:    $g_k^{\max} = \max_{s \in S} \mathbf{G}(s, k)$ ;
15:    $g_k^{\text{second}} = \max_{s \in S, \mathbf{G}(s, k) \neq g_k^{\max}} \mathbf{G}(s, k)$ ;
16:    $d_k = g_k^{\max} - g_k^{\text{second}}$ ;
17: Sort  $\mathbf{d}$  in descending order;  $k_d$  is the sorted UE indices.
18: Shared Iterative Allocation:
19: while  $k_d \neq \emptyset$  do
20:   for  $k = k_d$  do
21:     Sort  $\mathbf{G}(:, k)$  in descending order;  $\mathbf{S}_g$  is the sorted subband indices.
22:     for  $s = \mathbf{S}_g$  do
23:        $\mathcal{C}_{k,s} = \mathcal{A}_s \cap \mathcal{C}_k$ 
24:       if  $\mathcal{C}_{k,s} = \emptyset$  then
25:         Assign  $k$  to subband  $s$ :  $\mathcal{A}_s = \mathcal{A}_s \cup \{k\}$ ;
26:          $\alpha = 1$ ; // A free subband was found
27:         break
28:       else
29:          $\mathcal{A}_s^{\text{temp}} = \mathcal{A}_s^{\text{temp}} \cup \{k\}$ ;
30:         Compute  $\eta_{\text{temp}} = \eta_{\text{fct}}(\mathcal{A}_s^{\text{temp}})$ ;
31:         CN Criterion (if algorithm is CN):
32:         if  $\eta_{\text{temp}} \geq \eta_{\min}$  then
33:            $\mathbf{H}^{\text{test}} = [\mathbf{h}_{k,s}; \mathbf{h}_{i,s}, i \in \mathcal{C}_{k,s}]$ ;
34:            $\kappa_s^{\text{test}} = \text{cond}(\mathbf{H}^{\text{test}} \mathbf{D}_k \mathbf{H}^{\text{test}H})$ ;
35:         else
36:            $\kappa_s^{\text{test}} = \infty$ ;
37:         break
38:         CC Criterion (if algorithm is CC):
39:         if  $\eta_{\text{temp}} \geq \eta_{\min}$  and orthogonality of  $k$  with all UEs  $i \in \mathcal{C}_{k,s}$  is verified, i.e.,  $\frac{|\mathbf{h}_{i,s} \mathbf{D}_k^H \mathbf{h}_{k,s}|}{\|\mathbf{h}_{i,s} \mathbf{D}_k\| \|\mathbf{h}_{k,s} \mathbf{D}_k\|} < \beta_{\min}$ 
40:           then
41:             Assign  $k$  to subband  $s$ :  $\mathcal{A}_s = \mathcal{A}_s \cup \{k\}$ ;
42:             break
43:         Remove allocated UEs from  $k_d$ 
44:         if  $\alpha = 0$  then // If no free subband was found, apply CN criterion
45:           Select subband:  $s^* = \arg \min_s \kappa_s^{\text{test}}$ ;
46:           Assign  $k$  to subband  $s$ :  $\mathcal{A}_{s^*} \leftarrow \mathcal{A}_{s^*} \cup \{k\}$ ;
47:         else
48:           Set  $\alpha \leftarrow 0$ ; // Reset flag for next UE
49:         if Algorithm is CC then
50:           Update the orthogonality threshold:  $\beta_{\min} = \beta_{\min} + \Delta \beta_{\min}$ ;

```

In summary, while the CN-based method offers robust allocation with strong stability guarantees, it is computationally heavier than the CC-based approach. The BFS algorithm, though computationally light, is limited in its applicability due to its restrictive allocation model. Together, these methods offer a spectrum of trade-offs between complexity, interference mitigation, and spectral efficiency, providing a versatile toolkit for CF mMIMO frequency resource allocation.

3.5 Numerical Results

This section presents a comprehensive performance evaluation of the proposed resource allocation strategies in user-centric cell-free massive MIMO (UC-CFmMIMO) systems. Building on the realistic simulation environment detailed in Section 3.3, and the algorithms introduced in Section 3.4, we now assess how the CN-based and CC-based methods perform under varying deployment and network configurations. The analysis covers key performance indicators including spectral efficiency (SE), user packing efficiency (UPE), subband utilization, and system scalability, with comparisons against the BFS baseline algorithm.

Impact of Correlation Threshold in CC Algorithm

We begin by analyzing how the channel correlation threshold β_{\min} influences the performance of the CC-based algorithm. Figure 3.3 presents the average data rate per AP as a function of β_{\min} , evaluated under two configurations: (i) $L = 100, N = 4$ and (ii) $L = 400, N = 1$. Initially, as β_{\min} increases from 0 to approximately 0.3, the average data rate remains relatively high, indicating that strict orthogonality conditions are effective in limiting interference. However, beyond $\beta_{\min} \approx 0.4$, a sharp decline

is observed. This reflects a degradation in signal quality due to relaxed correlation constraints that permit more users with interfering channels to share subbands.

Interestingly, as $\beta_{\min} \rightarrow 0.5$, the data rate curve stabilizes, indicating that the system approaches full user allocation. This behavior highlights a trade-off in the CC strategy: lower β_{\min} enforces stricter orthogonality at the cost of excluding some users, while higher values improve allocation but introduce interference.

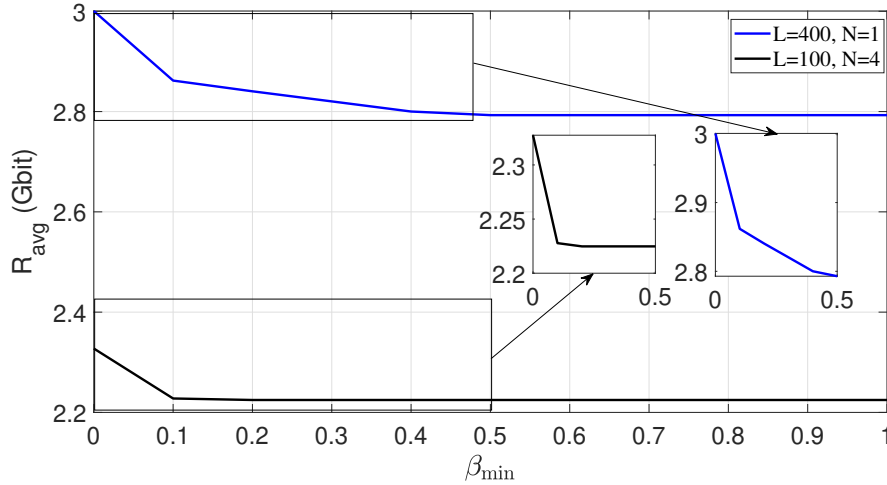


Figure 3.3: Comparison of average data rates as a function of varying β_{\min} using the CC algorithm for $L = 100, N = 4$ and $L = 400, N = 1$.

Subband Resource Utilization and User Packing Efficiency

Next, we evaluate the capacity of each algorithm to efficiently utilize subbands. Figure 3.4 illustrates the user packing efficiency (UPE) and the percentage of successfully allocated users as the number of subbands S varies from 15 to 80. These results are obtained with a fixed $\beta_{\min} = 0.4$ under the deployment $L = 400, N = 1$.

Both CN and CC algorithms demonstrate strong performance in limited-spectrum scenarios, achieving $\text{UPE} > 1$ and maintaining near-100% user allocation across all values of S . This reflects their ability to multiplex multiple users on a single subband without exceeding interference or stability constraints. In contrast, the BFS strategy

fails to scale under resource constraints; only 38% of users are allocated when $S = 15$, and the UPE remains close to 1 due to its one-user-per-subband restriction.

As the number of subbands increases, the UPE naturally decreases for all methods due to reduced contention, yet CN and CC continue to outperform BFS in both allocation success and spectrum efficiency.

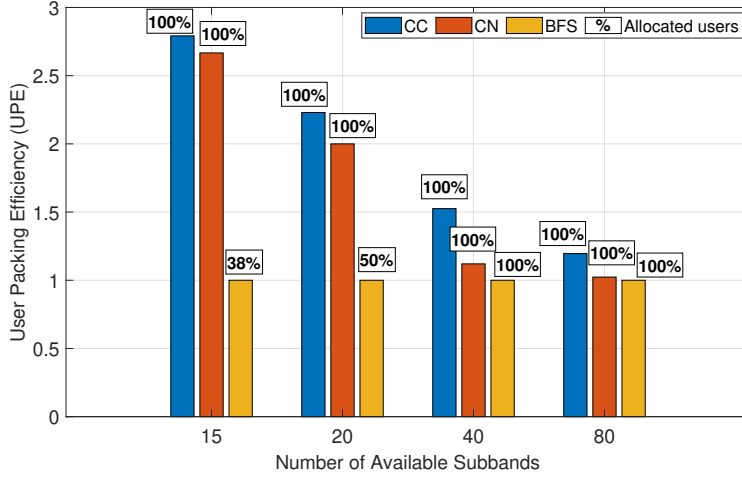


Figure 3.4: UPE and allocation success under subband variation for the setup $L = 400, N = 1$.

Subband Availability Analysis via KDE

To further understand how system parameters affect subband usage, we examine the distribution of free subbands using kernel density estimation (KDE). This provides insights into how efficiently each algorithm spreads users over the available spectrum.

Figure 3.5 shows the free subband distribution for the CC algorithm under two deployment setups, with $\beta_{\min} = 0.4$. The scenario with higher AP density exhibits a wider spread and a right-shifted peak, suggesting that more subbands remain unused due to enhanced spatial resolution and better user separation. Conversely, the lower-AP setup yields a sharper, narrower peak, indicating denser subband usage and limited flexibility.

For the CN-based algorithm (Figure 3.6), the differences between setups are less favorable. Despite having fewer APs with more antennas per AP ($N = 4$), the spatial correlation between antenna elements reduces diversity, limiting subband reuse and stability. These KDE insights reinforce the idea that AP densification, rather than simply increasing antenna count, yields more favorable spectral behavior in CF mMIMO systems.

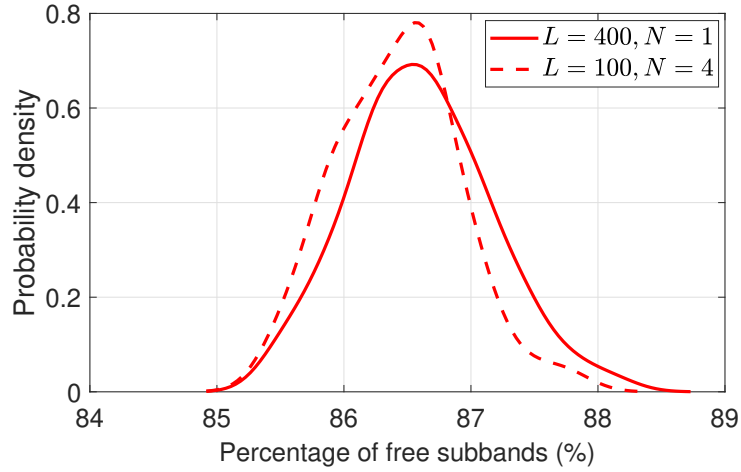


Figure 3.5: KDE of free subbands in the CC algorithm for two simulated scenarios with $\beta_{min} = 0.4$.

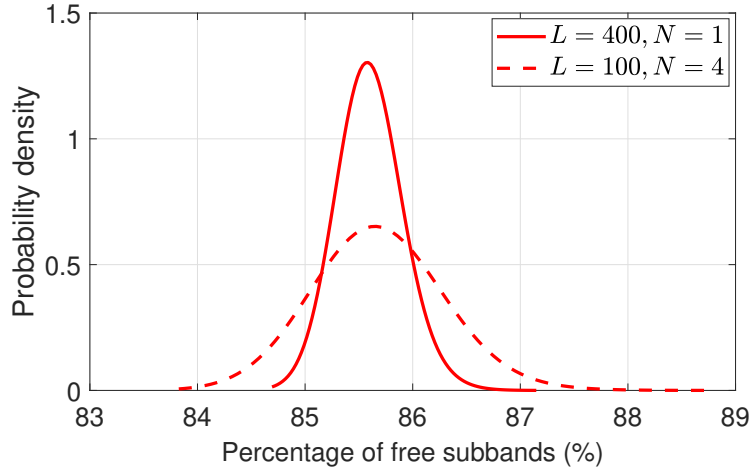


Figure 3.6: KDE of free subbands in the CN algorithm for the two deployment setups.

Spectral Efficiency Distribution under Allocation Strategies

Finally, we evaluate the system-level performance through cumulative distribution functions (CDFs) of the achieved SE, shown in Figures 3.7 and 3.8. In setup 1 ($L = 100, N = 4$), the CC algorithm delivers superior SE, particularly for $\beta_{\min} = 0.05$, which enforces strict orthogonality and thus minimizes intra-subband interference. The CN algorithm also performs well, offering stable and fair SE distribution, while BFS lags due to its limited allocation flexibility.

In setup 2 ($L = 400, N = 1$), the performance gap widens further. With more APs, the CC strategy benefits from finer user separation and denser coverage, leading to a higher proportion of users achieving strong SE values. These results underscore the scalability and robustness of the proposed algorithms, particularly in spectrum-constrained environments (only 20 subbands are available in this evaluation). The ability of both CC and CN to maintain high SE under such constraints highlights their practical utility for next-generation network deployments.

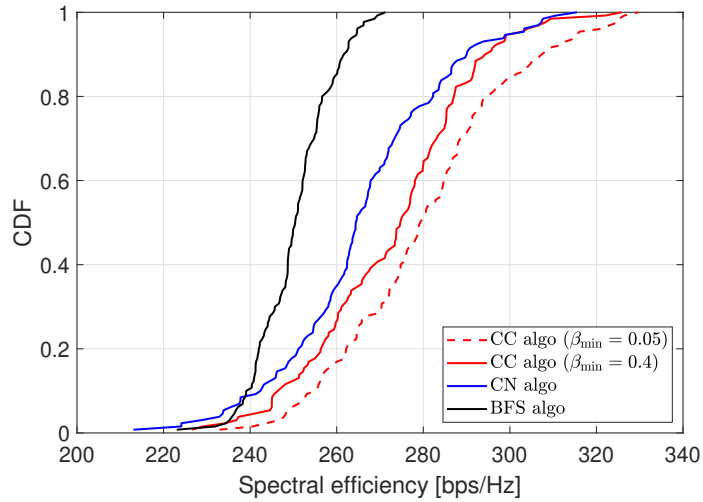


Figure 3.7: CDF of spectral efficiency in setup 1 ($L = 100, N = 4$) for $\beta_{\min} = 0.05$ and $\beta_{\min} = 0.4$.

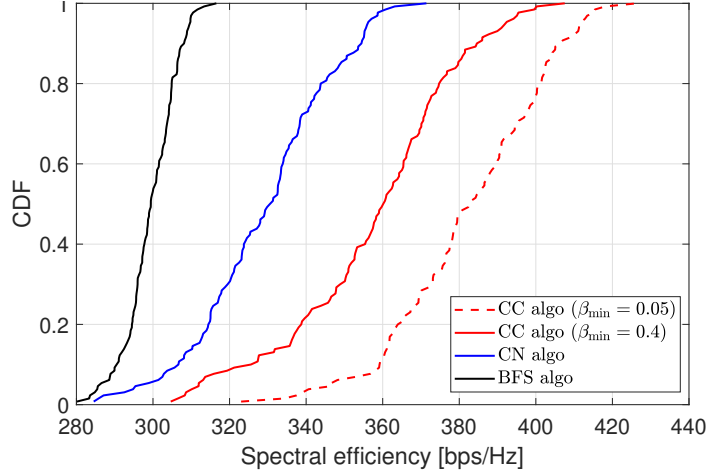


Figure 3.8: CDF of spectral efficiency in setup 2 ($L = 400, N = 1$) for $\beta_{\min} = 0.05$ and $\beta_{\min} = 0.4$.

Summary of Observations

The results demonstrate the effectiveness of the proposed heuristic algorithms in improving resource allocation in CF mMIMO systems. Key findings include:

- The CC algorithm offers significant flexibility through its tunable β_{\min} , allowing trade-offs between interference and user allocation.
- Both CC and CN strategies outperform BFS in user allocation success, subband reuse, and SE, particularly under constrained spectrum.
- AP densification (increased L) is more beneficial than simply increasing antennas per AP (increased N) for subband utilization and diversity gains.

These insights confirm the suitability of heuristic allocation strategies in scalable, interference-sensitive UC-CFmMIMO deployments.

3.6 Conclusion and Future Scope of Work

This chapter presented a comprehensive exploration of heuristic-based frequency resource allocation strategies for user-centric cell-free massive MIMO (UC-CFmMIMO) systems. The work was motivated by the practical need for scalable and low-complexity algorithms capable of operating effectively under realistic channel conditions, especially in dense and dynamic environments such as urban vehicular networks.

To establish a rigorous testing framework, we employed the WINNER II channel model, which accurately captures the spatial and frequency-selective characteristics of real-world propagation environments. The channel data generated using this model formed the foundation for evaluating the proposed algorithms across different configurations, including varying access point densities, antenna deployments, and available subband resources.

Two novel heuristic algorithms were introduced, one based on minimizing the condition number of aggregated channel matrices, and the other on enforcing spatial orthogonality between users sharing a subband. Both approaches were carefully adapted to suit the decentralized and interference-sensitive nature of CF mMIMO systems. A third, simpler benchmark algorithm (BFS) was also implemented to provide a baseline comparison.

Simulation results demonstrated the significant advantages of the proposed methods over the BFS baseline. The CN and CC algorithms were capable of maintaining high spectral efficiency even under limited subband availability and dense user scenarios. Particularly, the CC algorithm exhibited flexible behavior through its tunable correlation threshold, allowing it to balance between strict interference control and inclusive user allocation. Moreover, results showed that increasing the number of distributed

APs was more effective for enhancing performance than increasing the number of antennas per AP, due to the benefits of finer spatial resolution and improved diversity.

Overall, the chapter validates the effectiveness of condition-aware and correlation-sensitive heuristics in addressing the spectrum allocation challenges inherent to CF mMIMO architectures. These algorithms enable improved spectrum reuse, fairer user scheduling, and greater system robustness, all while maintaining manageable computational complexity.

Looking ahead, several extensions can be pursued to enhance this framework further. One promising direction involves the integration of learning-based methods, such as reinforcement learning or neural network models, to dynamically adapt allocation strategies to changing network conditions. Additionally, joint optimization of frequency allocation with power control and user scheduling would allow for more holistic resource management. Future studies could also investigate the incorporation of NOMA techniques, as well as consider delay-sensitive metrics to support latency-critical applications. Finally, evaluating the performance of these heuristics under hardware impairments and imperfect CSI scenarios would bring the analysis closer to real-world deployment conditions.

This chapter lays the groundwork for robust and scalable frequency allocation in cell-free networks and opens the path for more intelligent, adaptive, and cross-layer solutions in the next generation of wireless systems.

METAHEURISTIC SOLUTIONS FOR FREQUENCY RESOURCE
ALLOCATION IN UC CF MASSIVE MIMO

Publication Note

This chapter is based on the following peer-reviewed publication, accepted for presentation at the *IEEE Vehicular Networking Conference (VNC)*, and presented in June 2025 in Porto, Portugal [41].

4.1 Introduction

Metaheuristic algorithms have emerged as powerful tools for solving complex optimization problems across various scientific and engineering domains. These algorithms, inspired by natural phenomena such as biological evolution, thermodynamics, and collective intelligence, provide practical solutions to problems where traditional exact methods become intractable. Their strength lies in balancing global exploration with local exploitation, allowing them to escape local optima and converge toward high-quality solutions even in large, non-convex, or multi-objective landscapes.

Prominent examples include Genetic Algorithms (GA), Simulated Annealing (SA), and Ant Colony Optimization (ACO), each modeling a different process from nature. Unlike gradient-based methods, metaheuristics do not require differentiable or continuous functions and are inherently flexible, making them highly suitable for real-world problems that involve constraints, randomness, and non-linearity. Over

the years, these methods have been successfully applied in fields such as logistics, robotics, energy systems, and biomedical engineering.

In wireless communications, the growing complexity of network architectures, driven by the transition to 5G and 6G systems, has led to increased interest in metaheuristics. These networks demand dynamic and intelligent resource management strategies to handle diverse and evolving conditions such as user mobility, interference, energy constraints, and heterogeneous service requirements. Metaheuristic algorithms offer a compelling alternative to classical optimization approaches, enabling adaptive solutions for tasks like power control, user scheduling, beamforming, and frequency allocation.

As we move toward an increasingly connected world, technological advancements in wireless communications are crucial. While 5G networks are still expanding, attention is shifting to sixth-generation (6G) systems, which are expected to deliver improvements in data capacity, speed, reliability, and low-latency communication. 6G networks aim to meet the growing demands of future applications requiring unprecedented network performance [76].

One promising technology driving this evolution is cell-free massive Multiple-Input Multiple-Output (CFmMIMO). CFmMIMO revolutionizes traditional network architectures by deploying spatially distributed transmitters that cooperatively serve users, effectively removing fixed cell boundaries. This innovative "cell-less" approach integrates the advantages of Distributed Antenna Systems (DAS) and MIMO technology, ensuring seamless communication even in scenarios where conventional fixed cells fall short.

Vehicular networks represent a particularly compelling application for CFmMIMO due to their need for continuous and reliable communication in support of Intelligent

Transportation Systems (ITS). CFmMIMO has the potential to deliver uninterrupted coverage, low latency, and robust connectivity as vehicles move through different network zones, making it an ideal solution for high-performance, safety-critical applications such as autonomous driving and vehicle-to-everything (V2X) communications.

However, despite its potential, CFmMIMO faces significant challenges, particularly in dynamic environments such as vehicular networks. These challenges include issues related to scalability, computational complexity, energy efficiency, and resource allocation [62], which are further complicated by the Doppler effect caused by high-speed movement [14]. Various studies have explored resource allocation strategies, which can be categorized based on the type of resource being optimized, such as power and frequency allocation.

Power allocation and hybrid beamforming are among the key strategies for optimizing resources in cell-free networks. [92] proposed a joint approach for CFmMIMO, demonstrating significant sum-rate improvements using statistical channel state information (CSI) in resource-limited settings. Additionally, [59] focuses on optimizing power allocation to minimize inter-user interference using user-centric (UC) clustering approaches.

Research on frequency resource allocation has explored various approaches to enhance spectrum utilization in CF-mMIMO networks. For instance, [96] proposed opportunistic access point selection, assigning unique orthogonal subcarriers to individual users to eliminate interference and boost efficiency, though this approach may underutilize resources in dense scenarios. Similarly, [99] investigated subcarrier-based precoding to improve reliability. Other studies have examined hybrid energy CF-mMIMO systems [49] and scalable backhaul optimization [168]. However, none of these works address the complexities of dense vehicular scenarios and the dynamic challenges inherent to such environments.

To address these gaps, our work introduces a UC-CFmMIMO multi-user allocation within shared subbands approach, enabling more efficient spectrum utilization by allowing multiple users to share the same subband while adhering to Quality of Service (QoS) constraints and managing dynamic user mobility. We formulate a joint multi-objective optimization framework that maximizes SE, ensures fairness, and minimizes interference, employing advanced tools like SUMO (Simulation of Urban MObility) [107], an open-source traffic simulator that leverages real traffic data to simulate vehicle movement in urban environments, and WINNER II [38] for channel characterization.

The main contributions of this work can be summarized as follows:

- We introduce a novel UC-CFmMIMO architecture that integrates frequency-selective channel modeling and bandwidth sharing strategies, specifically tailored for high-mobility vehicular networks. This design ensures a more adaptive spectrum allocation at the physical layer, enabling multiple users to efficiently share the same subband while meeting QoS constraints.
- To accurately model the dynamics of vehicular networks, we deploy urban mobility simulations using SUMO, leveraging real traffic data, and integrate channel characterization through MATLAB’s WINNER II module, which incorporates empirical measurements for realistic evaluations.
- We formulate a multi-objective optimization problem aimed at maximizing spectral efficiency (SE), ensuring fairness, and minimizing interference, providing enhanced resource utilization and improved user experience in dynamic network environments.
- To solve the optimization problem, we deploy a Simulated Annealing (SA) algorithm, chosen for its robustness in handling complex multi-objective problems.

Its performance is compared against Genetic Algorithm (GA) and Ant Colony Optimization (ACO), demonstrating significant gains in SE and a 40% reduction in frequency resource usage.

4.2 Channel Model

The channel model adopted in this chapter builds upon the system framework established in Chapter 2, where a user-centric cell-free massive MIMO (UC-CFmMIMO) architecture was defined. The primary structure of the system, comprising distributed access points (APs) connected to a central processing unit (CPU), user clustering, and coordinated downlink transmission, remains consistent with the previous modeling assumptions. However, unlike Chapter 2, which employed static or semi-dynamic channel realizations generated exclusively using the WINNER II channel model, the present work extends the realism and fidelity of the channel representation by incorporating a dynamic vehicular mobility layer. This is achieved through the integration of the Simulation of Urban Mobility (SUMO) platform, which introduces time-varying user positions and velocities based on realistic traffic patterns.

In Chapter 2, the WINNER II model served as a robust framework for capturing spatially correlated channel characteristics under different propagation scenarios such as urban macro (UMa), urban micro (UMi), and indoor environments. Although it offered accurate modeling of large-scale fading (path loss and shadowing) and small-scale fading (multi-path components), it lacked a temporal dimension that accounts for fast-changing topologies typical of vehicular networks. This limitation becomes particularly critical in the context of high-mobility environments, where vehicle speeds, intersections, traffic signals, and network topology dynamically impact the quality and stability of wireless links. Therefore, while the fundamental physi-

cal layer assumptions, including antenna configurations, carrier frequency, and power budgets, remain aligned with those presented earlier, the significant novelty in this chapter lies in the dynamic modeling of user mobility, which is seamlessly integrated with the wireless channel environment through SUMO.

To simulate vehicular movement and interaction with the network, SUMO provides a scalable and customizable framework capable of replicating real-world urban traffic patterns. In this work, we utilize actual map data imported from OpenStreetMap (OSM) to generate urban scenarios with multiple lanes, intersections, traffic lights, and routing logic. Each vehicle in the SUMO simulation is mapped to a user terminal (UT) in the CFmMIMO network, and its spatial trajectory over time is used to dynamically update the user’s location, speed, and acceleration. These variables directly influence the Doppler shifts and time-varying channel conditions experienced by each UT.

The channel coefficients between each access point and user terminal are updated periodically based on the mobility traces provided by SUMO. These updates occur over discrete time slots, with each time slot representing a coherent interval during which the channel can be considered quasi-static. For every such interval, the WINNER II model is invoked using the updated user and AP positions to regenerate the channel impulse responses. This hybrid modeling approach combines the spatial richness of WINNER II with the temporal granularity of SUMO, thereby capturing both the geometry-based and mobility-induced dynamics of the channel.

Formally, for a given AP m and UT k , the time-varying channel response $h_{mk}(t)$ can be described as a function of the relative distance $d_{mk}(t)$, line-of-sight (LoS) conditions, and Doppler spread:

$$h_{mk}(t) = \sqrt{\beta_{mk}(t)} \cdot g_{mk}(t) \tag{4.1}$$

Here, $\beta_{mk}(t)$ denotes the large-scale fading component, which includes distance-dependent path loss and log-normal shadowing, while $g_{mk}(t)$ represents the small-scale fading, modeled using a tapped-delay line structure with parameters derived from WINNER II. The time index t corresponds to the vehicular trajectory snapshots extracted from SUMO.

The Doppler shift for each user is dynamically calculated based on their instantaneous velocity vector $\vec{v}_k(t)$ and the angle of arrival (AoA) $\theta_{mk}(t)$, resulting in the Doppler frequency

$$f_{D,k}(t) = \frac{v_k(t)}{\lambda} \cos(\theta_{mk}(t)), \quad (4.2)$$

where λ is the carrier wavelength. This allows us to simulate realistic coherence times and the impact of fast fading on frequency allocation strategies, which is particularly relevant for the proposed multi-user subband sharing approach discussed in Section 2.4.

An important consideration in this model is the dynamic clustering of APs around each user, as prescribed by the UC-CFmMIMO paradigm. Unlike static cell-based architectures, the set of APs serving each user evolves over time as the user moves through the network. At each time instance, the system dynamically selects a subset of geographically proximate APs based on signal quality thresholds, load balancing constraints, and resource availability. This clustering mechanism is recomputed periodically in accordance with the updated location data from SUMO, ensuring that users maintain high signal-to-noise-plus-interference ratios (SINR) and continuous connectivity.

To manage computational complexity, we adopt a time discretization scheme in which the mobility and channel updates are performed at fixed intervals (e.g., every 100 ms), corresponding to realistic vehicular speeds and channel coherence times. Within each

interval, all channel computations are based on the latest available mobility state, which includes position, heading, and velocity. Moreover, since the frequency-selective nature of the channel is critical in resource allocation, we employ an orthogonal frequency-division multiple access (OFDMA) framework with a predefined number of subcarriers. For each subcarrier, independent yet correlated channel realizations are generated, taking into account the frequency correlation bandwidth derived from the WINNER II profiles.

To summarize, the proposed channel model incorporates several layers of realism that go beyond conventional static or geometry-based models. It maintains compatibility with the established CFmMIMO architecture of Chapter 2, while introducing novel temporal dynamics via the integration of SUMO-based mobility. This hybrid modeling approach is particularly well-suited for evaluating frequency resource allocation strategies under highly dynamic conditions, such as those encountered in intelligent transportation systems and vehicular networks. By synchronizing mobility data with channel generation, we achieve a time-evolving, spatially-aware, and frequency-resolved channel environment that supports the development and assessment of advanced metaheuristic optimization techniques explored in this chapter.

4.3 Simulation Setup And Data Generation

To evaluate the proposed frequency resource allocation framework within the UC-CFmMIMO architecture, we designed a simulation environment that integrates realistic vehicular mobility with dynamic channel modeling. This setup combines two key components: urban mobility data generated through SUMO and channel coefficients derived using the WINNER II channel model. The goal is to create a holistic, time-evolving testbed capable of capturing the complex interactions between user

mobility, spatial distribution of access points, and the frequency-dependent nature of the wireless medium.

The vehicular mobility simulation was conducted using the Simulation of Urban Mobility (SUMO), a microscopic traffic simulator widely used for Intelligent Transportation Systems (ITS) research. We defined an urban scenario inspired by the Manhattan grid layout, characterized by structured intersections, two-way streets, and variable traffic densities. The road topology was imported from OpenStreetMap (OSM) and refined to support high-mobility vehicle trajectories with realistic acceleration and deceleration behaviors. Figure 4.1 illustrates a top-down view of the Manhattan-style city map used in the SUMO simulations, showcasing the road network and vehicular traffic flow.



Figure 4.1: Manhattan city simulation scenario, SUMO view.

A total of four user terminals (UEs), representing connected vehicles, were initialized at different locations within the SUMO scenario. Their mobility traces were extracted over a predefined simulation duration, segmented into coherent time slots of 100 ms, consistent with realistic vehicular communication update intervals. As the vehicles moved through the simulated city, their positions, velocities, and headings were recorded and used as dynamic inputs to the channel generation process.

Figure 4.2 shows the trajectories of the four UEs, with filled circles indicating their initial positions and arrows representing direction and movement over time.

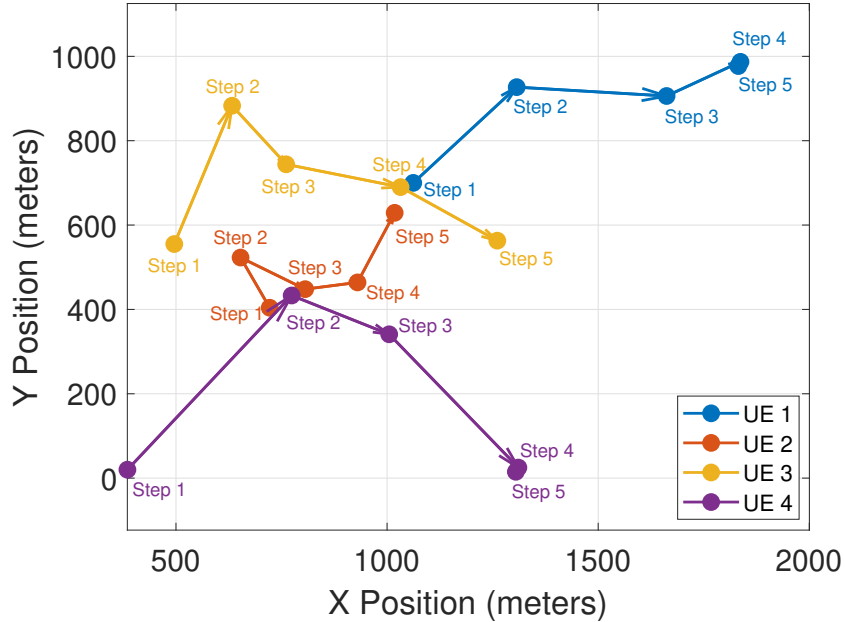


Figure 4.2: 4 UE positions and trajectories over mobility steps. The starting positions are indicated by filled circles, and arrows illustrate the direction of movement and the evolution of the vehicles' positions.

To model the wireless channel environment experienced by these moving UEs, we adopted a frequency-selective channel model based on WINNER II. For each time slot, updated AP-UE distances and angles were extracted and used to generate multi-path channel realizations. These channel responses were frequency-resolved, capturing the channel gain over a range of subcarriers. Figure 4.3 presents a snapshot of the frequency responses for ten AP-UE links corresponding to the first user pair. Each curve in the plot corresponds to a distinct access point-user link, highlighting the diversity and variability in channel gain across subcarriers.

In addition to frequency-domain representations, the Power Delay Profile (PDP) was computed to analyze the temporal dispersion characteristics of the channel. The PDP reflects how the signal energy is distributed over different delay paths, offering insight

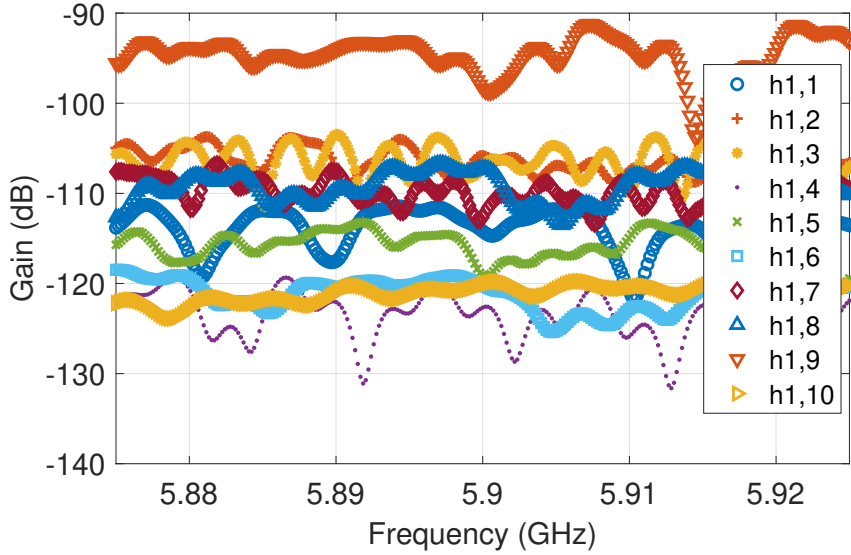


Figure 4.3: Frequency response of measured channel gains across 10 AP-UE links. Each curve represents the wireless channel gain for a specific AP-UE link in the first user pair, where $h_{1,1}$ corresponds to AP 1 and user 1, $h_{1,2}$ to AP 1 and user 2, and so on.

into multipath richness and time dispersion, factors that critically affect OFDM-based systems. Figure 4.4 shows the PDP results for the same 10 AP-UE links, revealing significant variation in delay spreads, which must be accounted for in the resource allocation and scheduling processes.

The full simulation environment, therefore, operates in a closed loop: user trajectories from SUMO influence the dynamic re-clustering of APs and trigger fresh WINNER II channel generations at each update interval. The resulting time-series of channel matrices provide the necessary input to the optimization framework described in the following sections, enabling precise evaluation of spectral efficiency, fairness, and interference management under realistic, mobility-driven scenarios.

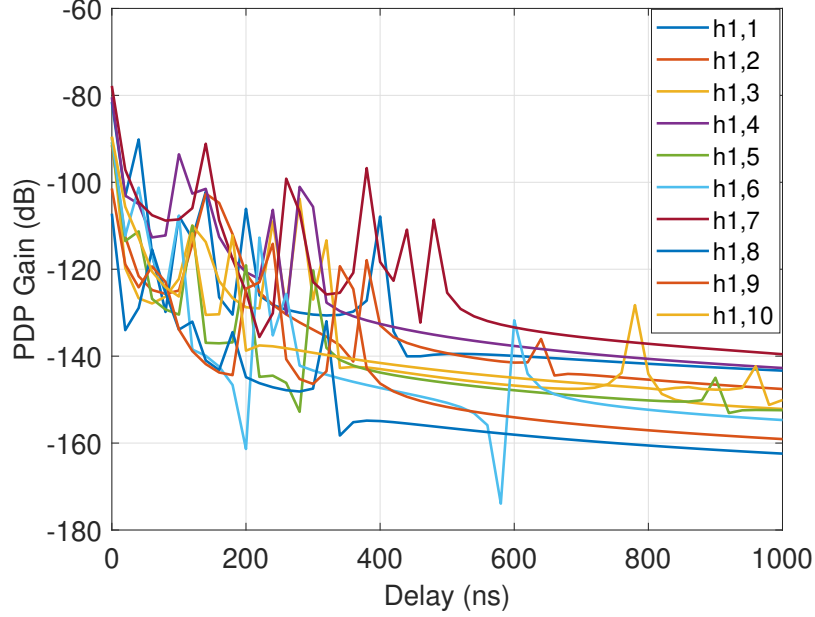


Figure 4.4: PDP of the channel gains for the 10 AP-UE links.

4.4 Problem Formulation

In Chapter 3, the user-to-resource allocation problem in vehicular networks was addressed using a heuristic algorithm based on simple metrics such as received signal strength or proximity to access points (APs). While effective in low-complexity scenarios, that approach lacked adaptability to dynamic environments and failed to guarantee quality of service (QoS) or fairness across users. In this chapter, we significantly extend that formulation by introducing a multi-objective optimization framework tailored for User-Centric Cell-Free Massive MIMO (UC-CFmMIMO) systems operating in high-mobility vehicular settings.

The system under consideration involves a downlink UC-CFmMIMO configuration comprising L spatially distributed APs, each equipped with N antennas, and K single-antenna vehicular users (UEs). The total available bandwidth B is divided into S frequency subbands. The assignment of users to subbands is governed by an allocation matrix A , where $A_{sk} = 1$ if user k is assigned to subband s , and 0 otherwise.

To efficiently manage the shared wireless resources in such a dynamic and frequency-selective environment, we define a joint optimization problem that simultaneously pursues three key objectives:

1. **Maximization of Spectral Efficiency (SE):** Ensuring high throughput across the system by maximizing the aggregate SE over all users and subbands. This is formalized as:

$$\eta_{\text{Total}} = \sum_{s=1}^S \sum_{k=1}^K \eta(A_{sk}), \quad (4.3)$$

where $\eta(A_{sk})$ denotes the spectral efficiency achieved by user k on subband s .

2. **Fairness in Resource Distribution:** To prevent disproportionate allocation of bandwidth, we introduce the Gini index I_{Gini} , which quantifies inequality in SE distribution:

$$I_{\text{Gini}} = \frac{1}{2K^2\bar{\eta}} \sum_{s=1}^S \sum_{i=1}^K \sum_{\substack{j=1 \\ j \neq i}}^K |\eta(A_{si}) - \eta(A_{sj})|, \quad (4.4)$$

where $\bar{\eta}$ is the average SE across all users.

3. **Interference Minimization:** To reduce mutual interference among users sharing the same subband, we leverage eigenvalue decomposition of the composite channel matrix. Specifically, we aim to maximize the minimum eigenvalue λ_{\min} of the matrix $H_s^\top D H_s$ for each subband s , where D is a block-diagonal matrix encoding user-AP association:

$$\lambda_{\min} = \min_{s \in \{1, \dots, S\}} (\min (\text{eig}(H_s^\top D H_s))). \quad (4.5)$$

These objectives are integrated into a unified optimization function as follows:

$$\max_A (w_\eta \cdot \eta_{\text{Total}} + w_{\text{EVD}} \cdot \lambda_{\text{min}} - w_{\text{Gini}} \cdot I_{\text{Gini}}), \quad (4.6)$$

where w_η , w_{EVD} , and w_{Gini} are the weights assigned to each objective to reflect their relative importance.

The optimization is subject to the following constraints:

$$\text{C1: } \sum_{k=1}^K \rho_k \leq \rho_{\text{max}} \quad (\text{Total power budget}), \quad (4.7)$$

$$\text{C2: } \eta(A_{sk}) \geq \eta_{\text{th}}, \quad \forall s, k \quad (\text{Minimum QoS per user}), \quad (4.8)$$

$$\text{C3: } \sum_{s=1}^S |A_{sk}| \leq 1, \quad \forall k \quad (\text{Single subband per user}), \quad (4.9)$$

$$\text{C4: } \sum_{s=1}^S |A_s| \leq K \quad (\text{User capacity constraint}). \quad (4.10)$$

This formulation allows for flexible, adaptive allocation of users to frequency resources, while explicitly accounting for frequency selectivity, user mobility, and inter-user coupling. By shifting from a heuristic-based approach to this rigorous optimization-based method, we are better equipped to guarantee service continuity and reliability, two critical requirements for vehicular communication systems, especially in the context of future 6G networks.

4.5 Proposed Resource Allocation Algorithms

Resource allocation in user-centric cell-free massive MIMO (UC-CFmMIMO) systems, particularly within vehicular environments, represents a formidable optimization challenge. The problem is shaped by non-convex objective functions, high-dimensional

search spaces, and discontinuous decision boundaries that stem from the interplay between user mobility, frequency-selective fading, and interference variability. These characteristics render classical optimization techniques, especially those relying on gradient information or convex relaxations, ineffective in providing robust and scalable solutions. As such, this work turns to a family of metaheuristic optimization strategies that excel in navigating complex, non-differentiable search landscapes.

Metaheuristic algorithms are well-suited for the type of dynamic and irregular solution space encountered in our system. Their stochastic nature allows for both global exploration and local refinement, enabling convergence toward high-quality solutions even under uncertainty and rapidly changing conditions. Among the wide spectrum of available techniques, we focus on three paradigms: Simulated Annealing (SA), Genetic Algorithm (GA), and Ant Colony Optimization (ACO). These algorithms have been tailored to solve the frequency subband allocation problem under the unified multi-objective framework previously introduced. Each of them adapts its underlying search mechanisms to account for the constraints of the UC-CFmMIMO architecture, including user-subband compatibility, quality-of-service (QoS) requirements, and interference suppression.

4.5.1 Simulated Annealing-Based Optimization

Simulated Annealing (SA) draws inspiration from the physical process of annealing in metallurgy, where a material is slowly cooled to reach a state of minimal energy. In the context of frequency resource allocation, SA begins with an initial allocation of users to subbands and iteratively explores neighboring solutions. Each candidate solution is evaluated using the composite fitness function defined in Section 4.4, which jointly captures spectral efficiency, fairness, and interference levels.

Algorithm 4.1: SA Algorithm for frequency resource allocation in a UC-CFmMIMO system

- 1: **Initialization Phase:**
 - 2: Set initial solution $\mathcal{A}^{(0)}$, initial temperature T_{init} , cooling parameter α , number of iterations, and weights w_{SEV} , w_{EVD} , w_{Gini} .
 - 3: Compute initial fitness value $f(\mathcal{A}^{(0)})$. // The fitness value $f(\mathcal{A})$ represents the objective function used to evaluate the quality of a given solution \mathcal{A} .
 - 4: Set current solution $\mathcal{A}_{\text{current}} = \mathcal{A}^{(0)}$ and current fitness value $f_{\text{current}} = f(\mathcal{A}^{(0)})$.
 - 5: **Training Phase:**
 - 6: **while** stopping criterion not met **do**
 - 7: Generate a new neighboring solution \mathcal{A}_{new} by moving a randomly selected user to a different subband.
 - 8: **Decision Phase:**
 - 9: Compute the new fitness value $f(\mathcal{A}_{\text{new}})$.
 - 10: **if** $f(\mathcal{A}_{\text{new}}) > f(\mathcal{A}_{\text{current}})$ **then**
 - 11: | Accept the new solution $\mathcal{A}_{\text{current}} = \mathcal{A}_{\text{new}}$.
 - 12: **else**
 - 13: | Accept \mathcal{A}_{new} with probability $P = \exp\left(\frac{f(\mathcal{A}_{\text{new}}) - f(\mathcal{A}_{\text{current}})}{f(\mathcal{A}_{\text{current}})}\right)$.
 - 14: **Update Phase:**
 - 15: Update the temperature $T = \alpha \times T$.
 - 16: **return** the best solution $\mathcal{A}_{\text{best}}$.
-

At each iteration, a new solution is generated by perturbing the current allocation, typically by reassigning a user to a different subband. If the new allocation yields an improved fitness, it is accepted. Otherwise, it may still be accepted with a probability that decreases as the temperature declines. This mechanism allows the algorithm to escape local optima during early exploration phases while encouraging convergence as the temperature lowers.

The stepwise procedure for the SA algorithm is detailed in Algorithm 4.1, where temperature control, fitness evaluation, and probabilistic acceptance govern the evolution of the solution.

4.5.2 Genetic Algorithm-Based Optimization

Genetic Algorithms (GAs) emulate the principles of evolution and natural selection. In this method, each candidate solution is encoded as a chromosome, where genes represent specific user-to-subband assignments. An initial population of chromosomes is randomly generated, and the fitness of each individual is evaluated according to the same multi-objective function used in SA.

Through successive generations, chromosomes are evolved using genetic operators: selection favors high-fitness individuals; crossover combines genetic material from parent chromosomes to generate offspring; and mutation introduces random alterations to preserve diversity. This evolutionary strategy allows the population to explore a broad search space while iteratively converging toward optimal allocations. The diversity within the population plays a crucial role in preventing premature convergence and enabling the discovery of globally competitive solutions.

4.5.3 Ant Colony Optimization-Based Strategy

Ant Colony Optimization (ACO) is inspired by the collective behavior of ants in discovering optimal paths to food sources. In our adaptation, artificial ants represent agents that construct frequency allocation paths by probabilistically assigning users to subbands based on pheromone intensities and heuristic desirability.

Each ant incrementally builds a complete allocation solution, influenced by the accumulated pheromone trails left by previous ants and by immediate utility metrics such as user spectral efficiency or interference cost. Over iterations, pheromones are updated to reinforce promising allocations, while evaporation prevents overexploitation

of suboptimal paths. This decentralized learning mechanism enables robust exploration and convergence, especially under dynamic channel and mobility conditions.

4.5.4 Computational Complexity

Each proposed metaheuristic exhibits a different computational profile, driven by its internal operations and control parameters. Simulated Annealing operates over a single solution and evolves it iteratively, leading to a complexity of $\mathcal{O}(N_{\text{iter}} \cdot F)$, where N_{iter} is the number of iterations and F is the cost of evaluating the fitness function. Its simplicity and structured cooling schedule make it an attractive option for time-constrained optimization in fast-changing vehicular networks.

The Genetic Algorithm, with its population-based design, incurs a higher computational cost of $\mathcal{O}(G \cdot P \cdot F)$, where G is the number of generations and P is the population size. Despite the higher cost, GA benefits from inherent parallelism, making it suitable for high-performance computing environments.

Ant Colony Optimization shares a similar complexity, expressed as $\mathcal{O}(N_{\text{iter}} \cdot A \cdot F)$, where A is the number of ants. While ACO may be slower to converge compared to SA, its capacity for distributed search and adaptability to dynamic changes offers valuable robustness in uncertain environments.

Collectively, these algorithms offer a flexible toolkit for addressing the multifaceted frequency allocation problem in UC-CFmMIMO systems. Their performance will be quantitatively assessed in the subsequent section, under a wide range of mobility and channel conditions, to highlight their respective strengths in balancing efficiency, fairness, and interference suppression.

4.6 Numerical Results

This section presents a comprehensive performance evaluation of the proposed frequency allocation framework under dynamic vehicular network scenarios. Through extensive simulations, we analyze and compare the effectiveness of Simulated Annealing (SA), Genetic Algorithm (GA), and Ant Colony Optimization (ACO) in optimizing the allocation of shared subband resources in UC-CFmMIMO systems. The evaluation spans multiple performance metrics, including convergence behavior, spectral efficiency (SE), resource utilization, and fairness. All simulations incorporate realistic user mobility patterns generated using SUMO and frequency-selective channel realizations modeled through WINNER II.

To begin, we examine the convergence characteristics of the metaheuristic algorithms under a fixed user distribution. As shown in Figure 4.5, SA demonstrates a steady progression toward higher fitness values, reaching approximately 0.91 after 4500 iterations. In contrast, GA and ACO exhibit faster convergence rates, stabilizing around 1000 iterations, but yield lower final fitness values, approximately 0.74 and 0.68, respectively. This behavior underscores the strength of SA in exploring complex solution spaces and achieving globally competitive results, though it comes at the expense of longer execution time.

To assess algorithm performance in dynamic settings, we simulate five distinct user distributions derived from SUMO mobility traces. These mobility steps reflect different vehicular topologies occurring at discrete intervals. As illustrated in Figure 4.6, all algorithms exhibit oscillatory convergence patterns caused by periodic changes in user locations and channel gains. Notably, SA maintains a significant advantage across all mobility snapshots, consistently converging to superior fitness values. For instance, at iteration 2500, SA reaches a fitness of 0.9, whereas GA and ACO plateau at 0.75 and

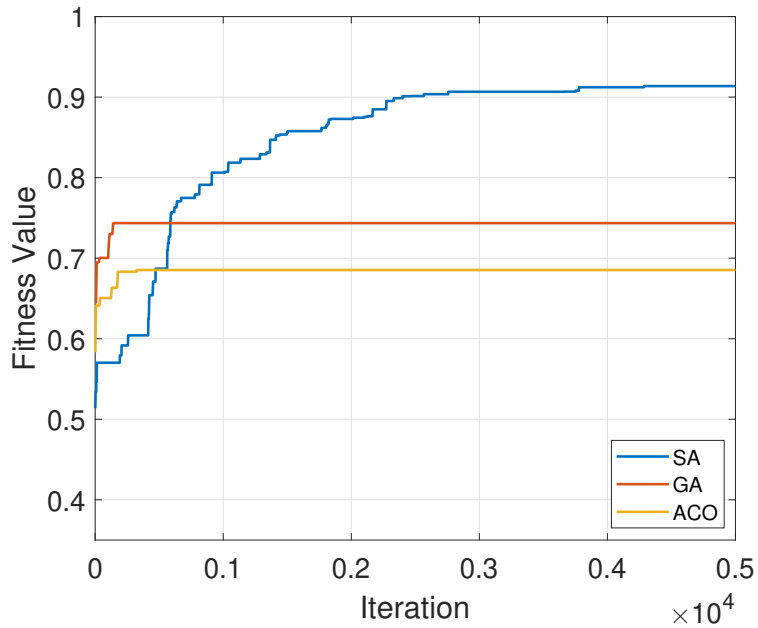


Figure 4.5: Convergence of fitness values across algorithms: Comparison for a single user distribution with 20 available frequency resources.

0.69, respectively. These results validate SA’s resilience to network dynamics and its capability to maintain high-quality allocations despite mobility-induced disruptions.

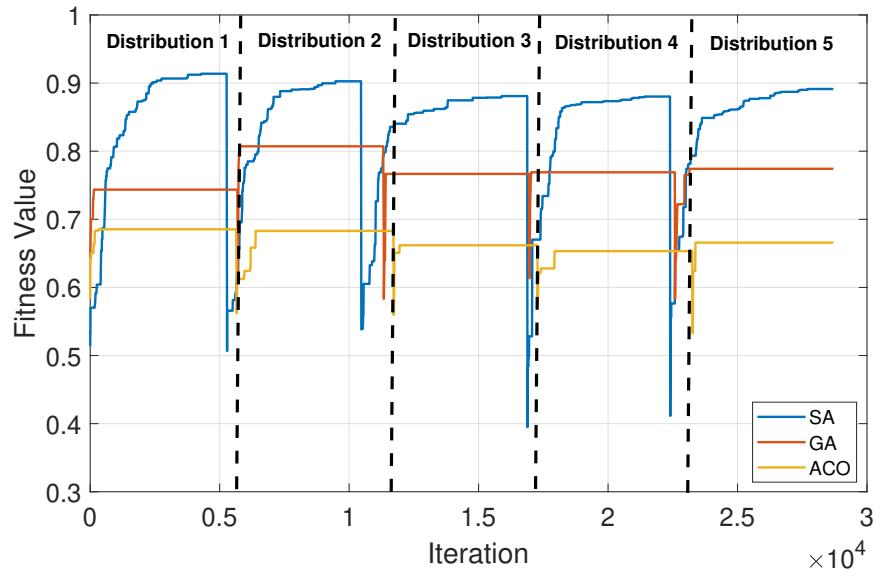


Figure 4.6: Convergence of fitness values across algorithms: Performance comparison over five distinct user distributions with 20 available frequency resources.

Next, we investigate the impact of varying the number of available subbands on spectral efficiency (SE). As depicted in Figure 4.7, increasing the subband count from 10 to 40 results in a proportional improvement in SE for all algorithms. However, SA consistently outperforms GA and ACO across all configurations. At $S = 20$, SA achieves 170 bps/Hz, compared to 131 bps/Hz and 127 bps/Hz for GA and ACO, respectively. With 40 subbands, SA peaks at 276 bps/Hz, reflecting its superior capacity to leverage expanded resource availability through deeper search exploration.

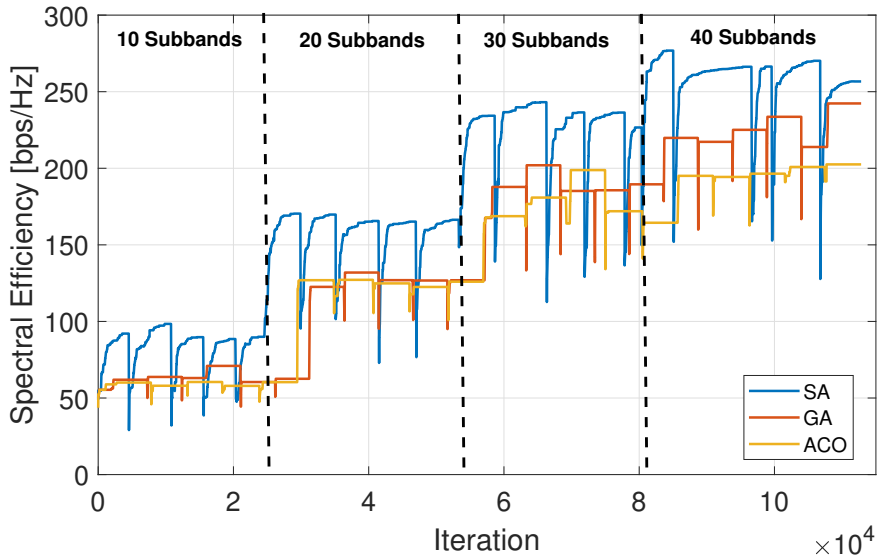


Figure 4.7: Convergence of SE performance across user distributions and varying subband resources.

The ability to conserve bandwidth by enabling user sharing on subbands is crucial in modern networks. Figure 4.8 reports the percentage of free bandwidth (i.e., unallocated subbands) as a function of total subband availability. SA consistently achieves the highest resource savings, starting from 27% at $S = 20$ and rising to 40.4% at $S = 40$. This indicates that SA not only optimizes spectral efficiency but also promotes efficient resource reuse, allowing additional users to be served without increasing bandwidth demands.

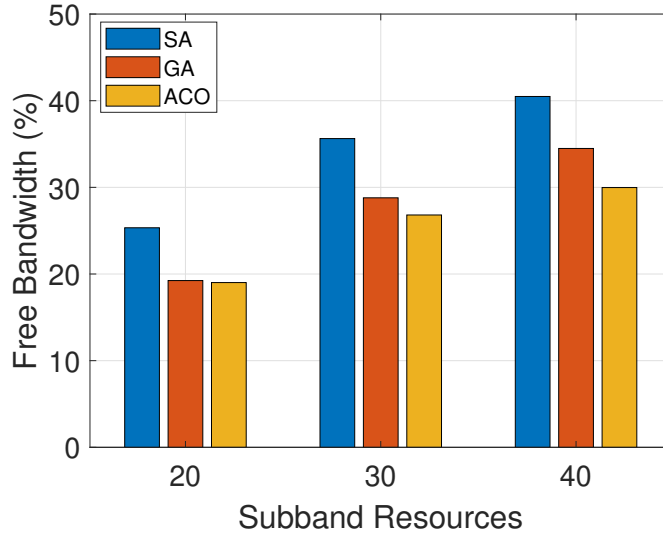


Figure 4.8: Percentage of free available bandwidth.

Fairness in resource allocation is another vital performance indicator, particularly in dense or heterogeneous networks. Figure 4.9 presents the Gini index for each algorithm, a measure of allocation fairness where lower values indicate more equitable distribution. SA shows the most significant improvement in fairness as the number of subbands increases, reducing the Gini index from 0.06 to 0.01. GA and ACO stabilize at 0.04 and 0.03, respectively. These findings further support SA’s effectiveness in balancing throughput maximization with fairness constraints.

Finally, we evaluate algorithm scalability under increased user density. The number of UEs is doubled from 40 to 80, while the number of APs and subband resources remains fixed at 40. Figure 4.10 illustrates the effect on SA’s convergence behavior. As expected, the increased user count introduces additional complexity, resulting in longer convergence time and a lower final fitness value. Specifically, SA reaches 0.76 for $K = 80$, compared to 0.90 for $K = 40$. Nonetheless, the algorithm maintains stability and continues to find high-quality solutions, confirming its robustness under load-intensive scenarios.

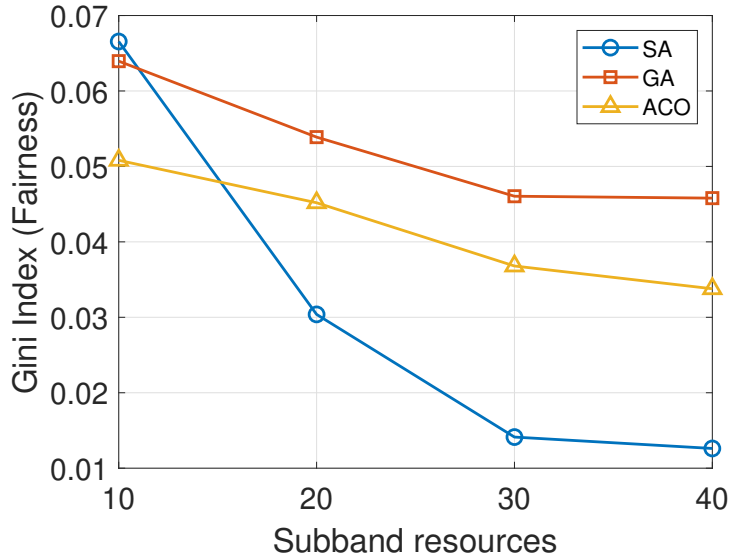


Figure 4.9: Gini Fairness.

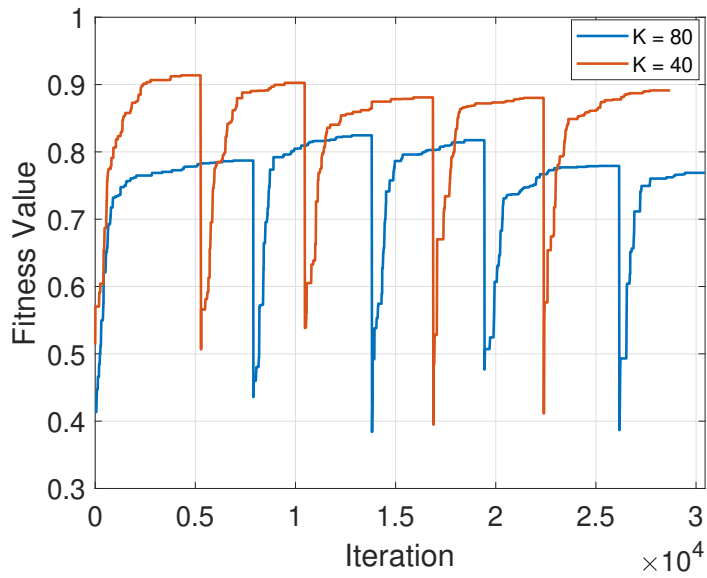


Figure 4.10: Convergence behavior of SA for different user densities ($K = 40$, $K = 80$).

In summary, the numerical evaluations demonstrate that Simulated Annealing consistently outperforms both Genetic Algorithm and Ant Colony Optimization across all considered metrics. It achieves superior spectral efficiency, greater bandwidth savings, enhanced fairness, and reliable adaptability to dynamic and high-density scenarios.

These results underscore its suitability as a robust optimization engine for frequency resource allocation in user-centric, cell-free massive MIMO vehicular networks.

4.7 Conclusion and Future Scope of Work

In this chapter, we addressed the problem of frequency resource allocation in user-centric cell-free massive MIMO (UC-CFmMIMO) systems under dynamic vehicular network conditions. Recognizing the limitations of traditional optimization methods in handling the complex, non-convex, and rapidly changing nature of this problem, we proposed a metaheuristic-based framework incorporating Simulated Annealing (SA), Genetic Algorithm (GA), and Ant Colony Optimization (ACO). Our approach integrates a high-fidelity simulation environment that couples realistic vehicular mobility patterns, generated via the SUMO traffic simulator, with frequency-selective channel models based on WINNER II. This hybrid setup enables an accurate and scalable testbed for evaluating resource allocation strategies in dense, high-mobility environments.

The numerical results demonstrate the robustness and efficiency of SA compared to GA and ACO, particularly in achieving superior spectral efficiency, fairness, and resource utilization across both static and dynamic user distributions. SA's ability to consistently adapt to ongoing changes in network topology, user positions, and interference patterns underlines its suitability for real-world vehicular communications. Furthermore, the algorithm maintains scalable performance even under increasing user density, highlighting its potential for future large-scale 6G networks.

Despite these promising outcomes, several avenues for future research remain open. First, while the current framework focuses on frequency allocation, extending the optimization to include joint power control, user scheduling, and beamforming could

lead to even greater performance gains. Additionally, incorporating energy efficiency constraints and latency-aware QoS metrics would align the optimization objectives more closely with emerging 6G use cases such as ultra-reliable low-latency communication (URLLC) and autonomous vehicular systems.

Another promising direction involves enhancing the intelligence of the optimization process through reinforcement learning or hybrid AI-metaheuristic approaches, which may offer faster adaptation to environmental changes without requiring full re-optimization. Furthermore, the integration of machine-learned mobility prediction models into the SUMO-based simulation could further improve the realism and anticipation capabilities of the resource allocation engine.

Lastly, real-time implementation and testing on hardware-in-the-loop platforms or with software-defined radios (SDRs) could provide practical validation of the proposed algorithms under actual network conditions.

Overall, this work lays a solid foundation for adaptive resource allocation in next-generation wireless systems and highlights the importance of flexible, intelligent optimization frameworks in supporting the increasingly dynamic nature of future networked environments.

REINFORCEMENT LEARNING-BASED APPROACHES TO FREQUENCY
RESOURCE ALLOCATION IN UC CF MASSIVE MIMO

Publication Note

This chapter is based on the following research work:

- The main content is currently under review for publication in the *Elsevier Physical Communication* journal [42].
- A related poster titled *Hybrid AI and Metaheuristic Solutions for Optimized Frequency Allocation in 6G Networks* was presented at the **BMW Group Summer School on Trust and Safety in Artificial Intelligence - Solving Challenges in Mobility**, held in July 2025 in Saint-Raphaël, France [43].

5.1 Introduction

The investigative trajectory underpinning this work reflects a progressive escalation in both the complexity of the addressed problem and the sophistication of the computational paradigms adopted. This evolution traces a methodological arc from traditional heuristic techniques to hybrid artificial intelligence solutions, tailored for frequency resource allocation in user-centric cell-free massive MIMO (UC-CFmMIMO) systems, an architecture poised to define the next generation of ultra-dense and dynamic wireless networks [172, 76, 23].

In the early stages of this research, heuristic strategies offered intuitive, low-complexity solutions suitable for small-scale scenarios. Their deterministic nature allowed for direct implementation, but as network topologies scaled and environmental dynamics intensified, especially in vehicular contexts, these methods proved inadequate in handling the non-convex, high-dimensional optimization landscape [90, 62, 44]. The limitations in adaptability and scalability prompted the exploration of more generalized metaheuristic frameworks.

Metaheuristic algorithms, such as Genetic Algorithms (GAs), Ant Colony Optimization (ACO), and Simulated Annealing, draw inspiration from evolutionary and biological processes to explore complex search spaces with stochastic robustness [145, 86, 68]. These methods introduced population diversity, adaptive learning, and probabilistic transitions that significantly improved spectral efficiency (SE), fairness, and interference management [41]. However, their reliance on offline processing and the lack of responsiveness to rapidly changing environmental conditions limited their utility in vehicular networks, where channel conditions and user mobility evolve quickly [158, 25].

To address these temporal constraints, this research pivoted toward Reinforcement Learning (RL), a paradigm that enables agents to learn optimal policies through interaction with their environment, without explicit system models [21, 24]. By framing frequency resource allocation as a Markov Decision Process (MDP), RL facilitates dynamic and context-aware decision-making that evolves over time, responding adaptively to user mobility, channel fluctuations, and varying service demands. Actor-Critic architectures, particularly the Deep Deterministic Policy Gradient (DDPG) algorithm, have proven well-suited for continuous action spaces and policy stability, making them ideal candidates for responsive control in large-scale MIMO systems [164, 166, 119].

This chapter presents the first RL-based framework developed within this thesis. It marks a critical methodological shift: from heuristic- and metaheuristic-guided optimization to model-free, data-driven intelligence. The proposed approach leverages the DDPG-based Actor-Critic architecture to enable online learning of frequency allocation strategies that balance SE, fairness, and interference mitigation in UC-CFmMIMO deployments. In contrast to the static nature of metaheuristic methods, this RL agent incrementally adapts its policy based on observed system feedback, enabling robust performance under the fast-changing conditions characteristic of vehicular wireless environments [109, 173].

While this chapter focuses on standalone RL, it also lays the conceptual foundation for the hybrid learning framework developed in the next chapter. The integration of metaheuristic global search (e.g., Aquila Optimizer) with RL-based local policy refinement exploits the complementary strengths of both paradigms, combining the sample efficiency and adaptability of RL with the exploratory diversity and convergence guarantees of nature-inspired search algorithms [104, 27, 68].

The remainder of this chapter is organized as follows. We begin with a detailed description of the system and channel model, followed by a formal definition of the reinforcement learning problem formulation, including state, action, and reward design. The implementation details of the RL agent are then described, and simulation results are presented to evaluate the performance against baseline metaheuristic approaches. Finally, key findings are discussed, along with insights that motivate the hybrid framework developed later in this thesis.

5.2 Channel Model

To support reinforcement learning (RL)-based resource allocation in realistic vehicular wireless environments, this chapter adopts a significant advancement in channel modeling methodology. While previous investigations utilized the WINNER II channel model, often paired with trajectory data from the Simulation of Urban Mobility (SUMO) tool, to simulate vehicular radio conditions, such approaches exhibit limitations in spatial consistency, trajectory smoothness, and environment-aware fading behaviors [38, 37, 107]. These limitations, although manageable in static or heuristic-driven optimization, pose serious challenges for learning algorithms that rely on temporally correlated feedback for policy updates.

To address these challenges, this work integrates the QuaDRiGa (QUAsi Deterministic RadIo channel GenerAtor) simulator [93], a state-of-the-art framework developed to emulate realistic and geometry-consistent wireless propagation. QuaDRiGa offers full 3D spatial-temporal consistency, supporting dynamic mobility, frequency-selective multipath fading, and directional antenna patterns, all critical for the accurate emulation of high-mobility environments in 6G and beyond [8, 94].

Unlike legacy models, QuaDRiGa simulates continuous-time channel evolution along user trajectories, embedding Doppler effects, angle spreads, and spatial filtering through antenna arrays in both Line-of-Sight (LoS) and Non-Line-of-Sight (NLoS) conditions [115, 85]. These characteristics are indispensable for reinforcement learning agents operating in partially observable and rapidly changing environments, where policy convergence depends on structured and gradual environmental transitions [155, 122].

The structural topology of the user-centric cell-free massive MIMO (UC-CFmMIMO) network is retained from prior chapters: a cooperative downlink system with L spatially distributed access points (APs) connected via fronthaul to a central processing unit (CPU), serving K single-antenna user terminals (UTs) via dynamic clustering. However, the channel modeling paradigm now shifts from episodic snapshot generation to coherent, trajectory-aware simulation. This provides reinforcement learning agents with temporally smooth and physically plausible channel state information (CSI), aligning well with the time-step-based learning loop of actor-critic architectures such as DDPG.

Formally, the channel impulse response between AP m and UT k at time t and delay τ is expressed as:

$$h_{mk}(t, \tau) = \sum_{l=1}^L a_l^{mk}(t) \delta(\tau - \tau_l^{mk}(t)) \quad (5.1)$$

where L denotes the number of multipath components, and each path is characterized by a time-varying complex gain $a_l^{mk}(t)$ and delay $\tau_l^{mk}(t)$. These parameters evolve as functions of the UT's mobility, determined by continuous spatial trajectories and dynamic scattering geometry.

The simulation scenario adheres to the 3GPP-defined Urban Microcell (UMi) environment [8]. Both clustered delay line (CDL) and geometry-based stochastic models (GBSMs) are supported, with environment-dependent LoS/NLoS determination, 3D angular spreads, and dual-polarized antenna arrays [78]. These specifications ensure compatibility with vehicular use cases such as V2X and ITS, where low latency and rapid channel variability must be accurately represented [134, 41].

Moreover, QuaDRiGa enables embedded mobility modeling without requiring external simulators. User positions, velocities, and directions are internally tracked and used to generate consistent channel evolution, ensuring that sequential actions taken

by the RL agent produce physically meaningful and smoothly transitioning system states. This is crucial for avoiding non-stationarities in the learning signal, which would otherwise degrade convergence performance [165, 150].

In summary, the adoption of QuaDRiGa introduces a geometrically coherent, time-evolving, and mobility-aware propagation model that bridges the gap between academic RL environments and real-world wireless systems. It not only preserves the architectural features of the UC-CFmMIMO network described previously, but also enables the deployment of learning-based resource allocation strategies in a high-fidelity simulation framework reflective of practical vehicular networks.

5.3 Simulation Setup and Data Generation

To rigorously assess the performance of the proposed reinforcement learning (RL)-based frequency allocation framework, a detailed simulation environment was developed to emulate the characteristics of dense vehicular communications in urban microcell scenarios. This environment is built on the QuaDRiGa simulator, configured with a system-level model representative of a user-centric cell-free massive MIMO (UC-CFmMIMO) architecture.

The simulation spans a $2\text{ km} \times 2\text{ km}$ area following the 3GPP TR 38.901 Urban Microcell (UMi) channel model guidelines [8]. The network consists of $L = 100$ distributed access points (APs), each employing a Uniform Circular Array (UCA) with $N = 4$ antennas positioned at a height of $h_{\text{AP}} = 12.5\text{ m}$. The mobile users, modeled as vehicular user equipments (UEs), are randomly deployed with $K = 40$ single-antenna devices, each utilizing a Uniform Linear Array (ULA) and operating at a height of $h_{\text{UE}} = 1.5\text{ m}$.

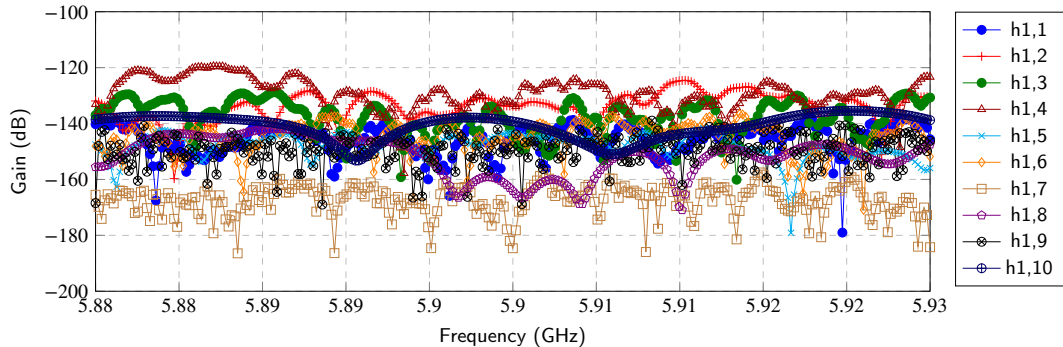


Figure 5.1: Channel frequency responses of the 10 AP-UE pair links.

The wireless system is configured to operate in the 5.9 GHz Intelligent Transportation Systems (ITS) band, as allocated for vehicular networks in 5G and beyond [108]. A bandwidth of $B = 50$ MHz is employed and segmented into 277 subbands, each comprising 12 OFDM subcarriers with a spacing of $B_{\text{RB}} = 180$ kHz, adhering to 5G NR numerology [140]. This fine-grained frequency partitioning enables detailed channel modeling and high-resolution resource allocation at the subband level, an essential feature for the RL agent’s input space.

The time-evolving channel frequency responses (CFRs) generated by QuaDRiGa serve as the environmental observations for the learning process. Figure 5.1 illustrates the CFRs for ten AP-UE links (AP 1 to UEs 1–10), showing strong frequency selectivity across the 5.875–5.925 GHz spectrum. These CFR variations capture the effects of multipath propagation, urban blockages, and mobility-induced Doppler shifts, factors critical for real-world frequency planning [115, 134].

Table 5.1 summarizes the simulation configuration, which includes spatial deployment, antenna configurations, power constraints, and signal structure. These parameters are designed to reflect a scalable, realistic vehicular UC-CFmMIMO deployment and ensure the validity of both training and testing phases for the RL-based scheduler.

Table 5.1: *QuaDRiGa Simulation Parameters.*

Parameter	Description	Value	Reference
f_c	Central Frequency	5.9 GHz	[108]
B	Total Bandwidth	50 MHz	[140]
B_{RB}	Subcarrier Spacing	180 kHz	[140]
UCA	AP Antenna Configuration	Uniform Circular Array	[182]
ULA	UE Antenna Configuration	Uniform Linear Array	[188]
R	Area of Coverage	2 km \times 2 km	[8]
L	Number of APs	100	[134]
N	Antennas per AP	4	[134]
K	Number of UEs	40	[134]
N_{UE}	Antennas per UE	1	[76]
h_{AP}	AP Height	12.5 m	[8]
h_{UE}	UE Height	1.5 m	[8]
τ_p	Pilot Sequence Length	10 symbols	[62]
P_{max}	Max Transmit Power (per AP)	200 mW	[62]
S	Number of Subbands	277	-
3GPP_38.901_UMi	Deployment Scenario	Urban Microcell	[8]

In summary, this simulation setup enables the generation of highly dynamic and frequency-selective channel environments, forming the input space upon which RL agents are trained. The detailed modeling of mobility, fading, and subband-level granularity provides a rich testbed for evaluating intelligent frequency resource allocation strategies.

5.4 Proposed Resource Allocation Algorithms

Building on the problem formulation previously established, this chapter introduces advanced computational strategies designed to solve the frequency resource allocation problem in user-centric cell-free massive MIMO (UC-CFmMIMO) systems. The wireless environment under consideration is characterized by high mobility, strong frequency selectivity, and spatial variability, which together give rise to a complex, non-convex optimization landscape. Traditional heuristics and offline solvers are insufficient in this context due to their inability to generalize over time, adapt to environmental variations, or respond promptly to changing system states.

To overcome these limitations, we develop a set of adaptive algorithms that approach the problem from complementary perspectives. The first is a nature-inspired metaheuristic technique, the Aquila Optimizer (AO), which efficiently explores complex solution landscapes through structured global and local search strategies. While AO excels at navigating rugged objective spaces, it lacks temporal adaptability, motivating the need for more responsive, learning-based methods.

To this end, we introduce a model-free reinforcement learning framework based on the Deep Deterministic Policy Gradient (DDPG) algorithm. This architecture is designed to learn a continuous policy that maps observed wireless conditions to optimal resource allocation decisions, without requiring an explicit model of the environment. By leveraging actor-critic learning and continuous action outputs, DDPG provides a powerful mechanism for adaptive frequency allocation in dynamic vehicular networks.

Finally, we present a hybrid algorithm that integrates the Aquila Optimizer into the DDPG training process. This hybrid framework, originally proposed in this thesis, combines the exploratory depth of AO with the adaptive intelligence of reinforcement learning, resulting in a solution that balances offline global optimization with online policy refinement. Together, these three methods offer a progressively richer set of tools for addressing the multifaceted challenges of frequency allocation in next-generation wireless systems.

5.4.1 Metaheuristic Optimization using Aquila Optimizer (AO)

The resource allocation problem addressed in this chapter builds upon the mathematical formulation introduced in Chapter 4, aiming to allocate frequency subbands to user terminals in a user-centric cell-free massive MIMO (UC-CFmMIMO) network. The optimization objective involves a composite utility function that balances spec-

tral efficiency (SE), user fairness (quantified via the Gini index), and interference suppression (through eigenvalue dispersion of the interference matrix) [143, 185, 45]. While the problem itself remains consistent, this section introduces a more adaptive and data-responsive approach to solving it, moving beyond static rule-based methods toward techniques that learn directly from observed input conditions without requiring explicit modeling of the full wireless environment [122, 178].

In highly dynamic vehicular settings, such as those modeled in this study, constructing an accurate and timely model of user mobility, multipath propagation, and interference dynamics becomes computationally prohibitive [134, 85]. Instead, we propose a strategy that learns to map raw observations of the radio environment (e.g., CFRs and user-AP associations) to effective resource allocation decisions. This perception-action framework allows the optimization method to reason about current system states and determine subband-user assignments that maximize overall utility, without the need to simulate or estimate the complete system dynamics at each time step [68, 155].

To initiate this approach, we explore metaheuristic optimization through the Aquila Optimizer (AO), a nature-inspired algorithm introduced by Abualigah et al. in 2021 [17]. AO mimics the adaptive hunting strategies of Aquila eagles, offering a balance between exploration and exploitation via four dynamic movement phases, as illustrated in Figure 5.2. Each phase corresponds to a mathematically encoded operator designed to navigate high-dimensional, rugged solution spaces with strong global and local search behavior [65, 144].

In the frequency resource allocation context, each candidate solution in AO encodes a full assignment of users to subbands. These candidate solutions evolve iteratively across generations using the following four search phases:

- **High Soar with Vertical Stoop:** Enables wide-ranging exploration using Lévy-flight-based jumps to traverse the global solution space [161].
- **Contour Flight with Short Glide Attack:** Guides search toward promising areas by combining current and best-known solutions to refine candidate selection.
- **Low Flight with Attack:** Implements localized intensification by narrowing the search around high-performing solutions.
- **Passive Glide with Random Walk:** Injects randomness to avoid premature convergence and maintain diversity among solutions.

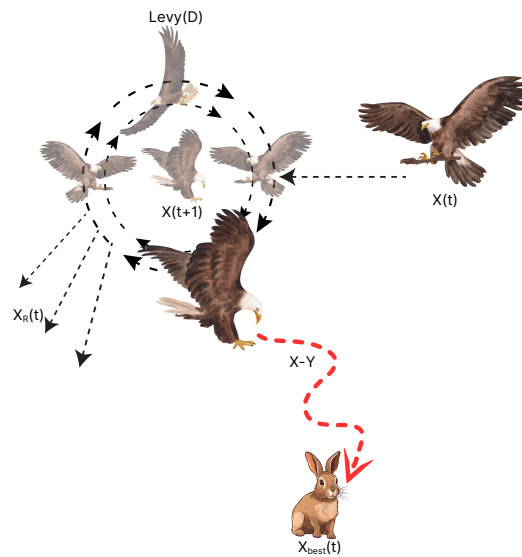


Figure 5.2: Illustration of the four hunting strategies in the Aquila Optimizer. Each phase models a distinct movement pattern balancing exploration and exploitation.

The suitability of AO for this problem is strongly grounded in the structural properties of the underlying wireless environment. The optimization landscape is inherently non-convex and high-dimensional, owing to frequency selectivity, dynamic interference conditions, and mobility-induced Doppler shifts [115, 41]. Furthermore, the joint maximization of SE, fairness, and interference mitigation introduces conflicting

objectives that are difficult to handle with traditional deterministic solvers. AO's dynamic phase-switching and Lévy-flight mechanisms allow it to maintain a robust search capability under these non-linear and stochastic constraints [178, 17].

However, while AO exhibits excellent global search behavior and robustness, it lacks memory: each optimization cycle starts afresh and does not adapt its strategy based on prior environmental feedback. This limitation motivates the introduction of reinforcement learning in the following section, which extends the optimization process by learning state-action policies that evolve over time [122, 150].

5.4.2 Reinforcement Learning-Based Resource Allocation

To overcome the limitations of episodic and non-adaptive optimization schemes, this section introduces a model-free reinforcement learning (RL) approach to the frequency resource allocation problem in UC-CFmMIMO systems. While metaheuristics like the Aquila Optimizer provide strong one-shot optimization capabilities, they lack the ability to improve performance over time or generalize across dynamically changing conditions. Model-free RL addresses this gap by enabling agents to autonomously learn policies through repeated interactions with the environment, without requiring a predefined model of system dynamics.

In model-free RL, decision-making is governed by the principle of trial-and-error learning. The agent perceives the system state, selects an action, and updates its policy based on the reward feedback received. This cycle repeats over time, allowing the agent to refine its behavior by accumulating experience. Importantly, the agent does not require prior knowledge of the underlying mobility patterns, interference statistics, or user-channel mappings. Instead, it infers optimal allocation strategies by observing how past actions influence long-term performance objectives. This makes

RL particularly suitable for wireless networks, where channel conditions, user distributions, and interference patterns are too complex to be modeled analytically [122, 150].

The proposed method adopts the Deep Deterministic Policy Gradient (DDPG) algorithm, an actor-critic framework designed for environments with continuous action spaces, as illustrated in Figure 5.3 [111]. The DDPG agent learns a deterministic policy that maps complex system observations, such as channel frequency responses (CFRs), historical allocations, and spectral congestion indicators, to frequency subband allocation decisions. Compared to discrete-action methods like Q-learning or Deep Q-Networks (DQN) [127], DDPG is more scalable in large systems, as it avoids the combinatorial explosion of action enumeration.

The environment is formalized as a Markov Decision Process (MDP), where the agent operates over sequential time steps t . At each step, it observes the state s_t , which encodes CFR matrices, user-subband mappings, and interference metrics. Based on this observation, the actor network generates a continuous action vector a_t , which determines the allocation decisions. The scalar reward r_t received in response reflects a weighted combination of spectral efficiency, fairness (via the Gini index), and interference suppression (via eigenvalue dispersion):

$$r_t = w_{SE} \cdot \eta(t) - w_{Gini} \cdot \text{Gini}(t) - w_{EVD} \cdot \text{EVD}(t) \quad (5.2)$$

This reward structure enables the agent to balance multiple system objectives over time.

The training process unfolds within a high-fidelity simulation environment powered by QuaDRiGa, which generates spatially and temporally consistent CFRs under realistic vehicular mobility. Unlike conventional simulators that rely on static snapshots,

QuaDRiGa ensures coherent evolution of the wireless environment, enabling the RL agent to learn policies that adapt to smooth variations in user positions and fading characteristics.

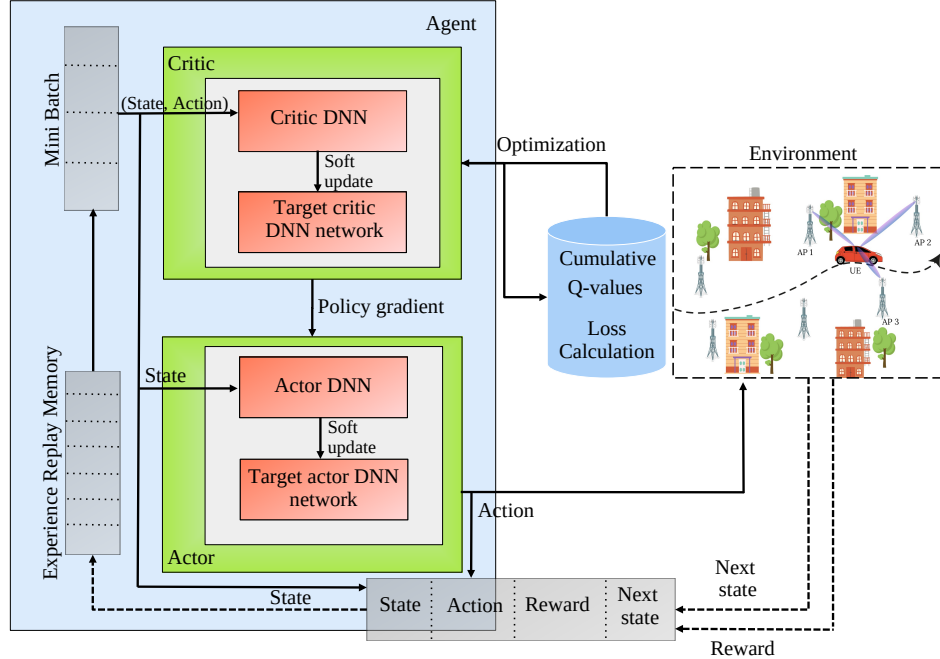


Figure 5.3: Deep Deterministic Policy Gradient (DDPG) agent for frequency sub-band allocation in UC-CFmMIMO systems. The actor network generates continuous allocation scores from observed CFRs, while the critic network estimates the value of state-action pairs for policy optimization.

By learning through interaction rather than pre-programmed rules, the RL agent adapts to new environments and user distributions without needing structural reconfiguration. This behavior is especially critical in UC-CFmMIMO networks, where user-centric clusters evolve, interference profiles shift, and subband reuse patterns must remain agile. Ultimately, RL enables the design of frequency allocation policies that are responsive, fair, and efficient, despite the stochastic, frequency-dependent nature of modern wireless systems.

However, one major challenge in model-free RL is exploration: during training, agents must sample enough of the solution space to identify good policies, yet avoid instabil-

ity caused by overly random behavior. To mitigate this, the next section introduces a hybrid approach that leverages the Aquila Optimizer as a guided exploration mechanism, thereby improving learning efficiency and convergence stability.

5.4.3 Hybrid Optimization Framework: AO-Assisted Actor-Critic Learning

While both metaheuristic and reinforcement learning (RL) techniques offer powerful capabilities for resource allocation in UC-CFmMIMO systems, each has limitations when applied in isolation. Metaheuristic approaches, such as the Aquila Optimizer (AO), excel in global exploration of complex solution spaces but lack memory and adaptability, resulting in static decision patterns that do not improve over time [17, 144]. On the other hand, RL frameworks like Deep Deterministic Policy Gradient (DDPG) are highly adaptive and capable of learning fine-grained policies through environmental interaction, but they often suffer from inefficient exploration and slow convergence in high-dimensional, non-convex spaces [150, 111, 74].

To overcome these complementary limitations, we propose a hybrid optimization framework that integrates AO with the actor-critic structure of DDPG. The core idea is to exploit AO’s ability to generate high-quality exploratory actions in the early stages of training, thereby guiding the RL agent toward promising regions of the action space. Meanwhile, the actor-critic mechanism refines these actions over time using gradient-based learning and reward-driven policy improvement. This hybrid design reflects a broader trend in AI optimization research, where combining nature-inspired and learning-based methods has shown superior performance in complex environments [68, 174].

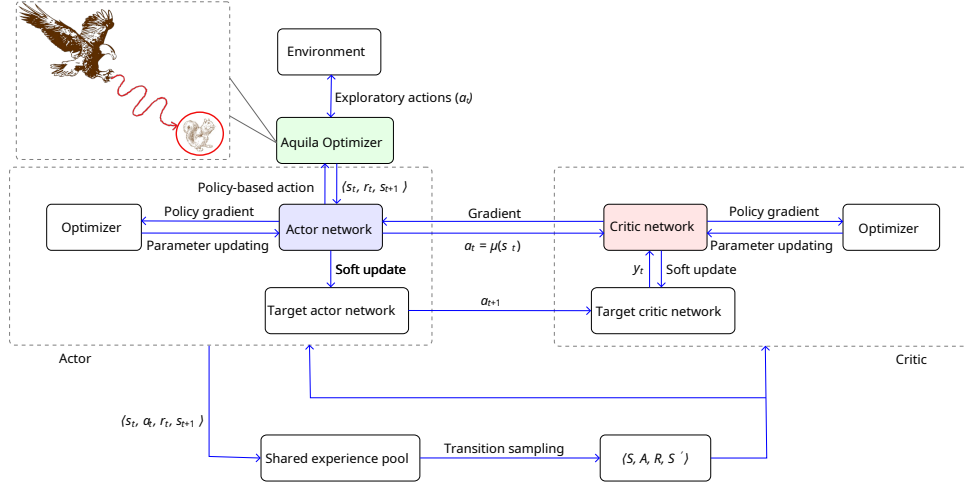


Figure 5.4: Hybrid AO-enhanced reinforcement learning architecture integrating Aquila-based exploration with DDPG’s actor-critic framework.

The hybrid agent operates as follows. At the beginning of each training episode, the system initializes the actor and critic networks along with their target counterparts. During each interaction step, the AO module proposes exploratory actions based on the current system state, which are then applied to the environment. The resulting state transitions and rewards are stored in a replay buffer, forming a shared experience pool that feeds the critic network. Using these samples, the critic estimates the Q-value of state-action pairs, while the actor updates its policy via the deterministic policy gradient. Target networks are softly updated to stabilize training and prevent divergence.

As illustrated in Figure 5.4, the AO component augments the actor’s decision pathway by enriching the exploration process, especially in the initial training stages where uninformed random exploration can lead to suboptimal convergence. By steering exploration toward high-potential solutions, AO improves the diversity and quality of experiences stored in the buffer, ultimately enhancing the sample efficiency and learning stability of the DDPG agent [68, 155]. Over time, the actor network learns

Algorithm 5.1: Hybrid AO with AC-RL

```

1: Initialize: Actor network  $\mu(s|\theta^\mu)$ , Critic network  $Q(s, a|\theta^Q)$ 
2:   Initialize Target networks:  $\theta^{\mu'} \leftarrow \theta^\mu$ ,  $\theta^{Q'} \leftarrow \theta^Q$ 
3:   Initialize replay buffer  $\mathcal{D}$ 
4: for each episode do
5:   Reset environment and obtain initial state  $s_0$ 
6:   for each timestep  $t$  do
7:     Exploration: Use AO to generate exploratory action  $a_t$ 
8:     Execute action  $a_t$  in the environment, observe reward  $r_t$  and next
      state  $s_{t+1}$ 
9:     Store transition  $(s_t, a_t, r_t, s_{t+1})$  in replay buffer  $\mathcal{D}$ 
10:    Critic Update:
11:      Sample a mini-batch  $(s, a, r, s')$  from  $\mathcal{D}$ 
12:      Compute target value:  $y_t = r + \gamma Q'(s', \mu'(s')|\theta^{Q'})$ 
13:      Compute loss:  $L = (y_t - Q(s, a|\theta^Q))^2$ 
14:      Update Critic network  $\theta^Q$  by minimizing  $L$ 
15:    Actor Update:
16:      Compute policy gradient  $\nabla_{\theta^\mu} J = \mathbb{E}[\nabla_a Q(s, a|\theta^Q) \nabla_{\theta^\mu} \mu(s|\theta^\mu)]$ 
17:      Update Actor network  $\theta^\mu$  using gradient ascent
18:    Target Networks Soft Update:
19:       $\theta^{Q'} \leftarrow \tau \theta^Q + (1 - \tau) \theta^{Q'}$ 
20:       $\theta^{\mu'} \leftarrow \tau \theta^\mu + (1 - \tau) \theta^{\mu'}$ 

```

to replicate and refine the strategies initially suggested by AO, leading to faster convergence toward high-quality policies.

The full hybrid algorithm is detailed in Algorithm 5.1, where the integration between AO’s global search and DDPG’s adaptive learning is explicitly implemented at each decision step. This structure enables the framework to address the key optimization goals in UC-CFmMIMO systems, namely maximizing spectral efficiency, reducing interference, and maintaining fairness, under dynamic and frequency-selective channel conditions.

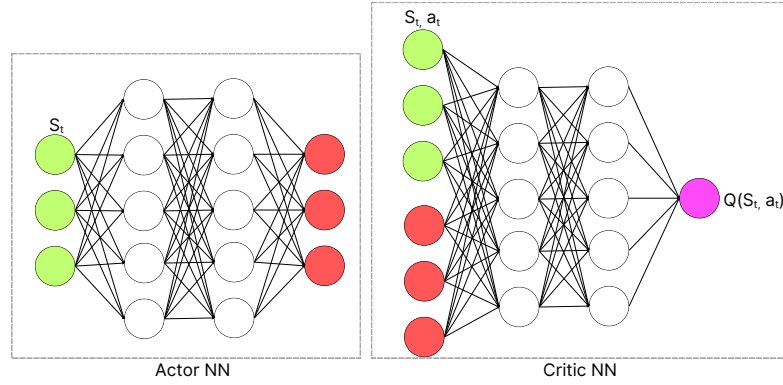


Figure 5.5: Architecture of Actor and Critic deep neural networks (DNNs).

5.4.4 Architecture and Training Dynamics of the DDPG Framework

The actor-critic reinforcement learning strategy employed in this work is based on the Deep Deterministic Policy Gradient (DDPG) algorithm, which enables effective control in continuous action spaces, an essential property for fine-grained subband allocation in CFmMIMO systems. The architecture is composed of two core components: an actor network that learns a deterministic policy for resource allocation, and a critic network that evaluates the expected return for each action-state pair.

As shown in Figure 5.5, both the actor and critic are implemented as deep neural networks (DNNs). The actor receives a high-dimensional input vector representing the system state, which includes user-cluster associations, CFR matrices, and interference indicators. It processes this input through two fully connected layers with ReLU activation, and produces a continuous-valued allocation vector. The final softmax layer ensures normalized output suitable for subband selection. The critic, in contrast, takes the concatenated state-action pair and estimates the scalar Q-value through a similar layered structure. This parallel network design allows the agent to independently model the policy and the value function while enabling joint optimization during training [111, 151].

Training follows a standard actor-critic update protocol. The critic is updated by minimizing the temporal difference (TD) error:

$$\mathcal{L}_{\text{critic}} = \mathbb{E}[(y_t - Q(s_t, a_t))^2], \quad (5.3)$$

where the target value y_t is computed using the target networks:

$$y_t = r_t + \gamma Q'(s_{t+1}, \mu'(s_{t+1})). \quad (5.4)$$

Critic weights θ_Q are updated via gradient descent:

$$\theta_Q \leftarrow \theta_Q - \alpha_Q \nabla_{\theta_Q} \mathcal{L}_{\text{critic}}. \quad (5.5)$$

Simultaneously, the actor is trained to maximize the Q-value of the selected actions by ascending the gradient of the expected return:

$$\nabla_{\theta_\mu} J = \mathbb{E} \left[\nabla_a Q(s, a) \Big|_{a=\mu(s)} \nabla_{\theta_\mu} \mu(s) \right], \quad (5.6)$$

with actor parameters updated as:

$$\theta_\mu \leftarrow \theta_\mu + \alpha_\mu \nabla_{\theta_\mu} J. \quad (5.7)$$

To stabilize learning, target networks for both actor and critic are maintained and softly updated:

$$\theta' \leftarrow \tau \theta + (1 - \tau) \theta', \quad (5.8)$$

where τ is a small smoothing parameter. This approach mitigates rapid shifts in Q-value estimation and prevents oscillations in policy learning [127, 67].

The agent also leverages a replay buffer to store state transitions (s_t, a_t, r_t, s_{t+1}) , from which random mini-batches are drawn during training. This breaks temporal correlation between samples and improves sample efficiency [113, 148]. Exploration is initially driven by adding noise to the actor’s output or by sampling AO-generated exploratory actions in the hybrid framework. Over time, the exploration rate is reduced to favor exploitation of the learned policy.

Overall, this training pipeline provides a robust mechanism for learning effective, environment-aware frequency allocation strategies in large-scale, user-dense wireless systems. Its modular design also allows seamless integration with metaheuristic guidance, as demonstrated in the hybrid approach.

5.4.5 Hyperparameter Tuning and Optimization of the DDPG Agent

Effective training of deep reinforcement learning models is highly sensitive to the choice of hyperparameters, which govern the stability, convergence rate, and generalization of learned policies. In the context of the proposed DDPG-based resource allocation framework, we employed a random search strategy to explore combinations of critical hyperparameters, including learning rates, discount factors, batch sizes, buffer sizes, and the target network update coefficient.

Random search has been widely recognized as a robust hyperparameter optimization technique in deep learning applications [32], offering higher search efficiency than grid search in high-dimensional spaces. For this study, each hyperparameter was sampled uniformly within empirically motivated bounds from reinforcement learning literature and prior DDPG implementations [81, 111]. The selected ranges are summarized in Table 5.2, which includes values for the actor and critic learning rates (α_π, α_Q) , the discount factor γ , soft update coefficient τ , and exploration noise magnitude.

Table 5.2: Hyperparameter Ranges Used in Random Search.

Hyperparameter	Range	Reference
Actor learning rate (θ_π)	10^{-5} to 10^{-3}	[60]
Critic learning rate (θ_Q)	10^{-5} to 10^{-3}	[60]
Discount factor (γ)	0.9 to 0.99	[180]
Replay buffer size	10^4 to 10^6	[160]
Batch size	32 to 256	[29]
Soft update coefficient (τ)	0.001 to 0.01	[29]
Exploration noise magnitude	0.1 to 0.5	[117]

To evaluate the impact of each sampled configuration, six training trials were executed using different hyperparameter sets. Performance was assessed based on convergence speed, cumulative reward stability, and the evolution of the actor and critic loss functions. Figures 5.6 and 5.7 illustrate the progression of loss values over time for each configuration.

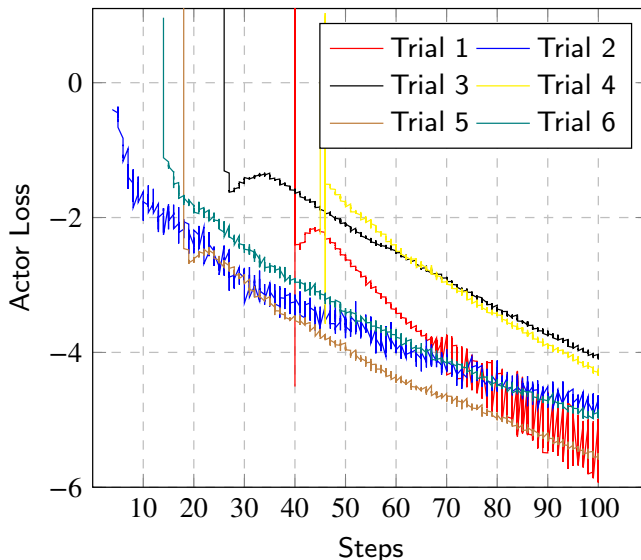


Figure 5.6: Evolution of actor loss for six hyperparameter configurations. Trial 5 exhibits the most consistent convergence.

Among all tested configurations, Trial 5 emerged as the best-performing setup. It achieved stable and rapid convergence in both actor and critic loss, reaching a final actor loss of approximately -6 and exhibiting minimal Q-value variance. This outcome

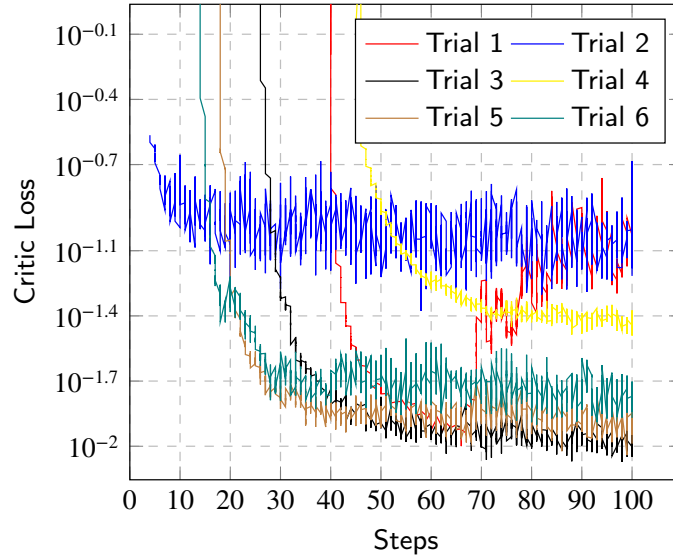


Figure 5.7: Critic loss curves across training trials. Trial 5 achieves the lowest final error with minimal variance.

indicates effective policy learning and value approximation under complex vehicular CFmMIMO conditions. The corresponding hyperparameters included a learning rate of 0.00226 for both actor and critic networks, a discount factor $\gamma = 0.882$, a replay buffer size of 30,397, and a batch size of 272. These values struck a favorable balance between aggressive learning and stable updates, allowing the agent to both explore and converge efficiently.

This result underscores the importance of principled hyperparameter selection in reinforcement learning applications. Without exhaustive search, the random strategy enabled efficient discovery of a configuration that significantly outperformed others in training consistency and final reward potential. The selected parameters were adopted in all subsequent evaluations of the DDPG and hybrid frameworks.

5.4.6 Computational Complexity Analysis

This section analyzes the computational complexity associated with the three resource allocation strategies explored in this work: Alternating Optimization (AO), Actor-Critic Reinforcement Learning (AC-RL), and the proposed Hybrid Reinforcement Learning Method (HRLM), which integrates AO into the reinforcement learning loop.

Alternating Optimization (AO): AO relies on deterministic updates over a population of candidate solutions and is well-suited to structured optimization problems involving continuous variables. Its complexity arises from repeated evaluations of the objective function and matrix operations such as channel projections and precoder updates. The per-iteration cost scales quadratically with the population size N , and linearly with the number of users K , subbands S , and access points L . For a total of T iterations, the computational complexity of AO is given by:

$$\mathcal{C}_{\text{AO}} = \mathcal{O}(T \cdot N^2 \cdot K \cdot S \cdot L). \quad (5.9)$$

While AO achieves good performance in terms of spectral efficiency and fairness, its computational cost becomes significant as network scale increases, limiting its scalability in systems with strict timing constraints.

Actor-Critic Reinforcement Learning (AC-RL): In contrast to AO, AC-RL is a learning-based method whose complexity is governed by the training of neural networks via forward and backward propagations. The key computational load originates from the mini-batch processing of transitions, backpropagation through multiple dense layers, and gradient updates of both actor and critic networks. Let B be the batch size, D the number of layers, and N_{neurons} the number of neurons per

layer. The per-iteration training complexity is approximately:

$$\mathcal{C}_{\text{AC-RL}} = \mathcal{O}(T \cdot B \cdot D \cdot N_{\text{neurons}}^2). \quad (5.10)$$

This complexity is independent of the number of users or subbands during inference, enabling efficient decision-making under tight timing requirements after training, but the offline training phase is computationally intensive and requires careful tuning and regularization to ensure generalization.

Hybrid Reinforcement Learning with AO (HRLM): The HRLM framework combines the strengths of both AO and AC-RL by injecting AO-based exploration into the actor-critic loop, particularly during early training epochs. While the core training cost remains that of AC-RL, an additional AO-driven search phase introduces an auxiliary complexity component that depends on the AO population size P , the number of AO iterations per training step I , and the network parameters K and S . The total complexity of HRLM becomes:

$$\mathcal{C}_{\text{HRLM}} = \mathcal{O}(T \cdot B \cdot D \cdot N_{\text{neurons}}^2) + \mathcal{O}(P \cdot I \cdot K \cdot S). \quad (5.11)$$

This formulation maintains the adaptive benefits of deep reinforcement learning while leveraging the structure of AO to guide early-stage exploration. Despite the added cost, HRLM improves sample efficiency and convergence speed, offering a practical trade-off between training overhead and policy quality.

Summary: Table 5.3 summarizes the asymptotic complexities of all three approaches. The hybrid HRLM design stands out as a scalable and efficient strategy, particularly well-suited for dynamic, frequency-selective environments where policy adaptability and structural guidance are both critical.

Table 5.3: *Asymptotic Computational Complexity of the Proposed Methods*

Method	Complexity Expression
Alternating Optimization (AO)	$\mathcal{O}(T \cdot N^2 \cdot K \cdot S \cdot L)$
Actor-Critic RL (AC-RL)	$\mathcal{O}(T \cdot B \cdot D \cdot N_{\text{neurons}}^2)$
Hybrid RL with AO (HRLM)	$\mathcal{O}(T \cdot B \cdot D \cdot N_{\text{neurons}}^2) + \mathcal{O}(P \cdot I \cdot K \cdot S)$

In summary, this section introduces a complete and scalable learning-based solution to frequency resource allocation in CFmMIMO networks. It combines the global search ability of metaheuristics with the adaptability of reinforcement learning, forming a powerful framework for efficient and adaptive decision-making in complex wireless systems.

5.5 Numerical Results

This section presents an in-depth evaluation of the proposed reinforcement learning and hybrid resource allocation approaches for UC-CFmMIMO systems operating under frequency-selective channels in dense vehicular environments. The objective is to benchmark the performance of the hybrid AO-AC-RL solution (referred to as HYM) against two standalone baselines: the Aquila Optimizer (AO) and the Actor-Critic-based Reinforcement Learning model (AC-RL, also referred to as RLM). The assessment encompasses various metrics, including convergence behavior, spectral efficiency (SE), fairness, and scalability with increasing user densities and available subband resources.

The numerical simulations are conducted based on the channel frequency responses generated via the QuaDRiGa simulator, using the 3GPP UMi-Street Canyon model. The UC-CFmMIMO architecture operates at 5.9 GHz with a bandwidth of 50 MHz subdivided into 277 subbands. The system includes $L = 100$ access points (APs),

each equipped with $N = 4$ antennas, serving $K = 40$ user equipments (UEs) with single-antenna configurations.

Figure 5.8 illustrates the convergence of the objective function over iterations for each of the three algorithms. The AO demonstrates the slowest convergence, stabilizing around an objective value of 0.6, reflecting its lack of adaptation over time. Although it provides a globally explorative search, it lacks the temporal refinement capability required in highly dynamic systems. On the other hand, the AC-RL model exhibits faster convergence, reaching a higher objective value close to 0.95. However, it suffers from moderate fluctuations, hinting at occasional instability and suboptimal policy refinement due to insufficient exploration. The hybrid model, which combines the structured exploration of AO with the adaptive learning power of AC-RL, surpasses both in terms of convergence speed and final performance. It quickly reaches an objective value near 1.0 and remains stable, demonstrating a well-balanced exploration-exploitation trade-off.

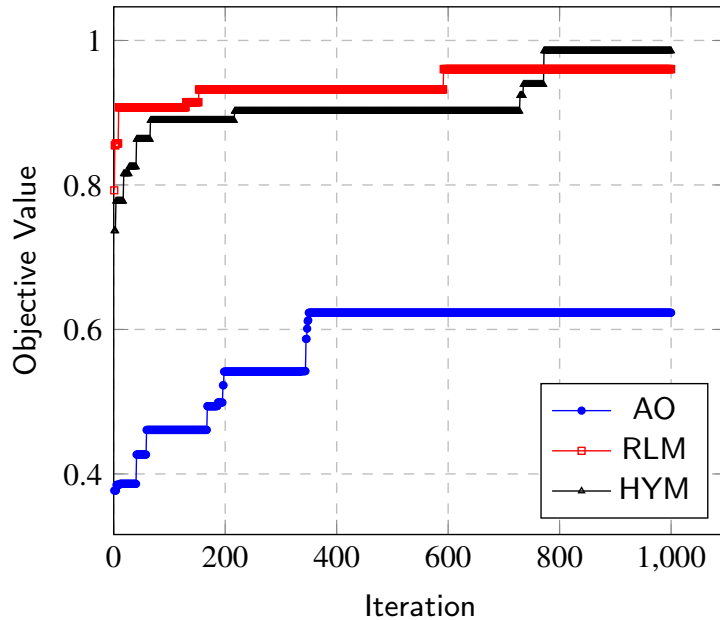


Figure 5.8: Objective value convergence comparison for AO, AC-RL, and HYM approaches.

To further examine the impact of the allocation strategies on system throughput, Figure 5.9 plots the evolution of spectral efficiency (SE) over time. AO stabilizes at approximately 100 bps/Hz, confirming its limited adaptability. The AC-RL approach improves this to nearly 200 bps/Hz but exhibits oscillations that may affect reliability. In contrast, the hybrid HYM method achieves the highest and most stable SE, surpassing 200 bps/Hz. This outcome underscores the value of combining AO’s exploration with AC-RL’s policy optimization to unlock higher SE in challenging wireless settings.

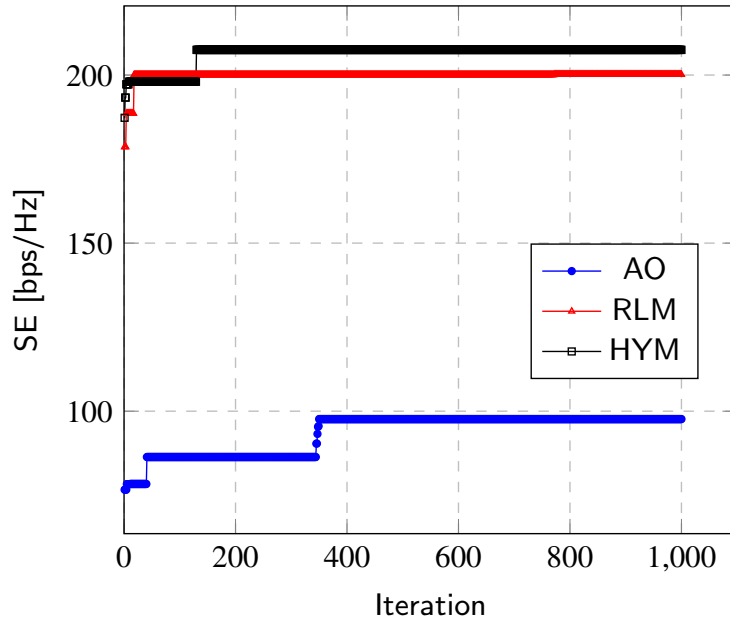


Figure 5.9: Spectral efficiency (SE) evolution across iterations for the three algorithms.

Beyond throughput, fairness in frequency resource distribution is critical for system-wide quality of service. The Gini index is adopted to quantify fairness, where lower values indicate more equitable distribution among users. Figure 5.10 shows that AO maintains a Gini index of around 0.05, implying a fairly uniform allocation but at the cost of efficiency. AC-RL tends to prioritize SE, leading to slightly higher imbalance with a Gini index near 0.1. The hybrid solution achieves the best fairness-efficiency balance, gradually converging to a Gini index of approximately 0.02 while

maintaining high SE. This result confirms the hybrid strategy’s ability to adaptively manage conflicting optimization goals.

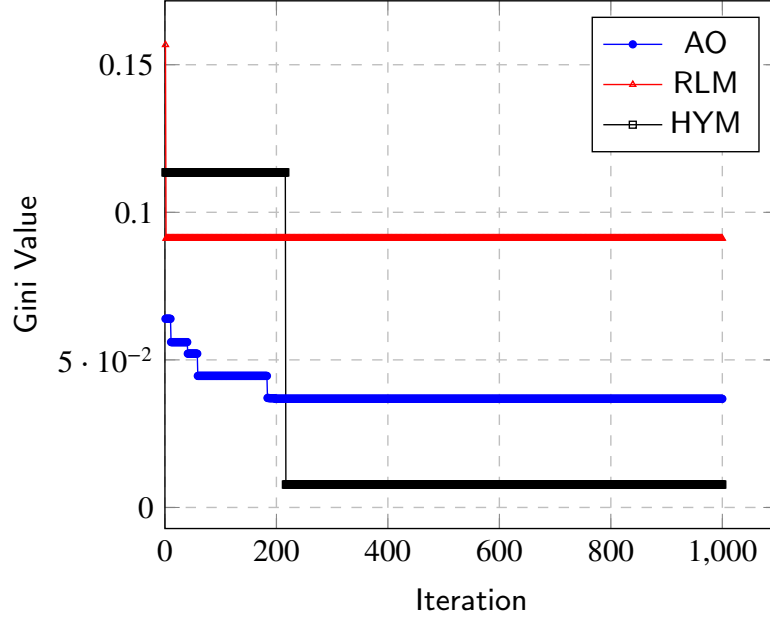


Figure 5.10: Gini index evolution over iterations for AO, AC-RL, and HYM.

To evaluate the scalability and robustness of the proposed hybrid framework under network densification, we analyze the SE performance with increasing UE densities while keeping the number of available subbands constant at 40. Figure 5.11 displays the SE results for 40, 60, and 80 UEs. As expected, performance decreases with more UEs due to intensified interference and resource contention. However, the hybrid method maintains acceptable SE, reducing gracefully from about 200 bps/Hz to 110 bps/Hz, indicating its scalability and resilience under congestion.

Finally, Figure 5.12 assesses how increasing the number of available subbands influences SE. As more subbands become available (40, 80, and 120), the SE rises accordingly, with the hybrid model consistently outperforming its counterparts. At 120 subbands, SE reaches around 225 bps/Hz, showcasing the hybrid method’s capacity to efficiently exploit additional spectrum.

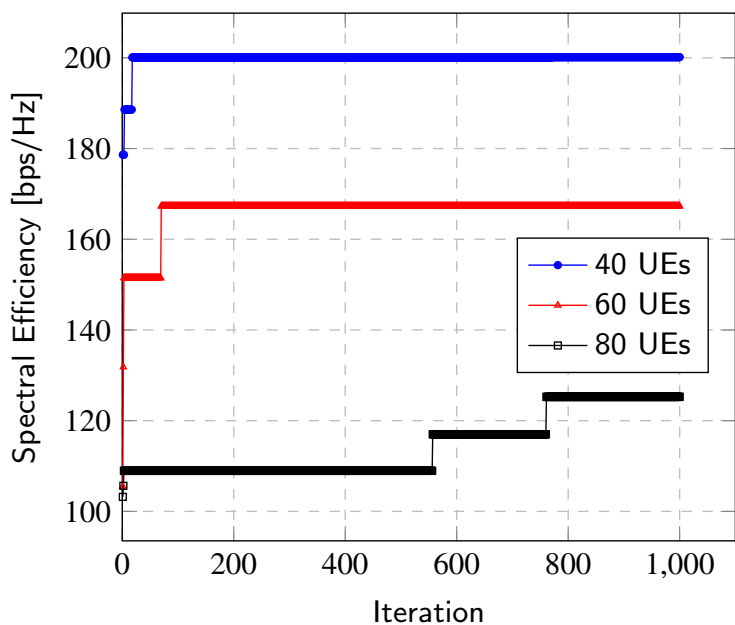


Figure 5.11: SE comparison across increasing user densities (40, 60, and 80 UEs).

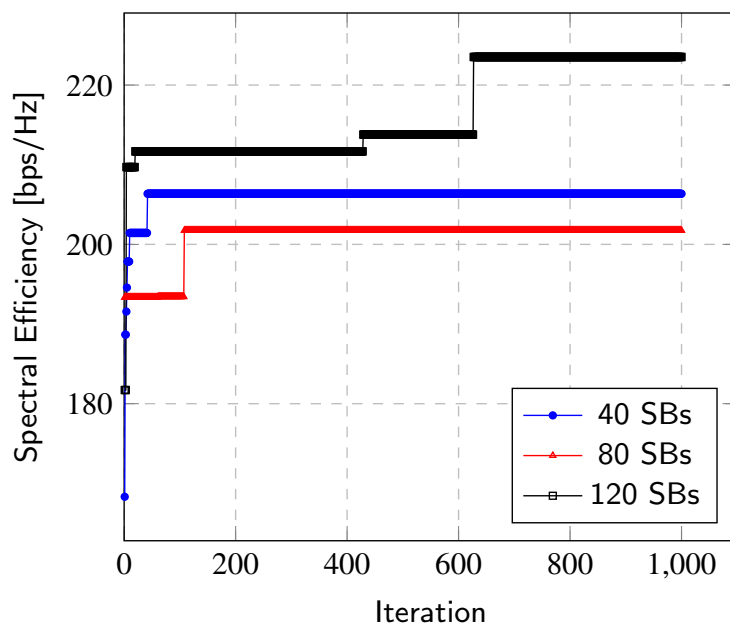


Figure 5.12: SE variation with different subband allocations (40, 80, and 120 subbands).

In summary, the numerical results demonstrate that while AO and AC-RL offer distinct benefits, their combination within the proposed hybrid framework yields superior

performance across all measured criteria. The HYM solution not only enhances SE and fairness but also maintains robustness under dense and dynamic network conditions, thereby providing a compelling strategy for responsive frequency resource allocation in next-generation UC-CFmMIMO systems.

5.6 Conclusion and Future Scope of Work

In this chapter, we presented a comprehensive investigation into learning-based strategies for frequency resource allocation in user-centric cell-free massive MIMO (UC-CFmMIMO) systems, operating under dynamic and frequency-selective wireless environments. Building upon the limitations observed in purely heuristic and metaheuristic methods, this chapter introduced a novel, adaptive framework that integrates reinforcement learning (RL) and bio-inspired optimization to effectively manage the complexity of dense vehicular communication systems.

The reinforcement learning solution was developed using an Actor-Critic (AC-RL) architecture based on the Deep Deterministic Policy Gradient (DDPG) algorithm. This model-free approach enabled the agent to learn allocation policies by interacting with the environment, without requiring a priori modeling of system dynamics. The actor network proposed subband allocations based on state observations, while the critic network evaluated the quality of these decisions, leading to gradual policy improvement over time. Despite its adaptability and sample efficiency, standalone RL showed sensitivity to exploration quality, especially during early training stages.

To address this challenge and further enhance convergence, we proposed a hybrid strategy combining the Aquila Optimizer (AO) with the AC-RL model. This hybrid approach leveraged AO's structured exploration behavior to enrich the agent's action space, particularly in the early stages of learning. By guiding the reinforcement

learning process toward promising regions of the solution space, the hybrid method improved both convergence speed and final performance. Simulation results confirmed that this integrated framework outperforms both AO and AC-RL individually in terms of spectral efficiency, fairness, and robustness to user density and network dynamics.

The success of this hybrid learning framework highlights the potential of combining structured optimization with adaptive, data-driven control in next-generation wireless systems. However, several opportunities remain open for future research:

- **Practical Deployment:** Extending the current simulation-based framework to support time-sensitive decision-making on physical testbeds or software-defined radio platforms would provide important practical validation.
- **Multi-Agent Reinforcement Learning (MARL):** Incorporating cooperative or competitive multi-agent systems, where multiple RL agents coordinate resource allocation across distributed APs, could further decentralize control and improve scalability.
- **QoS-Driven Learning Objectives:** Future work could integrate latency constraints, energy efficiency targets, and user-specific QoS profiles into the reward function, making the agent sensitive to more diverse performance metrics.
- **Transfer and Meta-Learning:** Leveraging transfer learning could allow pre-trained agents to quickly adapt to new environments, while meta-learning could enable fast retraining in response to topology or traffic pattern changes.
- **Explainability and Interpretability:** Exploring explainable RL models would help interpret and validate the learned allocation policies, which is essential for safety-critical applications such as vehicular networks and industrial automation.

In conclusion, this chapter marks a significant step toward intelligent, adaptive resource management for UC-CFmMIMO systems. The hybrid learning paradigm introduced here provides a powerful foundation for future research in autonomous wireless networks and aligns closely with the goals of 6G and beyond.

Chapter 6

ADVERSARIAL MACHINE LEARNING IN UC-CFMMIMO: VULNERABILITIES IN FREQUENCY-DOMAIN CHANNEL PREDICTION

Publication Note

This chapter is based on the following peer-reviewed publication, accepted for presentation at the *30th European Symposium on Research in Computer Security (ESORICS 2025)*, to be held in Toulouse, France, from 22 to 26 September 2025 [71].

6.1 Introduction

The methodological arc pursued throughout this thesis has progressively advanced from rule-based and metaheuristic optimization techniques to data-driven, model-free intelligence for frequency resource allocation in user-centric cell-free massive MIMO (UC-CFmMIMO) systems. In doing so, it has addressed the escalating complexity of wireless environments, especially vehicular scenarios characterized by mobility, fading, and spectral dynamics, through increasingly adaptive computational paradigms. As the architectural shift toward native AI continues to define 6G system design, a critical and often underexplored dimension now demands attention: the *security and robustness* of the machine learning (ML) models that drive such intelligent control systems.

In previous chapters, the emphasis was placed on maximizing system performance metrics such as spectral efficiency, fairness, and interference mitigation via intelligent

scheduling and predictive modeling. These approaches, while effective in idealized settings, implicitly assume the *reliability and trustworthiness* of the underlying learning components. However, recent advances in adversarial machine learning (AML) have revealed that ML models, particularly those integrated into physical-layer functions, are susceptible to *imperceptible, malicious perturbations* capable of degrading performance and compromising system stability [138, 30, 184].

This chapter investigates, for the first time within this thesis, the *security vulnerabilities* of ML-based gain prediction models in UC-CFmMIMO architectures operating under *realistic vehicular conditions*. We explore a black-box adversarial threat model that leverages surrogate learning and frequency-domain attacks to manipulate channel state predictions, which are critical inputs for resource allocation. In doing so, the chapter marks a conceptual transition from control and optimization to *trust and resilience*, framing adversarial robustness as a prerequisite for the safe deployment of intelligent 6G networks [153, 48].

Particularly, we focus on the exploitation of frequency-selective fading and the temporal dynamics of vehicular networks to *craft subtle, transferable adversarial perturbations* using the Fast Gradient Sign Method (FGSM) [73]. These perturbations are injected via *uplink pilot contamination*, a realistic attack vector in modern MIMO systems [189, 131]. Despite their low magnitude, the crafted signals induce *significant deviations in channel gain predictions*, triggering downstream misallocations and fairness violations, while remaining difficult to detect using conventional ML-based anomaly detectors [15, 35].

This security-centric inquiry is tightly coupled to the broader goals of this thesis: enabling scalable, intelligent, and robust UC-CFmMIMO networks. By exposing critical vulnerabilities in ML-based prediction pipelines, the present chapter provides not only a cautionary perspective but also a technical foundation for future research

into *adversarially resilient resource management strategies*. In the context of vehicular networks, where latency, reliability, and safety are paramount, such robustness is not merely desirable but essential.

The contributions of this chapter can be summarized as follows:

- **Systematic adversarial modeling:** We formalize a black-box adversarial attack strategy in UC-CFmMIMO systems, targeting frequency-domain channel gain prediction modules through surrogate-based FGSM perturbations [71].
- **Stealth-aware attack design:** A local anomaly detector is embedded in the attacker pipeline to evaluate the detectability of perturbations prior to injection, simulating real-world stealth constraints [41, 35].
- **Simulation-driven validation:** Using QuaDRiGa for geometry-based channel modeling in urban vehicular scenarios, we empirically evaluate the degradation in prediction accuracy, detection sensitivity, and subband-user allocation consistency [41, 71].
- **Security-performance tradeoff analysis:** We demonstrate that even undetected adversarial inputs lead to measurable disruptions in scheduling decisions and fairness, emphasizing the need for adversarially robust ML architectures in physical-layer control [123, 124].

The remainder of this chapter is structured as follows. Section ?? reviews the background on adversarial machine learning in wireless systems. Section 6.2 describes the system architecture and the frequency-domain prediction pipeline. Section 6.3 formalizes the adversarial model and attack assumptions. Section 6.4 details the perturbation generation and stealth assessment procedures. In Section 6.5.2, we present simulation results and analyze their implications. Finally, Section 6.6 concludes the

chapter with reflections on adversarial resilience in 6G-enabled vehicular communications.

6.2 Channel Model

In continuity with the simulation framework introduced in Chapter 5, this chapter retains the same high-fidelity channel modeling setup based on the QuaDRiGa (QUAsi Deterministic RadIo channel GenerAtor) simulator [93]. Originally adopted to support reinforcement learning under realistic urban mobility conditions, this model now serves a dual purpose: it provides a physically coherent channel environment for evaluating the stealth, transferability, and impact of adversarial perturbations targeting frequency-domain channel gain predictors.

QuaDRiGa is specifically designed to simulate three-dimensional, time-evolving wireless propagation environments, incorporating directionality, frequency selectivity, and Doppler effects, features that are indispensable for modeling vehicular UC-CFmMIMO deployments in 6G networks [8, 94]. It supports both clustered delay line (CDL) and geometry-based stochastic channel models (GBSMs), enabling realistic characterization of Line-of-Sight (LoS) and Non-Line-of-Sight (NLoS) conditions across dense urban microcellular environments.

The structural parameters of the simulated network are preserved from prior chapters: $L = 100$ distributed access points (APs), each with $N = 4$ antennas, jointly serve $K = 40$ single-antenna user terminals (UTs) in a $2 \text{ km} \times 2 \text{ km}$ urban area. APs are connected to a central processing unit (CPU) via fronthaul links to enable centralized scheduling and gain estimation. The system operates in the 5.88–5.92 GHz vehicular communication band, partitioned into S orthogonal frequency subbands, each governed by dynamic channel conditions.

The downlink channel between AP l and UT k on subband s is denoted as $h_{k,l,s} \in \mathbb{C}^{1 \times N}$ and generated through QuaDRiGa’s GSCM model, embedding realistic temporal evolution and multipath dynamics. The aggregated global channel vector is expressed as:

$$\mathbf{h}_{k,s} = [h_{k,1,s}, h_{k,2,s}, \dots, h_{k,L,s}] \in \mathbb{C}^{1 \times NL} \quad (6.1)$$

and constitutes the input to the ML-based channel gain predictor at the CPU.

For adversarial evaluation, the realism and continuity of this channel model are essential. They ensure that perturbations crafted via surrogate models trained on proxy measurements remain transferable to the target environment, a critical assumption in black-box attack scenarios [138, 71]. Moreover, the dynamic yet consistent evolution of channel conditions enables the simulation of temporally localized attacks, such as pilot contamination events, that exploit short-term prediction vulnerabilities without triggering detection via abrupt anomalies.

As in the previous chapter, user mobility is internally managed by QuaDRiGa without reliance on external simulators such as SUMO. User trajectories, velocities, and angular dynamics are directly embedded into the channel generation process, producing coherent Doppler spreads and spatial fading patterns that mirror realistic urban vehicular environments [115, 85, 165].

In summary, the use of QuaDRiGa in this chapter provides not only geometric and temporal realism for system-level evaluation but also a robust foundation for adversarial experimentation. Its capabilities enable the attacker to collect proxy RF data in spatially similar locations, train surrogate models, and inject perturbations in a manner that respects the physics of the channel, thereby ensuring the feasibility and credibility of the black-box threat model analyzed herein.

6.3 Threat Model

As UC-CFmMIMO systems evolve toward AI-native architectures, the increasing reliance on machine learning for physical-layer tasks, such as channel gain prediction and resource scheduling, introduces new security concerns. Among these, adversarial machine learning (AML) has emerged as a potent threat vector capable of manipulating model outputs through carefully crafted inputs that remain imperceptible at the signal level [138, 30].

This section formalizes a threat model tailored to the 6G vehicular UC-CFmMIMO scenario under study. The proposed adversarial attack targets the ML-driven frequency-domain gain predictor, which plays a critical role in subband-user allocation. Our focus lies on a black-box, physically realizable adversary who lacks direct access to the model’s architecture or training data, but who can collect environmental observations and inject malicious pilot signals during the uplink phase.

The model captures both the technical feasibility and operational constraints of adversarial manipulation within a realistic wireless setting. By clearly defining the attack pipeline, objectives, system knowledge, and practical limitations, we ensure that the analysis remains grounded in plausible deployment scenarios and highlights vulnerabilities that are not just theoretical, but exploitable in practice.

We now detail the adversarial model, the attacker’s objectives, its alignment with 3GPP standardization perspectives, and the practical boundaries of the threat.

6.3.1 Protocol-Level Vulnerability of Pilot Signals in 3GPP Networks

A key enabler of the proposed adversarial attack lies in the inherent vulnerability of pilot signals within the 3GPP protocol stack. Despite the growing integration of artificial intelligence (AI) in physical-layer tasks across emerging 6G systems, the transmission of pilot signals remains largely unprotected at the protocol level. This section examines the structural role of pilot signals, their security posture, and the feasibility of exploiting them for adversarial injection in UC-CFmMIMO networks.

Role and Structure of Pilot Signals. In 3GPP-compliant wireless systems, pilot signals, also known as reference signals, are deterministic sequences transmitted by user equipment (UE) or access points (APs) to facilitate channel estimation. These include Sounding Reference Signals (SRS) in the uplink and Demodulation Reference Signals (DMRS) in both uplink and downlink, as standardized in 3GPP TS 38.211. Their construction is deterministic, using sequences such as Zadoff-Chu, Gold, or pseudo-random QPSK, and their positions in the OFDM time-frequency grid are publicly defined and universally known to compliant devices [13].

Security Properties and Gaps. Unlike user-plane or control-plane data, which are protected via encryption and integrity checks defined in 3GPP TS 33.501, pilot signals operate purely at the physical layer. They are not encrypted, authenticated, or integrity-protected by design, so that any compliant receiver can decode them without additional overhead. While this facilitates low-latency channel estimation, it also leaves pilot signals exposed to adversarial manipulation.

Importantly, 3GPP standards currently lack mechanisms for per-symbol pilot authentication or cross-layer validation of pilot integrity. In scenarios involving massive MIMO or cell-free deployments, pilot reuse across multiple users becomes necessary

due to limited orthogonal sequences. This exacerbates vulnerability to spoofing and contamination, especially under user mobility and spatial reuse.

Attack Surface Realism. Given that pilot signal formats and positions are publicly known or inferable, a physically co-located adversary can accurately reproduce or slightly modify pilot sequences. Modern SDR platforms and ultra-wideband channel sounders enable precise timing and waveform generation in real-time. For example, [190] demonstrates a real-time channel sounder operating between 3 and 18 GHz with 2 GHz bandwidth per channel, designed for outdoor vehicular conditions. These tools make it feasible to collect training data, align with system timing, and inject signals with sub-microsecond precision.

Impact on AI-Based Channel Estimation. By exploiting these PHY-layer gaps, an adversary can inject adversarially perturbed pilot signals during the uplink training phase. Since these signals are used directly for estimating CSI, and in turn, feeding the ML-based gain predictor, any subtle perturbation introduced at this layer directly propagates into downstream resource allocation decisions. Crucially, because the attack targets a layer not covered by cryptographic protections, it remains undetected by conventional network-layer security mechanisms.

This gap between AI-driven physical-layer functionality and protocol-level security design represents a serious blind spot in current 6G architecture thinking. The feasibility and effectiveness of the proposed attack underscore the urgent need to re-evaluate pilot signal security, especially in AI-native architectures where ML models may be trusted inputs without proper validation.

6.3.2 Adversarial Model

The adversarial framework considered in this work reflects a realistic black-box threat model tailored to 6G vehicular UC-CFmMIMO networks, as illustrated in Figure 6.1. The attacker targets the ML-based frequency-domain channel gain predictor used at the central processing unit (CPU) to support subband allocation and beamforming decisions. The attacker operates externally with no access to the internal parameters or structure of the deployed model, but leverages passive measurements, channel reciprocity, and the transferability of adversarial examples to mount a two-phase attack. This setup models a physically realizable and scalable adversarial strategy in dynamic wireless environments.

Phase 1 — Passive Environmental Observation and Surrogate Model Construction. The attack begins with passive sensing. The adversary deploys a custom portable channel sounder within or near the operational region of the target UC-CFmMIMO deployment. While not co-located with access points (APs), the device is placed within a range that ensures spatially consistent multipath profiles with the legitimate users. This is supported by empirical findings on urban spatial correlation, where path loss and fading profiles exhibit high similarity across small geographic offsets [171].

To collect frequency-domain RF samples, the attacker may use commercially available or custom-built ultra-wideband (UWB) channel sounders. For instance, [190] presents a real-time UWB sounder operating over 3–18 GHz with 2 GHz bandwidth per channel, designed to support real-time acquisition in outdoor environments with fine temporal and spectral resolution. Such tools make it feasible for adversaries to collect realistic high-dimensional channel data without interfering with system operations.

Using this proxy dataset, the attacker trains a surrogate model $\hat{g}(\cdot)$ to approximate the behavior of the legitimate gain prediction module $g(\cdot)$. The model is selected to be differentiable, enabling the use of gradient-based adversarial algorithms. This phase exploits adversarial transferability by approximating the input-output mapping of the target model, even under black-box constraints [138].

Phase 2 — Adversarial Injection via Uplink Pilot Contamination. After crafting perturbations using the surrogate model, the adversary moves to the injection phase. A realistic attack pathway is enabled by impersonating a legitimate user and transmitting forged pilot sequences during the uplink training phase. Pilot contamination remains a known vulnerability in multi-user massive MIMO systems, where repeated or reused pilots can be exploited to inject artificial CSI at the receiver [189, 131].

This action does not require sophisticated hardware modifications; programmable SDR platforms such as USRP or BladeRF, widely used in academic and industry-grade testbeds, can be employed to transmit precisely timed uplink pilots on selected subcarriers. These systems allow attackers to align transmission timing, frequency band, and modulation parameters with legitimate UEs, making spoofing viable in realistic vehicular deployments.

To minimize detection risk, the adversary incorporates a locally trained anomaly detector that evaluates the stealthiness of each crafted perturbation. The classifier is trained using the same proxy data used for the surrogate model, and serves as a filter to ensure only low-detectability samples are injected, enhancing the attack’s stealth and persistence in live systems [35, 15].

This two-phase attack is designed to be both effective and stealthy under realistic conditions. It makes no assumptions about the internal structure of the victim model

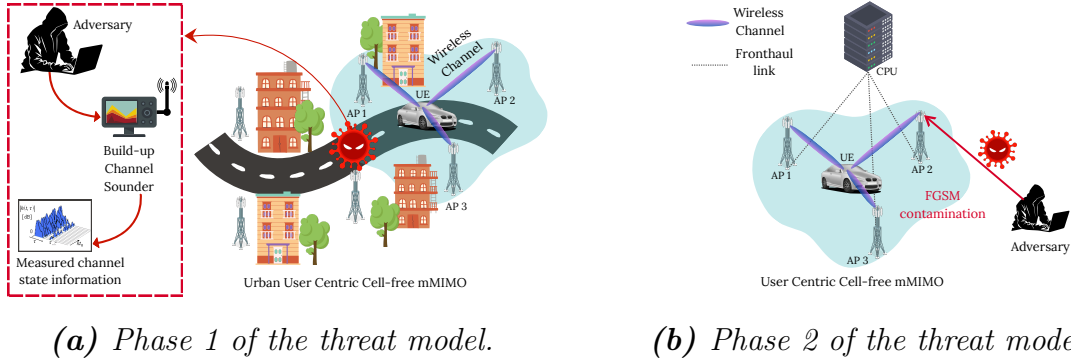


Figure 6.1: Overview of the two attack phases in the proposed threat model.

and requires no privileged access to system components. Instead, it relies on physical-layer phenomena, channel reciprocity, spatial consistency, and pilot reusability, combined with well-established ML vulnerabilities. As such, it exemplifies a plausible and concerning attack path in future AI-driven wireless infrastructures.

6.3.3 Adversary’s Goal

The primary objective of the adversary is to disrupt the machine learning-based frequency-domain channel gain prediction process in a stealthy and targeted manner. Specifically, the attacker seeks to induce small, imperceptible perturbations to the physical-layer uplink signals, namely pilot sequences, such that the resulting channel state information (CSI) estimates deviate from their true values. These deviations, once passed through the gain predictor, lead to erroneous channel gain forecasts that ultimately degrade the downstream resource allocation logic, including subband-user scheduling and power control.

This adversarial effect is crafted under the following operational goals:

- **Degradation of Resource Allocation Accuracy:** By corrupting the gain prediction output, the adversary causes suboptimal pairing between users and

subbands. This misalignment can result in increased inter-user interference, fairness violations, or overall reductions in spectral efficiency, all without compromising the structural validity of the ML output.

- **Stealth and Detection Evasion:** The attacker operates under the constraint of remaining undetected by any onboard or edge-based misbehavior detection systems (MDS). Perturbations are intentionally kept within a narrow ℓ_∞ or ℓ_2 norm bound and are filtered through a local anomaly detector prior to injection. This ensures that the manipulated input remains statistically consistent with clean data distributions [15, 35].
- **Transferability of Adversarial Examples:** The adversary must ensure that perturbations crafted using a locally trained surrogate model $\hat{g}(\cdot)$ are effective against the unknown target model $g(\cdot)$ deployed at the CPU. This requires the attack to generalize across variations in model architecture, training data, and hyperparameters, exploiting the well-documented transferability property of adversarial machine learning [138, 30].
- **Physical Feasibility and Protocol Compliance:** The attack must operate within the constraints of the 3GPP protocol stack. The injection is performed over pilot-bearing OFDM symbols, using realistic timing and frequency alignment achievable via SDR-based transmission. No cryptographic credentials or control-plane access is required, ensuring the attack remains compliant with current physical-layer assumptions [13, 189].

The adversary’s goal is thus not to create overt denial-of-service or catastrophic failure but rather to induce subtle, high-impact degradations in ML-driven decision-making pipelines. This type of attack reflects a new class of strategic, protocol-aware threats

tailored to intelligent wireless systems, where physical-layer inputs directly influence algorithmic decisions and system-wide performance.

6.3.4 Adversary’s Capability, Limitations, and the 3GPP Security Perspective

The integration of machine learning (ML) into the physical layer of 6G networks is advancing rapidly, driven by the promise of dynamic, data-driven decision-making in tasks such as beamforming, channel prediction, and resource allocation. However, this architectural shift has outpaced the evolution of formal security frameworks, particularly within the 3GPP standardization ecosystem, which remains focused on traditional cryptographic and access-layer threats.

Standardization Gaps in AI/ML Security. Current 3GPP technical specifications, such as TS 33.501 [12], define comprehensive encryption and integrity protection mechanisms for the control-plane (NAS, RRC) and user-plane (PDCP). However, no such provisions exist for ML models operating at the physical layer. Inputs to these models, such as channel estimates derived from pilot signals, are assumed trustworthy, despite being unauthenticated and unencrypted in practice.

This vulnerability stems from the fundamental design of physical-layer reference waveforms. PHY-layer signals such as pilot signals, Sounding Reference Signals (SRS), Demodulation Reference Signals (DMRS), and Channel State Information Reference Signals (CSI-RS) are all transmitted as raw, deterministic waveforms. Their structures and positions within the OFDM time-frequency grid are fully specified by 3GPP TS 38.211 [13], making them publicly known to all compliant devices. Critically, these signals are neither encrypted nor protected by integrity checks, as their function requires immediate decodability by receivers for channel estimation purposes.

As a result, adversaries with physical proximity and minimal hardware capabilities can observe, mimic, or slightly perturb these reference signals without violating any protocol constraints. This creates a regulatory blind spot: adversaries can manipulate pilot-bearing OFDM symbols at the PHY layer to influence AI outputs, while remaining fully compliant with transmission requirements. These vulnerabilities are particularly severe in ML-based gain prediction pipelines, where minor input perturbations can propagate into major misallocations in frequency resources.

Adversary’s Capabilities. Within this unprotected design space, the adversary is modeled as a physically co-located entity capable of both passive sensing and active pilot injection. The attacker does not require access to the internal structure or weights of the deployed ML model but can train a local surrogate $\hat{g}(\cdot)$ using RF samples collected via a wideband channel sounder or software-defined radio (SDR) [190]. The attacker can observe pilot structures and timing from over-the-air signals, leveraging their deterministic nature and public specification.

During the injection phase, the attacker uses SDR hardware (e.g., USRP, BladeRF) to transmit forged or modified pilot signals at the same time-frequency slots expected by the receiver. Timing, waveform shape, and modulation format can be synchronized with legitimate signals using well-known reverse-engineering techniques, such as synchronization to PSS/SSB frames in NR systems. No knowledge of cryptographic keys, authentication tokens, or system-side APIs is required.

Limitations and Assumptions. Despite its capabilities, the adversary is bounded by several practical and physical-layer constraints:

- *No access to model internals:* The attacker operates under a strict black-box assumption. All knowledge of the system is inferred from observations or replicated via proxy modeling.

- *No control-plane privileges:* The adversary cannot modify system scheduling, pilot assignments, or user association policies. It relies solely on over-the-air interference.
- *Local-only deployment:* The attack is scoped to a specific geographic region where the adversary can remain near legitimate users. While realistic for vehicular or roadside scenarios, it does not scale to cloud-based or multi-region attacks.
- *Power and spectral masking:* Transmissions must adhere to power masks to remain undetectable by spectrum monitors. The attacker balances perturbation strength against stealth.

This capability profile aligns with known real-world exploits demonstrated in MIMO systems [189], and reflects a credible threat posture under current 3GPP assumptions. As AI continues to move closer to the wireless PHY layer, the absence of corresponding attacker models and trust boundaries in standardization efforts presents a critical gap in system resilience.

6.4 Adversarial Attack Strategy

To operationalize the threat model presented earlier, this section introduces the adversarial attack strategy used to compromise the ML-based channel gain predictor. The approach follows a black-box attack paradigm, assuming no access to the model’s architecture, internal weights, or training data. Instead, the attacker relies on surrogate modeling, adversarial transferability, and uplink pilot injection to degrade prediction accuracy and disrupt downstream resource allocation.

The core of the attack uses the Fast Gradient Sign Method (FGSM) [73], a single-step gradient-based attack originally designed for classification models. In our case, the method is adapted to regression, where the model outputs continuous-valued channel gain estimates. FGSM perturbs an input vector in the direction of the gradient that maximally increases the model’s prediction error. Although traditionally applied to classification, FGSM has been successfully adapted to tasks like channel estimation and signal classification in wireless systems [30, 184].

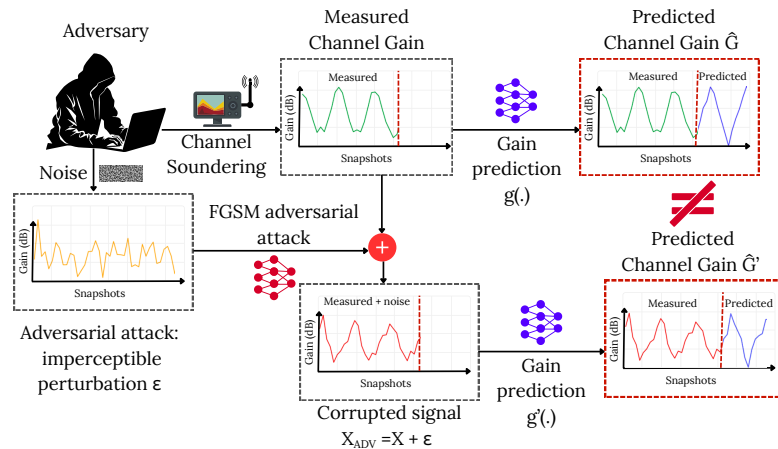


Figure 6.2: Overview of the adversarial attack based on FGSM.

As shown in Figure 6.2, the attack process unfolds in two main stages. In the first stage, the adversary trains a differentiable substitute model using proxy data collected from the surrounding wireless environment. This model acts as a surrogate for the target gain predictor. In the second stage, the attacker uses this model to craft perturbations that, when injected into the system via pilot contamination, mislead the gain predictor at the CPU.

Attack Pipeline Overview

The complete adversarial pipeline is described in Algorithm 6.1. It includes both the preparation of adversarial samples and their deployment against real-world data to evaluate prediction degradation and detectability.

Algorithm 6.1: *Adversarial Attack Construction and Evaluation Pipeline*

Require: Proxy dataset X_{proxy} , perturbation range $\{\epsilon_i\}$, real dataset X_{real}

Ensure: Adversarial samples X_{adv} , classifier C

1: **Step I: Attack Preparation on Proxy Data**

2: **I. Train Substitute LSTM Model**

3: Train a surrogate model \hat{M} on X_{proxy}

4: **II. Optimize Perturbation Level**

5: **for** each ϵ_i in a predefined set **do**

6: Compute gradient: $\nabla_X \mathcal{L}(\hat{M}, X_{\text{proxy}})$

7: Generate adversarial inputs: $X_{\text{adv}}^{\epsilon_i} = X_{\text{proxy}} + \epsilon_i \cdot \text{sign}(\nabla_X \mathcal{L})$

8: Evaluate prediction degradation for each ϵ_i

9: Select ϵ^* balancing stealth and impact

10: **III. Train Anomaly Detector**

11: Use X_{proxy} and $X_{\text{adv}}^{\epsilon^*}$ to train classifier C_{ϵ^*}

12: **Step II: Evaluation on Real Data**

13: **for** each ϵ_j in evaluation set **do**

14: Generate $X_{\text{real}}^{\text{adv}}[\epsilon_j]$ using \hat{M}

15: Test C_{ϵ^*} on $X_{\text{real}}^{\text{adv}}[\epsilon_j]$

16: Measure detectability and impact on gain prediction

17: **return** Final adversarial samples $X_{\text{adv}}^{\epsilon_j}$ and classifier C_{ϵ^*}

Step I: Attack Preparation

The first phase is entirely attacker-side and uses only proxy data. A substitute model \hat{M} , based on an LSTM architecture to capture temporal dependencies in the input, is trained using clean channel data collected via passive sensing (line 3). This model is then used to compute FGSM perturbations across a set of candidate ϵ values, each representing a different tradeoff between attack effectiveness and stealth (lines 5–9).

After evaluating their impact on prediction accuracy, a candidate ϵ^* is selected that maximizes degradation without introducing large input anomalies. This choice reflects the attacker’s lack of access to system-defined thresholds, and instead relies on empirical tuning through proxy experimentation.

Next, the attacker trains a binary anomaly detector C_{ϵ^*} using clean and adversarial inputs. This classifier simulates the decision boundary of a potential misbehavior detection system (MDS), allowing the adversary to pre-filter crafted inputs for stealth before deployment (line 11).

Step II: Deployment and Evaluation

In the second phase, the attack is transferred to real data. Using the same surrogate model and several ϵ_j values, the attacker perturbs real inputs, e.g., pilot-bearing vectors captured during live traffic (line 14). These adversarial inputs are then evaluated for two criteria: (1) their ability to degrade the gain predictor’s output, and (2) their detectability by the anomaly classifier C_{ϵ^*} trained earlier.

Because both the substitute model and the detector are trained solely on proxy data, this pipeline reflects a realistic black-box scenario. The success of the attack thus hinges on the transferability of adversarial perturbations and the degree to which

ML-based gain predictors generalize from spatially similar, but not identical, channel environments [138, 30].

6.5 Experiments

Following the formulation of the threat model and the definition of the adversarial pipeline, this section provides a comprehensive evaluation of the attack’s impact from both a predictive and system-level perspective. The experimental process begins by examining the susceptibility of machine learning-based channel gain predictors to input perturbations, specifically those crafted via the FGSM algorithm in a black-box setting. The attack, launched using a locally trained surrogate model, aims to degrade gain prediction accuracy while evading detection, thereby compromising the integrity of the scheduling process in UC-CFmMIMO networks.

To assess the consequences of this manipulation, we simulate a realistic vehicular communication environment with high spatial-temporal fidelity using QuaDRiGa, and evaluate how perturbations affect not only the regression outputs but also the downstream allocation of spectral resources. Machine learning models used for gain prediction, including LSTM-based architectures and ensemble regressors, are first benchmarked under clean conditions to establish a reliable reference. The perturbations are then introduced progressively, and their effects are observed through detailed error analysis, model robustness evaluation, and downstream inconsistencies in resource scheduling.

This framework allows us to trace the propagation of adversarial influence from raw physical-layer inputs to upper-layer decision-making, thereby exposing a previously underexplored vulnerability in AI-enabled wireless infrastructure.

6.5.1 Evaluation Framework and Predictive Models

To rigorously evaluate the effects of adversarial perturbations on model reliability and system-level behavior, we first benchmark a set of channel gain predictors under clean conditions. These models represent both the attack surface and the potential target architectures that may be deployed in real-world UC-CFmMIMO systems. The focus of this phase is to establish a reliable performance baseline and validate the assumptions underlying the black-box attack pipeline.

The predictive task involves estimating the frequency-domain channel gain on each subband, based on previous time samples of spatially aggregated channel state information (CSI). Accurate prediction at this stage is critical, as the results are directly consumed by the subband allocation algorithm during scheduling. The more accurate the gain forecast, the better the system can ensure fairness, minimize interference, and optimize spectral efficiency.

Model Selection Rationale. The architecture used by the attacker to craft adversarial perturbations must be differentiable. Therefore, a Long Short-Term Memory (LSTM) model is adopted as the surrogate model, leveraging its ability to learn temporal patterns from sequential input data. The LSTM’s gradient accessibility makes it suitable for applying the Fast Gradient Sign Method (FGSM) to generate adversarial samples.

However, the black-box nature of the threat model implies that the attacker cannot assume the same model is deployed at the CPU. To test the transferability of the perturbations, we evaluate three other predictive models: a second LSTM (used as the attack target), a Random Forest (RF) regressor, and a Gradient Boosted Trees (XGB) model. These alternatives represent non-differentiable and ensemble-based architectures that are common in wireless signal prediction pipelines.

Data Preparation and Training. All models are trained using time-series channel data generated via QuaDRiGa in a 6G vehicular context. The data reflects subband-specific gain fluctuations for each user terminal across time. 80% of the dataset is allocated for training, and 20% is used for validation. For the black-box simulation, the surrogate LSTM model is trained on spatially distinct proxy data to emulate what an attacker would realistically observe in the field.

Metrics for Evaluation. To ensure a comprehensive evaluation of predictive accuracy, we compute the following metrics for each model:

- **Mean Squared Error (MSE):** Penalizes large deviations in predictions.
- **Mean Absolute Error (MAE):** Reflects average absolute prediction error.
- **Root Mean Squared Error (RMSE):** Provides interpretable error magnitudes.
- **Coefficient of Determination R^2 :** Measures how well the predictions explain the variance in the data.
- **Explained Variance Score:** Assesses proportion of variance captured by the model.

Figure 6.3 shows a representative example of an LSTM model’s predictive performance on clean test data. The model effectively captures temporal fluctuations in the gain profile, validating its relevance for deployment and its susceptibility to input perturbation.

Clean Performance Results. Table 6.1 reports the performance of all four models on the clean validation set. The LSTM models outperform the ensemble-based alternatives in every metric, which is expected given their architectural advantage in

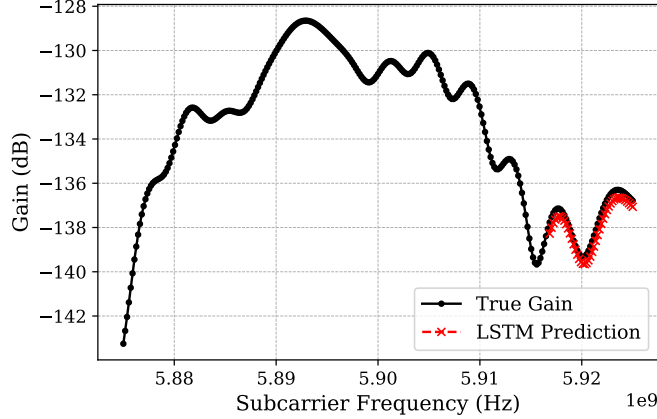


Figure 6.3: Temporal prediction of frequency-domain channel gain using LSTM on a representative AP-UE pair. The model accurately tracks gain evolution, validating its predictive capacity.

modeling sequential data. Notably, the substitute LSTM achieves nearly identical accuracy to the target LSTM, further supporting its use as a reliable attacker-side proxy.

Table 6.1: Clean performance of predictive models on the validation set

Model	MSE	MAE	RMSE	R^2	Expl. Var.
LSTM (target)	0.097	0.198	0.311	0.948	0.948
Random Forest	0.123	0.232	0.351	0.936	0.936
Gradient Boosting	0.112	0.224	0.334	0.941	0.941
LSTM (substitute)	0.095	0.196	0.308	0.949	0.949

These results confirm the vulnerability of high-performing ML models, particularly LSTMs, when used for predictive tasks in dynamic wireless environments. Their differentiable nature, while beneficial for learning, also exposes them to gradient-based adversarial attacks. The next section will assess how perturbations, crafted from the substitute model, degrade predictive performance across all targets, under various perturbation intensities.

6.5.2 Adversarial Robustness

This section presents an empirical evaluation of the predictive robustness of ML-based gain estimation models under adversarial attack. The aim is twofold: to quantify the degradation in predictive accuracy due to perturbations, and to assess the extent to which adversarial samples remain transferable and stealthy across model families and perturbation intensities.

Evaluation Setup. Perturbations are generated using FGSM with respect to the LSTM substitute model trained on proxy data. The attack is deployed across a sweep of perturbation strengths $\epsilon \in \{0.1, 0.5, 1.0, 2.0, 5.0\}$ and corruption ratios $\rho \in \{10\%, 20\%, 50\%, 100\%\}$, which simulate partial to full-scale input contamination. For each combination of ϵ and ρ , adversarial examples are generated and fed to the LSTM target, Random Forest (RF), and Gradient Boosting (XGB) models.

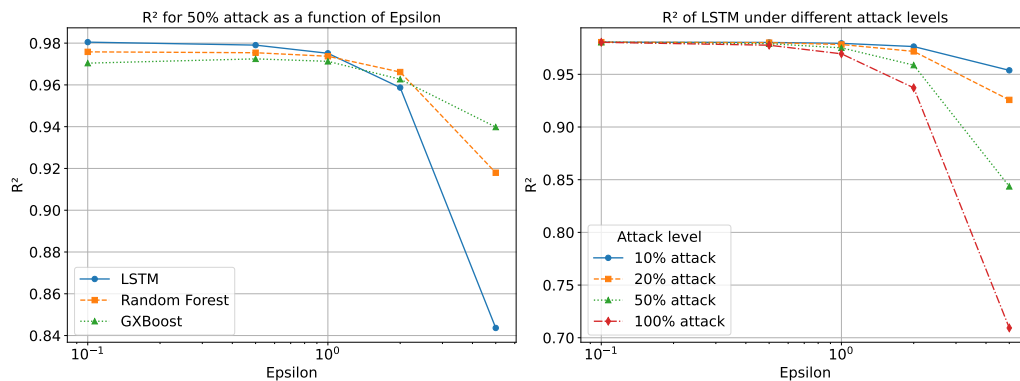
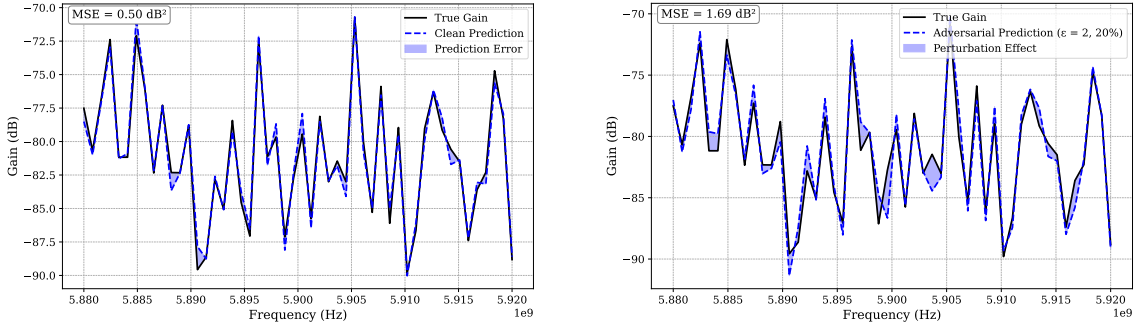


Figure 6.4: Effect of perturbation strength and corruption percentage on R^2 . The left panel shows model-wise degradation at 50% corruption. The right panel shows LSTM degradation across varying corruption ratios.

Model Performance Degradation. Figure 6.4 illustrates the decline in R^2 as a function of both ϵ and corruption percentage. The LSTM model exhibits the sharpest drop due to its architectural similarity to the surrogate. For $\epsilon = 1.0$ and $\rho = 50\%$, the R^2 drops below 0.90, signaling a strong disruption in prediction fidelity. Notably,

even tree-based models like RF and XGB, although architecturally unrelated to the attacker’s model, experience noticeable degradation, confirming that adversarial perturbations maintain significant transferability across regression paradigms.

Visual Inspection of Perturbation Impact. To better understand the perceptibility and distortion of the adversarial examples, Figure 6.5 compares LSTM gain predictions under clean and adversarial inputs for the same AP-UE link. While the visual difference in the prediction curves is subtle, the underlying Mean Squared Error increases from 0.50 dB^2 to 1.69 dB^2 , demonstrating the stealthy yet impactful nature of the attack.



(a) Clean LSTM prediction.

(b) Adversarial LSTM prediction (FGSM, $\epsilon = 0.5$).

Figure 6.5: Comparison of predicted frequency-domain gain under clean and adversarial conditions for the same user and antenna. The adversarial case shows greater deviation and a higher MSE, despite visually subtle differences.

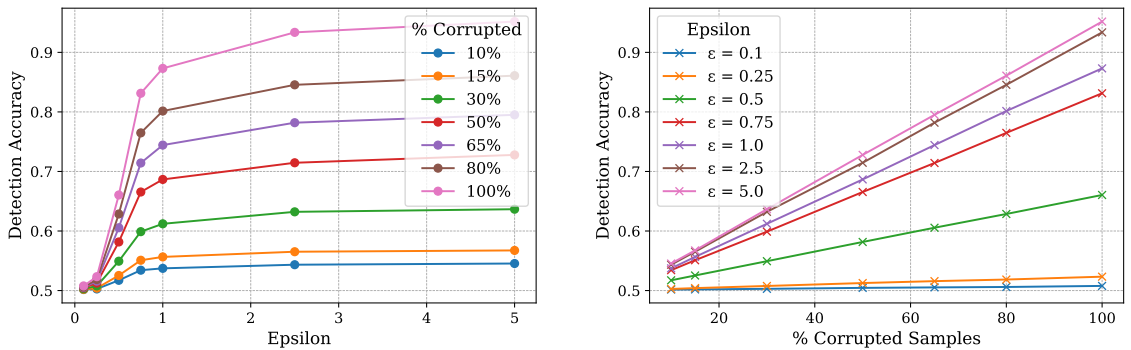
Detectability and Misbehavior Classifier Evaluation. While the adversarial impact is significant, the perturbations are crafted to remain statistically inconspicuous. To test this, a binary anomaly detection task is conducted using several classifiers trained to distinguish between clean and adversarial inputs. The inputs for detection are raw channel feature vectors, and the classifiers are trained on a balanced 50% clean / 50% adversarial dataset. Table 6.2 shows that tree-based detectors, particularly Random Forest, achieve the highest detection accuracy, above 94%. However,

linear models like SVM underperform, highlighting the difficulty of separating perturbed and unperturbed samples in non-linear spaces.

Table 6.2: Detection accuracy of different classifiers on mixed (50% clean, 50% adversarial) test data. Attacks were generated using FGSM based on the LSTM substitute model.

Model	Detection Accuracy
Decision Tree	91.17%
Random Forest	94.19%
KNN	91.62%
SVM	89.71%

Figure 6.6 further analyzes detection accuracy as a function of perturbation intensity and corruption level using the Random Forest detector. As expected, detection becomes easier as ϵ increases or as the fraction of adversarial inputs grows. However, for $\epsilon \leq 0.5$ and $\rho \leq 20\%$, detection rates decline sharply, which coincides with the parameter regions used by a stealth-conscious attacker.



(a) Impact of perturbation strength ϵ on detection accuracy. (b) Impact of corruption level ρ on detection accuracy.

Figure 6.6: Detection accuracy behavior under varying perturbation parameters using a Random Forest classifier.

Summary. The results in this subsection confirm the adversarial vulnerability of ML-based gain predictors under black-box attacks. Perturbations generated using a surrogate LSTM model not only degrade the performance of the same model family but also transfer across model architectures. Furthermore, although high-accuracy

detectors exist, their performance degrades substantially under subtle perturbations, a condition likely favored by attackers seeking stealth and persistence.

The next subsection investigates how these prediction errors, once propagated into the scheduling engine, affect consistency in subband-user allocation decisions.

6.5.3 Impact on Resource Allocation Consistency

While the previous subsection established the vulnerability of gain prediction models under adversarial perturbations, it remains essential to quantify the downstream effects on system behavior, specifically, the stability of frequency resource allocation decisions. In AI-native UC-CFmMIMO networks, scheduling decisions are directly informed by predicted channel gain vectors. As such, even marginal deviations at the prediction layer can cause cascaded inconsistencies in subband-user mappings, potentially leading to performance degradation, fairness violations, and spectral inefficiency.

Measuring Allocation Instability. To capture the misalignment between allocation decisions under clean and adversarial conditions, we adopt the Jaccard similarity index as a measure of consistency. Let $\mathcal{A}_{\text{clean}}$ and \mathcal{A}_{adv} denote the subband-user allocation matrices generated using clean and perturbed gain predictions, respectively. The Jaccard index is computed for each subband as:

$$\text{Jaccard}(i) = \frac{|\mathcal{A}_{\text{clean}}^i \cap \mathcal{A}_{\text{adv}}^i|}{|\mathcal{A}_{\text{clean}}^i \cup \mathcal{A}_{\text{adv}}^i|}$$

where \mathcal{A}^i denotes the set of users allocated to subband i . A lower Jaccard index implies greater deviation between the two allocation outcomes.

Results and Interpretation. Figure 6.7 presents the Jaccard similarity results under different attack intensities. Even at low corruption levels ($\rho = 10\%$), the difference in allocation patterns becomes significant as ϵ increases. For $\epsilon = 0.5$, many subbands retain a relatively stable mapping (Figure 6.7a), but the presence of several outliers indicates localized allocation instability. As the perturbation intensity increases to $\epsilon = 2.0$ (Figure 6.7b), the mean Jaccard similarity decreases substantially, confirming widespread disruption in the allocation process.

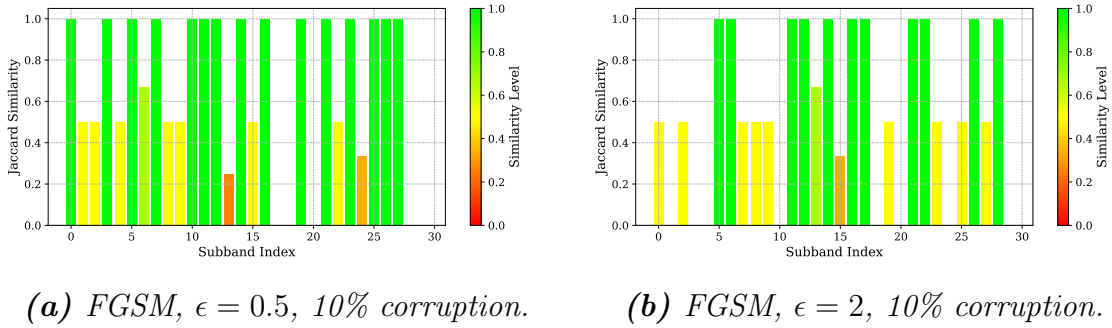


Figure 6.7: Jaccard similarity between subband-user allocations under clean and adversarial CSI.

This behavior highlights the non-linear amplification of prediction noise within the resource allocation pipeline. Since scheduling relies on comparative metrics, e.g., selecting the highest-gain user per subband, even small perturbations in a subset of predictions can lead to different ranking outcomes, thereby altering the final allocation.

System-Level Implications. The observed instability in subband-user allocation under adversarial conditions has significant system-level ramifications. Even modest perturbations in gain prediction can lead to the misallocation of frequency resources, wherein users with genuinely higher gains are bypassed in favor of adversarially perturbed alternatives. This results in suboptimal scheduling, increased inter-user interference, and fairness violations, particularly in dense and dynamic vehicular networks. Due to the combinatorial nature of scheduling, even localized perturbations in a sub-

set of users can propagate into widespread reallocation decisions, which are difficult to isolate or recover from without re-executing the entire optimization pipeline.

These findings underscore that the impact of adversarial noise extends well beyond the regression layer. Once injected into the physical-layer input, the perturbation propagates through the machine learning pipeline to disrupt core operational logic in the network stack. This exposes a structural vulnerability in AI-native wireless architectures, specifically, the lack of resilience in the mapping from prediction to action. The results strongly motivate future work on end-to-end robustness strategies, including perturbation-tolerant scheduling mechanisms and cross-layer anomaly detection systems that can intercept adversarial drift before it affects critical allocation decisions.

6.6 Conclusion and Future Scope of Work

This chapter has introduced and validated a novel adversarial attack targeting frequency resource allocation in user-centric cell-free massive MIMO networks. By exploiting the lack of physical-layer authentication in 3GPP-compliant pilot signals and the architectural opacity of ML-based gain predictors, the proposed strategy demonstrates how a stealthy adversary, operating in a realistic black-box setting, can inject minimally visible perturbations that propagate across the learning and scheduling pipeline.

The use of a gradient-based surrogate model enabled the generation of adversarial samples with high transferability, degrading prediction accuracy across diverse model architectures. These perturbations led to measurable inconsistencies in subband-user allocation, as quantified through Jaccard similarity analysis, revealing how even modest input corruption can produce system-level instability. Moreover, while anomaly

detectors could identify severe perturbations with reasonable accuracy, their performance deteriorated under low- ϵ , low- ρ regimes, conditions that an attacker would naturally favor for stealth.

These findings reveal a critical security gap in AI-native wireless infrastructure: the fragility of ML-driven control decisions under adversarial manipulation. This vulnerability is particularly pronounced in architectures like UC-CFmMIMO, where physical-layer estimations are tightly coupled to high-stakes resource allocation mechanisms.

Looking forward, several directions emerge for enhancing the resilience of such systems:

- **Adversarially robust learning architectures:** Future work should explore training strategies that increase resistance to perturbations, including adversarial training and model ensembling across heterogeneous architectures.
- **Cross-layer anomaly detection:** Developing lightweight, PHY-integrated detectors that operate jointly across the prediction and scheduling layers may improve detection performance under stealth conditions.
- **Secure pilot design:** Revisiting the pilot signal specification to incorporate authentication or randomized perturbation masking could reduce the risk surface at the protocol level.
- **Adaptive scheduling under uncertainty:** Designing resource allocation schemes that are robust to uncertainty in gain estimates, through confidence-aware optimization or bounded regret strategies, can mitigate the effects of adversarial drift.

Ultimately, this work opens a broader conversation about the intersection of adversarial machine learning and wireless system design, and motivates a cross-disciplinary effort to engineer resilient, intelligence-driven 6G networks.

CONCLUSIONS AND FUTURE RESEARCH DIRECTIONS

7.1 Conclusions

This thesis has presented a comprehensive framework for addressing the challenges of frequency resource allocation in User-Centric Cell-Free massive MIMO (UC-CFmMIMO) systems, with a particular focus on high-mobility scenarios such as vehicular networks. In light of the evolving demands of Beyond 5G (B5G) and upcoming 6G networks, characterized by stringent latency, reliability, and scalability requirements, this work responds with methods that are both theoretically grounded and practically applicable.

The research began by establishing a realistic foundation for system modeling through the integration of frequency-selective channel characterization using the WINNER II and QuaDRiGa toolkits. This allowed for an accurate representation of Doppler effects, subband diversity, and mobility-induced variability, which are essential for designing effective resource allocation strategies in dynamic urban environments.

Building upon this foundation, the thesis introduced heuristic algorithms based on physical-layer metrics, specifically the condition number and channel correlation. These methods demonstrated significant improvements in spectral efficiency and user packing efficiency, particularly under dense and interference-prone conditions. To further enhance resource optimization, a utility-based multi-objective framework was proposed, enabling a balanced trade-off among throughput maximization, fairness, and interference suppression. Metaheuristic techniques, including Simulated Annealing (SA), Genetic Algorithms (GA), and Ant Colony Optimization (ACO), were em-

ployed to solve this complex optimization task with notable success, especially under large-scale network constraints.

Recognizing the need for adaptability in dynamic and time-sensitive environments, the thesis transitioned to a learning-based paradigm. A novel hybrid framework was developed by combining the Aquila Optimizer (AO) with an Actor-Critic Deep Deterministic Policy Gradient (DDPG) reinforcement learning agent. This integration leveraged the structured exploration of AO with the adaptive learning capabilities of DDPG, resulting in superior convergence speed, robustness under variable user densities, and efficient allocation of frequency resources. Simulation results consistently showed that the hybrid model outperformed standalone techniques across metrics such as spectral efficiency, Gini-based fairness, and resilience to interference.

In its final contribution, the thesis investigated the vulnerability of AI-based wireless resource management to adversarial threats. A black-box attack model was designed to demonstrate how subtle perturbations, crafted without access to the internal system, could significantly disrupt frequency allocation by targeting the channel prediction pipeline. This finding not only revealed a critical risk but also emphasized the necessity of incorporating robustness and security into future learning-based wireless protocols.

Overall, this research delivers a layered, adaptable, and secure approach to physical-layer resource allocation in UC-CFmMIMO systems. It aligns with the technical goals of 3GPP Release 19 and anticipates the emerging requirements of 6G networks, offering practical tools and theoretical insights for enabling next-generation intelligent transportation systems and other mission-critical applications. By bridging classical optimization, deep learning, and adversarial resilience, this work sets the stage for scalable and trustworthy wireless connectivity in increasingly mobile and complex environments.

7.2 Future Research Directions

While this thesis has proposed a comprehensive framework for intelligent and secure frequency resource allocation in UC-CFmMIMO systems under high mobility, several promising directions remain open for further investigation.

One natural extension is the integration of hardware constraints into the proposed optimization and learning frameworks. While the current models focus on throughput, fairness, and interference management, incorporating power consumption metrics at both user and access point levels would align resource allocation strategies more closely with practical deployment requirements in 6G and IoT contexts.

Another avenue is to explore coordination among multiple learning agents in dense deployments. The hybrid RL model proposed in this thesis can be extended to multi-agent settings, where distributed agents collaborate or compete to allocate spectrum resources. Investigating the impact of partial observability, communication overhead, and agent-to-agent interactions will be essential for scalable learning-based wireless systems.

Furthermore, online learning and continual adaptation present important opportunities. Vehicular environments are inherently dynamic, and models trained offline may degrade over time. Incorporating continual learning mechanisms that adapt in real-time without catastrophic forgetting can significantly improve robustness and long-term performance.

In parallel, the security and trustworthiness of learning-driven wireless systems warrant deeper investigation. The adversarial threat model introduced in this thesis opens the door to a broader exploration of defense mechanisms, such as adversar-

ial training, certified robustness, or blockchain-inspired trust validation for federated wireless agents.

Finally, aligning with ongoing standardization efforts, future work could contribute to the co-design of protocol stacks that integrate learning-based decision making at the physical and MAC layers, and study how these mechanisms can be standardized in future 3GPP releases. This includes challenges related to interpretability, convergence guarantees, and compliance with low-latency service constraints.

Taken together, these directions aim to evolve the proposed models into real-world deployable systems, supporting secure, adaptive, and intelligent wireless communication in the high-mobility, high-density landscape of future networks.

BIBLIOGRAPHY

- [1] 3GPP. *NR; Multiplexing and channel coding (Release 15)*. Tech. rep. TS 38.212. Available: <https://www.3gpp.org/DynaReport/38212.htm>. 3rd Generation Partnership Project (3GPP), 2018.
- [2] 3GPP. *NR; NR and NG-RAN Overall Description; Stage-2 (Release 15)*. Tech. rep. TS 38.300. Available: <https://www.3gpp.org/DynaReport/38300.htm>. 3rd Generation Partnership Project (3GPP), 2019.
- [3] 3GPP. *NR; Physical channels and modulation (Release 15)*. Tech. rep. TS 38.211. Available: <https://www.3gpp.org/DynaReport/38211.htm>. 3rd Generation Partnership Project (3GPP), 2018.
- [4] 3GPP. *NR; Physical layer procedures for data (Release 15)*. Tech. rep. TS 38.214. Available: <https://www.3gpp.org/DynaReport/38214.htm>. 3rd Generation Partnership Project (3GPP), 2018.
- [5] 3GPP. *NR; Physical layer; General description (Release 15)*. Tech. rep. TS 38.201. Available: <https://www.3gpp.org/DynaReport/38201.htm>. 3rd Generation Partnership Project (3GPP), 2018.
- [6] 3GPP. *NR; Radio Resource Control (RRC); Protocol specification (Release 16)*. Tech. rep. TS 38.331. Available: <https://www.3gpp.org/DynaReport/38331.htm>. 3rd Generation Partnership Project (3GPP), 2020.
- [7] 3GPP. *Service Data Adaptation Protocol (SDAP) Specification (Release 15)*. Tech. rep. TS 37.324. Available: <https://www.3gpp.org/DynaReport/37324.htm>. 3rd Generation Partnership Project (3GPP), 2018.

- [8] 3GPP. *Study on channel model for frequencies from 0.5 to 100 GHz (Release 16)*. Tech. rep. TR 38.901. V16.1.0. 3rd Generation Partnership Project (3GPP), 2020. URL: <https://www.3gpp.org/DynaReport/38901.htm>.
- [9] 3GPP. *TR 38.913 - Study on scenarios and requirements for next generation access technologies*. Tech. rep. Version 14.3.0. 3rd Generation Partnership Project (3GPP), 2017.
- [10] 3GPP. *TS 38.211 - NR; Physical channels and modulation*. Tech. rep. Version 17.x.x. 3rd Generation Partnership Project (3GPP), 2024.
- [11] 3GPP. *TS 38.212 - NR; Multiplexing and channel coding*. Tech. rep. Version 17.x.x. 3rd Generation Partnership Project (3GPP), 2024.
- [12] *3GPP TS 33.501: Security architecture and procedures for 5G system*. Tech. rep. Version 17.8.0. 3rd Generation Partnership Project (3GPP), 2023.
- [13] *3GPP TS 38.211: NR; Physical channels and modulation*. Tech. rep. Version 17.6.0. 3rd Generation Partnership Project (3GPP), 2023.
- [14] A. Anand, C. R. Murthy, and R. Chopra. “Impact of mobility on the downlink performance of cell-free massive MIMO systems”. In: *Physical Communication* 61 (2023), p. 102178.
- [15] A. Abhulimhen-Iyoha, G. Ditzler, and S. Krishnan. “Isolation Forest and Support Vector Machine for detecting adversarial examples in autonomous vehicles”. In: *IEEE Transactions on Intelligent Vehicles* 7.1 (2022), pp. 123–134.
- [16] L. Abualigah, D. Yousri, M. Abd Elaziz, et al. “Aquila optimizer: a novel meta-heuristic optimization algorithm”. In: *Computers & Industrial Engineering* 157 (2021), p. 107250.
- [17] L. Abualigah, D. Yousri, M. Abd Elaziz, et al. “Aquila optimizer: A novel meta-heuristic optimization algorithm”. In: *Computers & Industrial Engineering* 157 (2021), p. 107250. DOI: 10.1016/j.cie.2021.107250.

- [18] M. Ajmal et al. “Cell-free massive multiple-input multiple-output challenges and opportunities: A survey”. In: *ICT Express* (2023).
- [19] H. F. Alhashimi et al. “A Survey on Resource Management for 6G Heterogeneous Networks: Current Research, Future Trends, and Challenges”. In: *Electronics* 12.3 (2023), p. 647.
- [20] M. Alkhaled et al. “Adaptive User Grouping Algorithm for the Downlink Massive MIMO Systems”. In: *Proc. IEEE Wirel. Commun. Netw. Conf.* IEEE. Apr. 2016, pp. 1–6.
- [21] A. Alwarafy, M. Abdallah, B. S. Ciftler, et al. “Deep reinforcement learning for radio resource allocation and management in next-generation heterogeneous wireless networks: A survey”. In: *arXiv preprint arXiv:2106.00574* (2021).
- [22] H. A. Ammar, R. Adve, S. Shahbazpanahi, et al. “Distributed Resource Allocation Optimization for User-Centric Cell-Free MIMO Networks”. In: *Proc. IEEE Global Communications Conference (GLOBECOM)*. 2022, pp. 341–346. DOI: 10.1109/GLOBECOM48099.2022.10000919.
- [23] M. Ammar, B. Nouredine, S. El-Badawy, and W. Hamouda. “User-centric cell-free massive MIMO-enabled mobile edge network for vehicular communications”. In: *IEEE Access* 9 (2021), pp. 78507–78522. DOI: 10.1109/ACCESS.2021.3082863.
- [24] Y. An, T. Qiu, W. Yu, et al. “Deep reinforcement learning for resource allocation in wireless networks: Recent advances and challenges”. In: *IEEE Transactions on Neural Networks and Learning Systems* 34.10 (2023), pp. 6124–6141. DOI: 10.1109/TNNLS.2022.3207420.
- [25] A. Anand, C. R. Murthy, and R. Chopra. “Impact of mobility on the downlink performance of cell-free massive MIMO systems”. In: *Phys. Commun.* 61 (2023), p. 102178.

- [26] A. Anand and C. R. Murthy. “Impact of Subcarrier Allocation and User Mobility on the Uplink Performance of Multi-User Massive MIMO-OFDM Systems”. In: *arXiv preprint arXiv:2108.05485* (2022).
- [27] R. Anandan, S. Abdur Rahman Seenuvasamurthi, and G. Vishnu Vardhan Rao. “CCOA-AdaLS: Hybrid beamforming using chaotic Chebyshev Aquila optimization for mmWave massive MIMO”. In: *International Journal of Communication Systems* (2024). DOI: 10.1002/dac.6069.
- [28] F. Arena et al. “A Review on IEEE 802.11p for Intelligent Transportation Systems”. In: *J. Sens. Actuator Networks* 9.2 (2020), p. 22.
- [29] N. M. Ashraf, R. R. Mostafa, R. H. Sakr, and M. Z. Rashad. “Optimizing hyperparameters of deep reinforcement learning for autonomous driving based on whale optimization algorithm”. In: *Plos One* 16.6 (2021), e0252754.
- [30] A. Bahramali, F. Gagnon, and M. L. et al. “Adversarial attacks on deep learning-based modulation recognition”. In: *IEEE Transactions on Cognitive Communications and Networking* 9.1 (2023), pp. 123–135.
- [31] M. Bashar, E. Björnson, and L. Sanguinetti. “Scalable Cell-Free Massive MIMO Systems With Local Signal Processing”. In: *IEEE Transactions on Wireless Communications* 20.4 (2021), pp. 2228–2242. DOI: 10.1109/TWC.2020.3042977.
- [32] J. Bergstra and Y. Bengio. “Random search for hyper-parameter optimization”. In: *Journal of Machine Learning Research* 13.Feb (2012), pp. 281–305.
- [33] E. Björnson and E. Jorswieck. “Optimal resource allocation in coordinated multi-cell systems”. In: *Found. Trends Commun. Inf. Theory* 9.2–3 (2013), pp. 113–381.

- [34] E. Björnson, L. Sanguinetti, H. Q. Ngo, and M. Debbah. “Making Cell-Free Massive MIMO Competitive With MMSE Processing and Centralized Implementation”. In: *IEEE Transactions on Wireless Communications* 19.1 (2020), pp. 77–90.
- [35] A. Boualouache and T. Engel. “A survey on machine learning-based misbehavior detection systems for 5G and beyond vehicular networks”. In: *IEEE Communications Surveys & Tutorials* 25.2 (2023), pp. 1128–1172.
- [36] K. Boutiba, M. Baga, and A. Ksentini. “Optimal radio resource management in 5G NR featuring network slicing”. In: *Comput. Netw.* 234 (2023), p. 109937.
- [37] Y. D. J. Bultitude and T. Rautiainen. *IST-4-027756 WINNER II D1.1.2 V1.2 WINNER II Channel Models*. Tech. Rep. EBITG, TUI, UOULU, CU/CRC, NOKIA, 2007.
- [38] Y. D. J. Bultitude and T. Rautiainen. *IST-4-027756 WINNER II D1.1.2 V1.2 WINNER II channel models*. Tech. rep. EBITG, TUI, UOULU, CU/CRC, NOKIA, 2007.
- [39] S. Buzzi, C. D’Andrea, and A. Zappone. “User-Centric 5G Cellular Networks: Resource Allocation and Comparison With the Cell-Free Massive MIMO Approach”. In: *IEEE Transactions on Wireless Communications* 17.11 (2018), pp. 6899–6913.
- [40] S. Chakraborty et al. “Efficient downlink power allocation algorithms for cell-free massive MIMO systems”. In: *IEEE Open J. Commun. Soc.* 2 (2020), pp. 168–186.
- [41] S. Cheggour and V. Loscri. “Frequency Channel Selectivity in Vehicular CF-MIMO Systems: a Multi-Objective Optimization Approach”. In: *VNC 2025 - IEEE Vehicular Networking Conference*. ⟨hal-05011230⟩. Porto, Portugal, June 2025.

- [42] S. Cheggour and V. Loscri. “Frequency Resource Management in 6G User-Centric CFmMIMO: A Hybrid Reinforcement Learning and Metaheuristic Approach”. In: *arXiv preprint arXiv:2505.22443* (2025).
- [43] S. Cheggour and V. Loscri. *Hybrid AI and Metaheuristic Solutions for Optimized Frequency Allocation in 6G Networks*. Poster presented at BMW Summer School on Artificial Intelligence and Wireless Technologies. Saint-Raphaël, France, July 2025.
- [44] S. Cheggour, E. P. Simon, and V. Loscri. “Advanced Resource Management in Cell-Free Massive MIMO Systems with WINNER II Channels”. In: *LAN-MAN 2025 - IEEE International Symposium on Local and Metropolitan Area Networks*. (hal-05062956). Lille, France, July 2025.
- [45] F. Chen, Z. Zhong, and L. Burry. “A performance metric for evaluating interference in MIMO networks based on eigenvalue spread”. In: *IEEE Transactions on Wireless Communications* 15.12 (2016), pp. 8081–8095. DOI: 10.1109/TWC.2016.2604827.
- [46] Z. Chen, E. Björnson, and E. G. Larsson. “Structured Massive Access for Scalable Cell-Free Massive MIMO Systems”. In: *IEEE Journal on Selected Areas in Communications* 39.4 (2021), pp. 1086–1100.
- [47] X. Cheng, Y. He, and J. Qiao. “Channel modeling for UCA and URA massive MIMO systems”. In: *Proc. 2020 Int. Conf. Comput., Netw. Commun. (ICNC)*. Feb. 2020, pp. 963–968.
- [48] H. F. Chou, S. Solanki, and V. N. H. et al. “Edge AI empowered physical layer security for 6G NTN: Potential threats and future opportunities”. In: *arXiv preprint arXiv:2401.01005* (2023).

- [49] F. Conceição, M. Gomes, V. Silva, and R. Dinis. “Resource allocation in cell-free massive MIMO networks with hybrid energy supply”. In: *Electronics* 13.13 (2024), pp. 1–8.
- [50] *Considerations and evaluation results for IMT-2020 for high mobility*. <https://www.3gpp.org/dynareport?code=TDocExMtg--R1-94--18796.htm>.
- [51] E. Dahlman, S. Parkvall, and J. Sköld. *5G NR: The Next Generation Wireless Access Technology*. 1st. Academic Press, 2018. ISBN: 9780128143230.
- [52] Ö. T. Demir et al. “Foundations of User-Centric Cell-Free Massive MIMO”. In: *Foundations and Trends® in Signal Processing* 14.3-4 (2021), pp. 162–472. ISSN: 1932-8346. DOI: 10.1561/2000000109.
- [53] O. T. Demir, E. Bjornson, and L. Sanguinetti. “Foundations of User-Centric Cell-Free Massive MIMO”. In: *Foundations and Trends in Signal Processing* 14.3-4 (2021), pp. 162–472. DOI: 10.1561/2000000109.
- [54] M. Dianati, X. Shen, and S. Naik. “A new fairness index for radio resource allocation in wireless networks”. In: *Proc. IEEE Wireless Commun. Netw. Conf. (WCNC)*. Vol. 2. Mar. 2005, pp. 712–717.
- [55] P. A. M. Dirac. *The Principles of Quantum Mechanics*. International Series of Monographs on Physics. Clarendon Press, 1981. ISBN: 9780198520115.
- [56] M. Drela and M. B. Giles. “Viscous-Inviscid Analysis of Transonic and Low Reynolds Number Airfoils”. In: *4th Applied Aerodynamics Conference*. AIAA 1986-1786. San Diego, CA: American Institute of Aeronautics and Astronautics, June 1986. DOI: 10.2514/6.1986-1786.
- [57] H. L. Dryden. “Aerodynamics of Cooling”. In: *Aerodynamic Theory: A General Review of Progress*. Ed. by W. F. Durand. Vol. 6. Springer, 1943. Chap. T.

- [58] M. Dryjanski, M. Maternia, and A. Kliks. “5G-Advanced and the Road to 6G: A Technical Overview of 3GPP Release 19”. In: *IEEE Access* 12 (2024), pp. 1–15. DOI: 10.1109/ACCESS.2024.XXXXXXX.
- [59] E. Nayebi, A. Ashikhmin, T. L. Marzetta, and B. D. Rao. “Performance of cell-free massive MIMO systems with MMSE and LSFD receivers”. In: *2016 50th Asilomar Conference on Signals, Systems and Computers*. Nov. 2016, pp. 203–207.
- [60] T. Eimer, M. Lindauer, and R. Raileanu. “Hyperparameters in reinforcement learning and how to tune them”. In: *International Conference on Machine Learning*. PMLR. 2023, pp. 9104–9149. URL: <https://proceedings.mlr.press/v202/eimer23a.html>.
- [61] A. Einstein. “Zur Elektrodynamik bewegter Körper”. German. In: *Annalen der Physik* 322.10 (1905). Translation: “On the Electrodynamics of Moving Bodies”, pp. 891–921. DOI: 10.1002/andp.19053221004.
- [62] F. Conceição, M. Gomes, V. Silva, and R. Dinis. “Survey on resource allocation for future 6G network architectures: Cell-free and radio stripe technologies”. In: *Electronics* 13.13 (2024), p. 2489.
- [63] M. Farzanullah. “Deep reinforcement learning for resource allocation in next-generation C-V2X and IIoT networks”. In: (2023).
- [64] W. Fedus, P. Ramachandran, R. Agarwal, et al. “Revisiting Fundamentals of Experience Replay”. In: *International Conference on Machine Learning*. ICML. PMLR, Nov. 2020, pp. 3061–3071.
- [65] I. Fister, X.-S. Yang, I. J. Fister, et al. “A comprehensive review of nature-inspired algorithms for optimization”. In: *International Journal of Computational Intelligence Systems* 8.4 (2015), pp. 667–695. DOI: 10.1080/18756891.2015.1016228.

- [66] M. S. Frikha, S. M. Gammar, A. Lahmadi, and L. Andrey. “Reinforcement and deep reinforcement learning for wireless Internet of Things: A survey”. In: *Computer Communications* 178 (2021), pp. 98–113.
- [67] S. Fujimoto, H. Hoof, and D. Meger. “Addressing function approximation error in actor-critic methods”. In: *International Conference on Machine Learning (ICML)* (2018), pp. 1587–1596.
- [68] X. Gao, L. Zhang, and R. Wu. “Metaheuristic Optimization Techniques in 6G Networks: Applications and Challenges”. In: *Algorithms* 17.2 (2024), p. 51. DOI: 10.3390/a17020051.
- [69] G. Geraci et al. “What will the future of UAV cellular communications be? A flight from 5G to 6G”. In: *IEEE Commun. Surv. Tutor.* 24.3 (2022), pp. 1304–1335.
- [70] M. Ghasemi, A. H. Mousavi, and D. Ebrahimi. “Comprehensive survey of reinforcement learning: From algorithms to practical challenges”. In: *arXiv preprint arXiv:2411.18892* (2024).
- [71] M. Ghorbel, S. Cheggour, V. Loscri, et al. “Machine Learning Vulnerabilities in 6G: Adversarial Attacks and Their Impact on Channel Gain Prediction and Resource Allocation in UC-CFmMIMO”. In: *Proceedings of the 30th European Symposium on Research in Computer Security (ESORICS)*. (hal-05127853). Toulouse, France, Sept. 2025.
- [72] F. Gómez-Cuba and M. Zorzi. “Twice simulated annealing resource allocation for mmWave multi-hop networks with interference”. In: *Proc. IEEE Int. Conf. Commun. (ICC)*. June 2020, pp. 1–7.
- [73] I. J. Goodfellow, J. Shlens, and C. Szegedy. “Explaining and harnessing adversarial examples”. In: *arXiv preprint arXiv:1412.6572* (2015).

- [74] S. Gu, E. Holly, T. Lillicrap, and S. Levine. “Deep reinforcement learning for robotic manipulation with asynchronous off-policy updates”. In: *IEEE International Conference on Robotics and Automation (ICRA)* (2017), pp. 3389–3396. DOI: 10.1109/ICRA.2017.7989385.
- [75] A. Guenther, D. D. Marshall, C. Ford, et al. *Cal Poly Thesis Template*. 2024. URL: <https://github.com/CalPolyCSC/thesis-template> (visited on 08/16/2024).
- [76] H. Q. Ngo, G. Interdonato, E. G. Larsson, et al. “Ultradense cell-free massive MIMO for 6G: Technical overview and open questions”. In: *Proceedings of the IEEE* (2024).
- [77] T. Han and D. Zhao. “Energy Efficiency of User-Centric, Cell-Free Massive MIMO-OFDM with Instantaneous CSI”. In: *Entropy* 24.2 (2022), p. 234. DOI: 10.3390/e24020234.
- [78] J. He, Y. Zhang, X. Ge, and J. Yang. “Joint channel modeling and antenna design for realistic 5G simulations: A geometry-based stochastic approach”. In: *IEEE Access* 8 (2020), pp. 171295–171307. DOI: 10.1109/ACCESS.2020.3024323.
- [79] W. He, F. Gao, and J. Zhang. “Graph Neural Networks for Scalable Resource Management in Wireless Networks”. In: *IEEE Transactions on Wireless Communications* 20.10 (2021), pp. 6562–6576. DOI: 10.1109/TWC.2021.3074373.
- [80] M. R. Head. *Entrainment in the Turbulent Boundary Layer*. ARC Reports and Memoranda 3152. Ministry of Aviation, Aeronautical Research Council, Sept. 1958.
- [81] P. Henderson, R. Islam, P. Bachman, et al. “Deep reinforcement learning that matters”. In: *Proceedings of the AAAI Conference on Artificial Intelligence* 32.1 (2018).

- [82] M. Hoffmann and P. Kryszkiewicz. “Evaluation of User-Centric Cell-Free Massive Multiple-Input Multiple-Output Networks Considering Realistic Channels and Frontend Nonlinear Distortion”. In: *Applied Sciences* 14.5 (2024), p. 1684. DOI: 10.3390/app14051684.
- [83] S. Huang, Y. Liu, and K. Yang. “Deep Reinforcement Learning for Resource Allocation in Massive MIMO”. In: *IEEE Communications Letters* 24.5 (2020), pp. 1052–1055. DOI: 10.1109/LCOMM.2020.2977082.
- [84] X. Huang, Y. Wang, S. Chen, et al. “Joint User Clustering and Graph Coloring Based Pilot Assignment for Cell-Free Massive MIMO Systems”. In: *Sensors* 23.11 (2023), p. 5014. DOI: 10.3390/s23115014.
- [85] Z. Huang, W. Li, Z. Han, and J. Li. “Mobility-aware channel modeling for V2X communications: A survey”. In: *IEEE Access* 8 (2020), pp. 64669–64684. DOI: 10.1109/ACCESS.2020.2986002.
- [86] A. Hussein, M. Anbar, M. Molhem, et al. “Channel allocation in 5G networks using ant colony optimization algorithm”. In: *Proc. 2024 6th Int. Youth Conf. Radio Electron., Electr. Power Eng. (REEPE)*. Feb. 2024, pp. 1–5.
- [87] Y. O. Imam-Fulani, N. Faruk, O. A. Sowande, et al. “5G frequency standardization, technologies, channel models, and network deployment: Advances, challenges, and future directions”. In: *Sustainability* 15 (2023), p. 5173.
- [88] G. Interdonato et al. “Ubiquitous Cell-Free Massive MIMO Communications”. In: *EURASIP J. Wirel. Commun. Netw.* 2019.1 (2019), pp. 1–13.
- [89] G. Interdonato and S. Buzzi. “Joint Optimization of Uplink Power and Computational Resources in Mobile Edge Computing-Enabled Cell-Free Massive MIMO”. In: *IEEE Trans. Commun.* (2023).
- [90] G. Interdonato, P. Frenger, and E. G. Larsson. “Scalability aspects of cell-free massive MIMO”. In: *arXiv preprint arXiv:1902.11275* (2019).

- [91] G. Interdonato, H. Q. Ngo, E. G. Larsson, and P. Frenger. “Ubiquitous Cell-Free Massive MIMO Communications”. In: *EURASIP Journal on Wireless Communications and Networking* 2019.1 (2019), p. 197. DOI: 10.1186/s13638-019-1507-0.
- [92] J. Bai, G. Wang, M. Wang, and J. Zhu. “Joint power allocation and hybrid beamforming for cell-free mmWave multiple-input multiple-output with statistical channel state information”. In: *Sensors* 24.19 (2024), p. 6276.
- [93] S. Jaeckel, L. Raschkowski, L. Bönsch, et al. “QuaDRiGa: A 3-D multi-cell channel model with time evolution for enabling virtual field trials”. In: *IEEE Transactions on Antennas and Propagation* 62.6 (2014), pp. 3242–3256. DOI: 10.1109/TAP.2014.2310220.
- [94] S. Jaeckel, L. Raschkowski, L. Thiele, and L. Bönsch. *QuaDRiGa 2.0 — A geometry-based stochastic channel model including UMTS and 5G extensions*. <https://quadriga-channel-model.de>. Fraunhofer Heinrich Hertz Institute, Release v2.0.0. 2020.
- [95] W. Jiang and H. D. Schotten. “Cell-free massive MIMO-OFDM transmission over frequency-selective fading channels”. In: *IEEE Communications Letters* 25.8 (2021), pp. 2718–2722.
- [96] W. Jiang and H. D. Schotten. “Opportunistic AP Selection in Cell-Free Massive MIMO-OFDM Systems”. In: *Proc. IEEE Veh. Technol. Conf.* IEEE. 2022, pp. 1–5.
- [97] Y. Jiang, Y. Shao, and M. D. Renzo. “Learning Resource Allocation Policies with GNNs in Cell-Free MIMO”. In: *IEEE Transactions on Wireless Communications* 21.8 (2022), pp. 6859–6874. DOI: 10.1109/TWC.2022.3166796.
- [98] J. Kassam et al. “A Review on Cell-Free Massive MIMO Systems”. In: *Electronics* 12.4 (2023), p. 1001.

- [99] B. Kianbakht et al. “Distributed and Centralized Subcarrier-based Precoding for Cell-Free Massive MIMO Networks”. In: *Proc. Iranian Conf. Electr. Eng.* IEEE. Aug. 2020, pp. 1–5.
- [100] J. Kim et al. “A study on frequency planning of MN system for 5G vehicular communications”. In: *Proc. Int. Conf. Inf. Commun. Technol. Converg.* IEEE. Oct. 2019, pp. 1442–1445.
- [101] J.-W. Kim, H.-D. Kim, K.-H. Shin, et al. “User-Centric Cell-Free Massive MIMO with Low-Resolution ADCs for Massive Access”. In: *Sensors* 24.16 (2024), p. 5088. DOI: 10.3390/s24165088.
- [102] T. Kim, H. Seo, and J.-H. Lee. “User-centric cell-free massive MIMO for high-mobility vehicular networks: Challenges and solutions”. In: *Vehicular Communications* 41 (2024), p. 100624. DOI: 10.1016/j.vehcom.2023.100624.
- [103] T. Kobayashi and W. E. L. Ilboudo. “T-soft update of target network for deep reinforcement learning”. In: *Neural Networks* 136 (2021), pp. 63–71.
- [104] M. Kölle, D. Seidl, M. Zorn, et al. “Optimizing Variational Quantum Circuits Using Metaheuristic Strategies in Reinforcement Learning”. In: *2024 IEEE International Conference on Quantum Computing and Engineering (QCE)*. Vol. 2. IEEE, Sept. 2024, pp. 323–328.
- [105] S. Kottwitz. *Example: a Venn diagram with PDF blending*. 2015. URL: <https://texample.net/tikz/examples/venn/> (visited on 08/16/2024).
- [106] P. Koutsovasilis and M. Beitelschmidt. “Comparison of model reduction techniques for large mechanical systems”. In: *Multibody System Dynamics* 20.2 (2008), pp. 111–128. ISSN: 1384-5640. DOI: 10.1007/s11044-008-9116-4.
- [107] D. Krajzewicz, J. Erdmann, M. Behrisch, and L. Bieker. “Recent development and applications of SUMO—Simulation of Urban Mobility”. In: *Int. J. Adv. Syst. Meas.* 5.3&4 (2012).

- [108] P. Kumar and K. B. Ali. “Intelligent Traffic System Using Vehicle-to-Vehicle (V2V) & Vehicle-to-Infrastructure (V2I) Communication Based on Wireless Access in Vehicular Environments (WAVE) Standard”. In: *Proc. Int. Conf. Reliab. Infocom Technol. Optim. (Trends Future Dir.)* IEEE. Oct. 2022, pp. 1–5.
- [109] J. Lee, H. Park, and S. Cho. “User-Centric Resource Allocation with Deep Reinforcement Learning in Cell-Free MIMO Systems”. In: *IEEE Internet of Things Journal* (2024). DOI: 10.1109/JIOT.2024.3350560.
- [110] C. Li, L. Xiao, and M. Li. “Soft Actor-Critic for Energy-Efficient Beamforming in Massive MIMO”. In: *IEEE Transactions on Green Communications and Networking* 7.1 (2023), pp. 243–256. DOI: 10.1109/TGCN.2022.3224622.
- [111] T. P. Lillicrap, J. J. Hunt, A. Pritzel, et al. “Continuous control with deep reinforcement learning”. In: *arXiv preprint arXiv:1509.02971* (2015). DeepMind Technologies. URL: <https://arxiv.org/abs/1509.02971>.
- [112] T. P. Lillicrap, J. J. Hunt, A. Pritzel, et al. “Continuous control with deep reinforcement learning”. In: *arXiv preprint arXiv:1509.02971* (2015).
- [113] L.-J. Lin. “Self-improving reactive agents based on reinforcement learning, planning and teaching”. In: *Machine learning* 8.3 (1992), pp. 293–321.
- [114] X. Lin, P. Liu, and A. Ghosh. “5G-Advanced: Evolution Towards 6G”. In: *IEEE Wireless Communications* 29.1 (2022), pp. 102–108. DOI: 10.1109/MWC.001.2100283.
- [115] B. Liu, S. Zhang, Y. Liu, and Y. He. “Ray-tracing-based channel modeling for evaluating V2X scenarios in urban microcells”. In: *IEEE Transactions on Vehicular Technology* 70.6 (2021), pp. 5372–5384. DOI: 10.1109/TVT.2021.3078390.

- [116] C. Liu and J. Zhen. “Diagonal Loading Beamforming Based on Aquila Optimizer”. In: *IEEE Access* 11 (2023), pp. 69091–69100. DOI: 10.1109/ACCESS.2023.3293403.
- [117] C. Liu and Y. Zhang. “Hyper-parameter optimization based on soft actor critic and hierarchical mixture regularization”. In: *arXiv preprint arXiv:2112.04084* (2021). URL: <https://arxiv.org/abs/2112.04084>.
- [118] X. Liu, H. Zhou, and Q. Guo. “Hierarchical Deep Reinforcement Learning for Joint Clustering and Resource Allocation”. In: *IEEE Transactions on Wireless Communications* 20.6 (2021), pp. 3560–3574. DOI: 10.1109/TWC.2021.3066029.
- [119] Y. Liu, Y. Sun, H. Zhang, and X. Wang. “Deep reinforcement learning-based resource allocation for cell-free massive MIMO systems”. In: *IEEE Wireless Communications Letters* 10.8 (2021), pp. 1721–1725. DOI: 10.1109/LWC.2021.3084446.
- [120] S. D. Liyanaarachchi, C. B. Barneto, T. Riihonen, and M. Valkama. “Experimenting Joint Vehicular Communications and Sensing with Optimized 5G NR Waveform”. In: *2021 IEEE 93rd Vehicular Technology Conference (VTC2021-Spring)*. IEEE, Apr. 2021, pp. 1–5.
- [121] G. A. Lopez, M. Taufer, and P. J. Teller. “Evaluation of IEEE 754 Floating-Point Arithmetic Compliance across a Wide Range of Heterogeneous Computers”. In: *Proceedings of the 2007 Conference on Diversity in Computing – TAPIA '07*. ACM Press, 2007, p. 1. ISBN: 978-1-59593-866-4. DOI: 10.1145/1347787.1347793.
- [122] N. C. Luong, D. N. Hoang, S. Gong, et al. “Applications of deep reinforcement learning in communications and networking: A survey”. In: *IEEE Communica-*

- tions Surveys & Tutorials* 21.4 (2019), pp. 3133–3174. DOI: 10.1109/COMST.2019.2916583.
- [123] B. Manoj, M. Sadeghi, and E. G. Larsson. “Adversarial attacks on deep learning based power allocation in a massive MIMO network”. In: *arXiv preprint arXiv:2101.12090*. 2021.
- [124] M. Manoj, N. Kalantari, and S. A. et al. “Adversarial attacks on deep learning-based power allocation in massive MIMO systems”. In: *IEEE International Conference on Communications (ICC)*. 2021, pp. 1–6.
- [125] B. Mao et al. “Sustainability assessment of speed regulation of urban traffic”. In: *IATSS Res.* 26.2 (2002), pp. 18–24.
- [126] R. A. Mathew and R. M. George. “Measurements and characterization of 5G wireless channel for mmWave massive MIMO system with circular rayline array pattern”. In: *Int. J. Appl. Eng. Res.* (). Year not specified.
- [127] V. Mnih, K. Kavukcuoglu, D. Silver, A. A. Rusu, et al. “Human-level control through deep reinforcement learning”. In: *Nature* 518.7540 (2015), pp. 529–533. DOI: 10.1038/nature14236.
- [128] M. Mohammadi, Z. Mobini, H. Q. Ngo, and M. Matthaiou. “Next-generation multiple access with cell-free massive MIMO”. In: *Proceedings of the IEEE* (2024).
- [129] F. Naaz, A. Nauman, T. Khurshaid, and S. W. Kim. “Empowering the vehicular network with RIS technology: A state-of-the-art review”. In: *Sensors* 24.2 (2024), p. 337.
- [130] M. Narandzic et al. *Matlab SW documentation of WIM2 model*. Tech. rep. WIM 2 Matlab documentation V1.0. doc, 2008.
- [131] D. Nashat and S. Khairy. “Statistical-based detection of pilot contamination attack for NOMA in 5G networks”. In: *Scientific Reports* 15.1 (2025), p. 3726.

- [132] H. Q. Ngo, A. Ashikhmin, H. Yang, et al. “Cell-Free Massive MIMO versus Small Cells”. In: *IEEE Transactions on Wireless Communications* 16.3 (2017), pp. 1834–1850.
- [133] H. Q. Ngo, G. Interdonato, E. G. Larsson, et al. “Ultradense cell-free massive MIMO for 6G: Technical overview and open questions”. In: *Proc. IEEE* (2024).
- [134] H. Q. Ngo, G. Interdonato, E. Nayebi, et al. “Cell-free massive MIMO for 5G and beyond”. In: *IEEE Wireless Communications* 28.4 (2021), pp. 110–117. DOI: 10.1109/MWC.001.2100020.
- [135] Ö. Özdoğan et al. “Performance of cell-free massive MIMO with Rician fading and phase shifts”. In: *IEEE Trans. Wirel. Commun.* 18.11 (2019), pp. 5299–5315.
- [136] Ö. Özdoğan, E. Björnson, and J. Zhang. “Performance of cell-free massive MIMO with Rician fading and phase shifts”. In: *IEEE Trans. Wireless Commun.* 18.11 (2019), pp. 5299–5315.
- [137] A. Paier, J. Karedal, N. Czink, et al. “Car-to-car radio channel measurements at 5 GHz: Pathloss, power-delay profile, and delay-Doppler spectrum”. In: *Proc. 2007 4th Int. Symp. Wireless Commun. Syst. (ISWCS)*. Oct. 2007, pp. 224–228.
- [138] N. Papernot, P. McDaniel, and I. Goodfellow. “Transferability in machine learning: from phenomena to black-box attacks using adversarial samples”. In: *arXiv preprint arXiv:1605.07277* (2016).
- [139] S. Park, J. Kim, and E.-K. Lee. “Federated Reinforcement Learning for Collaborative Multi-AP Networks”. In: *IEEE Transactions on Wireless Communications* 21.10 (2022), pp. 8404–8419. DOI: 10.1109/TWC.2022.3182367.
- [140] S. Parkvall et al. “NR: The New 5G Radio Access Technology”. In: *IEEE Commun. Stand. Mag.* 1.4 (2017), pp. 24–30.

- [141] J. Peisa, E. Dahlman, A. Bergman, et al. “5G Evolution: 3GPP Releases 16 and 17 Overview”. In: *Ericsson Technology Review* (2020). Available: <https://www.ericsson.com/en/reports-and-papers/ericsson-technology-review/articles/5g-evolution-3gpp-releases-16-and-17-overview>.
- [142] M. Plappert, R. Houthoof, P. Dhariwal, et al. “Parameter space noise for exploration”. In: *arXiv preprint arXiv:1706.01905* (2018).
- [143] C. Poggi, A. Albanese, and S. Marano. “On the application of the Gini index for fairness assessment in wireless systems”. In: *IEEE Communications Letters* 25.4 (2021), pp. 1126–1130. DOI: 10.1109/LCOMM.2020.3047996.
- [144] R. V. Rao. “Metaheuristic algorithms for engineering optimization: A review”. In: *Journal of Computational Design and Engineering* 6.3 (2019), pp. 302–322. DOI: 10.1016/j.jcde.2018.08.001.
- [145] N. M. H. Robbi, I. W. Mustika, and W. Widyawan. “A modified genetic algorithm for resource allocation in cognitive radio networks in the presence of primary users”. In: *Proc. 2019 Int. Seminar Intell. Technol. Appl. (ISITIA)*. Aug. 2019, pp. 19–23.
- [146] J. D. V. Sánchez et al. “Survey on Physical Layer Security for 5G Wireless Networks”. In: *Ann. Telecommun.* 76.3 (2021), pp. 155–174.
- [147] M. Sarker and A. O. Fapojuwo. “Uplink Power Allocation for RSMA-aided User-centric Cell-free Massive MIMO Systems”. In: *Proc. IEEE Veh. Technol. Conf.* IEEE. June 2023, pp. 1–5. DOI: 10.1109/VTC2023-Spring57618.2023.10200653.
- [148] T. Schaul, J. Quan, I. Antonoglou, and D. Silver. “Prioritized experience replay”. In: *arXiv preprint arXiv:1511.05952* (2015).

- [149] S. Shekhar, A. Subhash, M. Srinivasan, and S. Kalyani. “Joint Power-Control and Antenna Selection in User-Centric Cell-Free Systems with Mixed Resolution ADC”. In: *IEEE Transactions on Communications* 70.12 (2022), pp. 8400–8415. DOI: 10.1109/TCOMM.2022.3218835.
- [150] N. Shlezinger, Y. C. Eldar, O. Simeone, et al. “Reinforcement learning for wireless communications: Fundamentals, applications, and open issues”. In: *IEEE Journal on Selected Areas in Communications* 39.7 (2021), pp. 2056–2071. DOI: 10.1109/JSAC.2021.3067434.
- [151] D. Silver, G. Lever, N. Heess, et al. “Deterministic policy gradient algorithms”. In: *International Conference on Machine Learning (ICML)* (2014), pp. 387–395.
- [152] E. P. Simon et al. “Resource Allocation and Pairing Techniques in Multiuser Massive MIMO-NOMA”. In: *IEEE Syst. J.* (2023).
- [153] B. D. Son, N. T. Hoa, T. V. Chien, et al. “Adversarial attacks and defenses in 6G network-assisted IoT systems”. In: *IEEE Internet of Things Journal* (2024).
- [154] Q. Sun, H. Wu, and O. Petrosian. “Optimal power allocation based on meta-heuristic algorithms in wireless network”. In: *Mathematics* 10.18 (2022), p. 3336.
- [155] Y. Sun, M. Peng, S. Mao, et al. “Learning to optimize in wireless systems: A reinforcement learning-based approach”. In: *IEEE Transactions on Communications* 67.6 (2019), pp. 4165–4179. DOI: 10.1109/TCOMM.2019.2909802.
- [156] R. S. Sutton and A. G. Barto. *Reinforcement learning: An introduction*. MIT press, 2018.
- [157] S. Tang, X. Liu, and Y. Cheng. “Hybrid Deep Reinforcement Learning and Genetic Algorithms for Resource Allocation in 5G”. In: *IEEE Access* 11 (2023), pp. 10849–10861. DOI: 10.1109/ACCESS.2023.3248012.

- [158] T. A. Tilahun, M. Bennis, and H. Gacanin. “A DRL-based joint power and subcarrier allocation scheme in vehicular networks”. In: *IEEE Transactions on Vehicular Technology* 71.12 (2022), pp. 13493–13506. DOI: 10.1109/TVT.2022.3211042.
- [159] J. F. D. Valgas, D. Martín-Sacristán, and J. F. Monserrat. “5G New Radio Numerologies and their Impact on V2X Communications”. In: *Waves, Universitat Politecnica de Valencia*. 2018, pp. 15–22.
- [160] G. Vasan, M. Elsayed, S. A. Azimi, et al. “Deep policy gradient methods without batch updates, target networks, or replay buffers”. In: *Advances in Neural Information Processing Systems*. Vol. 37. 2025, pp. 845–891.
- [161] G. Viswanathan, V. Afanasyev, S. Buldyrev, et al. “Lévy-flight foraging patterns of wandering albatrosses”. In: *Nature* 381 (1996), pp. 413–415. DOI: 10.1038/381413a0.
- [162] B. Wang, Y. Wu, and J. Liu. “A Hybrid Ant Colony Optimization Approach for Distributed Antenna System Resource Management”. In: *Journal of Communications and Networks* 23.4 (2021), pp. 295–303. DOI: 10.23919/JCN.2021.000022.
- [163] G. Wang, P. Cheng, Z. Chen, et al. “Green cell-free massive MIMO: An optimization-embedded deep reinforcement learning approach”. In: *IEEE Transactions on Signal Processing* (2024).
- [164] M. Wang, X. Liu, F. Wang, et al. “Spectrum-efficient user grouping and resource allocation based on deep reinforcement learning for mmWave massive MIMO-NOMA systems”. In: *Scientific Reports* 14.1 (2024), p. 8884. DOI: 10.1038/s41598-024-34715-8.

- [165] M. Wang, Y. Zhou, X. Zhang, and H. Li. “Mobility-aware wireless resource allocation using deep reinforcement learning in vehicular networks”. In: *IEEE Transactions on Vehicular Technology* 69.10 (2020), pp. 11380–11394. DOI: 10.1109/TVT.2020.3018847.
- [166] R. Wang, M. Shen, Y. He, and X. Liu. “Joint access points-user association and caching placement strategy for cell-free massive MIMO systems based on soft actor-critic algorithm”. In: *IEEE Communications Letters* (2023).
- [167] Y. Wang, X. Zhang, and L. Xie. “A Hybrid PSO-SA Algorithm for Resource Allocation in Massive MIMO”. In: *IEEE Systems Journal* 16.1 (2022), pp. 1046–1057. DOI: 10.1109/JSYST.2021.3057645.
- [168] Z. Wang, J. Zhang, E. Björnson, and B. Ai. “Scalable cell-free massive MIMO networks using resource-optimized backhaul and PSO-driven fronthaul clustering”. In: *IEEE Commun. Lett.* 25.4 (2023), pp. 1348–1352.
- [169] Z. Wang, J. Zhang, E. Björnson, and B. Ai. “Uplink performance of cell-free massive MIMO over spatially correlated Rician fading channels”. In: *IEEE Commun. Lett.* 25.4 (2020), pp. 1348–1352.
- [170] K. Wieghardt and W. Tillmann. *On the Turbulent Friction Layer for Rising Pressure*. NACA Technical Memorandum 1314. National Advisory Committee for Aeronautics, Oct. 1951.
- [171] C. Wu, Y. Zhu, W. Wang, et al. “Improvement of the cluster-level spatial consistency of channel simulator with reference points transition method”. In: *IEEE Transactions on Vehicular Technology* 69 (2020), pp. 11447–11459.
- [172] W. Wu, X. Huang, and T. H. Luan. “AI-Native Network Digital Twin for Intelligent Network Management in 6G”. In: *arXiv preprint* 2410.01584 (2024).

- [173] K. Xu, S. Zhou, and G. Y. Li. “Federated reinforcement learning for resource allocation in V2X networks”. In: *IEEE Journal of Selected Topics in Signal Processing* (2024).
- [174] K. Xu, X. Yang, L. Sun, and H. Wang. “Hybrid intelligent optimization algorithm: A review”. In: *Applied Soft Computing* 114 (2022), p. 108122. DOI: 10.1016/j.asoc.2021.108122.
- [175] Y. Xu, S. Wang, and H. Zhou. “Pilot Allocation via Reinforcement Learning in Cell-Free Massive MIMO”. In: *IEEE Wireless Communications Letters* 11.3 (2022), pp. 540–544. DOI: 10.1109/LWC.2021.3135383.
- [176] Y. Xu, M. Zhang, and W. Han. “Hybrid ACO-GA for Distributed Antenna Resource Allocation”. In: *Journal of Communications and Networks* 25.1 (2023), pp. 15–27. DOI: 10.23919/JCN.2023.000002.
- [177] L. Yang, X. Li, and H. Zhang. “Fairness-Aware Scheduling in Heterogeneous 5G Networks Using Proportional Fairness”. In: *IEEE Transactions on Wireless Communications* 18.7 (2019), pp. 3391–3405. DOI: 10.1109/TWC.2019.2915063.
- [178] X.-S. Yang. “Nature-inspired metaheuristic algorithms: Success and new challenges”. In: *Soft Computing* 14.8 (2010), pp. 783–784. DOI: 10.1007/s00500-009-0460-7.
- [179] W. Yu, H. Wu, and Z. Zhang. “Multi-Agent Reinforcement Learning for Distributed Resource Allocation in Cell-Free MIMO”. In: *IEEE Transactions on Cognitive Communications and Networking* 7.3 (2021), pp. 624–638. DOI: 10.1109/TCCN.2021.3050981.
- [180] T. Zahavy, Z. Xu, V. Veeriah, et al. “A self-tuning actor-critic algorithm”. In: *Advances in Neural Information Processing Systems*. Vol. 33. 2020, pp. 20913–

20924. URL: https://proceedings.neurips.cc/paper_files/paper/2020/file/20a64c3e09657263cc465b082d1d5e53-Paper.pdf.
- [181] M. Zaher, E. Bjornson, and M. Petrova. “Soft Handover Procedures in mmWave Cell-Free Massive MIMO Networks”. In: *IEEE Transactions on Wireless Communications* 23.6 (Sept. 2022). Preprint on arXiv:2209.02548, pp. 1234–1247. DOI: 10.1109/TWC.2023.3330199.
- [182] G. Zhang. “Channel Characterization and Modeling for Future Wireless Communication Systems”. PhD thesis. 2023.
- [183] J. Zhang and E. G. Larsson. “Performance of Cell-Free Massive MIMO with Rician Fading and Phase Shifts”. In: *IEEE Transactions on Wireless Communications* 18.11 (2019), pp. 5295–5309. DOI: 10.1109/TWC.2019.2927064.
- [184] W. Zhang, G. Ditzler, and M. Krunz. “Application of adversarial machine learning in protocol and modulation misclassification”. In: *IEEE Transactions on Cognitive Communications and Networking* 9.3 (2023), pp. 789–801.
- [185] Y. Zhang, D. Xu, H. Zhu, and X. Wang. “Fairness-aware resource allocation in user-centric cell-free massive MIMO systems”. In: *IEEE Access* 10 (2022), pp. 41368–41379. DOI: 10.1109/ACCESS.2022.3166162.
- [186] Z. Zhang, L. Zhang, and D. Wu. “Joint AP Selection and Power Control for Cell-Free Massive MIMO Using Genetic Algorithms”. In: *IEEE Access* 8 (2020), pp. 12413–12425. DOI: 10.1109/ACCESS.2020.2965810.
- [187] J. Zhao, W. Xiang, and J. Guo. “Resource Allocation for OFDM-Based 5G Systems: Water-Filling Algorithms Revisited”. In: *IEEE Access* 8 (2020), pp. 45302–45317. DOI: 10.1109/ACCESS.2020.2978226.
- [188] Y. Zheng et al. “Ultra-massive MIMO channel measurements at 5.3 GHz and a general 6G channel model”. In: *IEEE Trans. Veh. Technol.* 72.1 (2022), pp. 20–34.

- [189] X. Zhou, L. Zhang, L. Song, and Z. Han. “On pilot spoofing attack in massive MIMO systems: Detection and countermeasures”. In: *IEEE Transactions on Information Forensics and Security* 15 (2020), pp. 2630–2645.
- [190] Y. Zhu, W. Xie, and M. M. Tentzeris. “A real-time ultra-wideband channel sounder from 3 to 18 GHz for outdoor multipath acquisition”. In: *IEEE MTT-S International Microwave Symposium (IMS)*. 2022.

Appendix A

CODE EXAMPLES

A.1 WINNER II channel model simulation

This appendix presents the full MATLAB code used to simulate the UC-CFmMIMO wireless channel using the WINNER II channel model. The script is structured for clarity and reproducibility.

Code Listing A.1: *channel_simulation.m: MATLAB script for WINNER II*

channel simulation with UC-CFmMIMO

```
1 %% Channel Generation for UC-CFmMIMO using WINNER II Model
2 % This script sets up a UC-CFmMIMO scenario with a single base station (BS)
3 % and multiple user equipments (UEs), simulating a high-mobility wireless
   channel
4 % at 5.8 GHz using the WINNER II model.
5
6 %% Initialization
7 nbrOfSetups = 1;
8 squareLength = 2000;
9 vec_K = [40];
10 Nue = 1;
11 L = 100;
12 Num_ant = [1];
13 betamin_arr = [0.4];
14
15 %% Frequency and Physical Constants
16 fc = 5.8e9;
17 bw = 20e6;
18 RB = 12 * 15e3;
```

```

19 fmin = fc - bw/2;
20 fmax = fc + bw/2;
21 Mf = floor(bw/RB);
22 frequencies = linspace(fmin, fmax, Mf);
23 df = frequencies(2) - frequencies(1);
24 lambda = 3e8 / fc;
25
26 %% Noise Parameters
27 sigma2_dbm = -174 + 10*log10(RB) + 10;
28 sigma2 = 10^(sigma2_dbm / 10) / 1000;
29
30 %% Time-Domain Sampling and Doppler
31 frameLen = 20;
32 TSDensity = 2;
33 MS_Speed = 15;
34 ds = (lambda / 2) / TSDensity;
35 dt = ds / abs(MS_Speed);
36 delay = (0:Mf-1) * (1 / bw);
37 distance = (0:frameLen-1) * ds;
38 time = (0:frameLen-1) * dt;
39 fd = fc * abs(MS_Speed) / 3e8;
40 dp = 1 / time(end);
41 doppler = (0:frameLen-1) * dp;
42 doppler = doppler - doppler(end)/2;
43
44 %% Antenna Array Configuration
45 for n2 = 1:length(vec_K)
46     K = vec_K(n2);
47     for n3 = 1:length(Num_ant)
48         N = Num_ant(n3);
49         for n4 = 1:length(betamin_arr)
50             betamin = betamin_arr(n4);

```

```

51     numLinks = K * L;
52
53     radius = N * lambda / (2 * 2 * pi);
54     AA(1) = winner2.AntennaArray('UCA', N, radius);
55     AA(2) = winner2.AntennaArray('ULA', Nue, 0.45 * lambda);
56
57     %% Layout Generation
58     BSIdx = cell(L, 1);
59     for l = 1:L
60         BSIdx{l} = 1;
61     end
62     MSIdx = repmat(2, 1, K);
63     cfgLayout = winner2.layoutparset(MSIdx, BSIdx, numLinks, AA,
64         squareLength);
65     cfgLayout.ScenarioVector = repmat(3, 1, numLinks);
66     cfgLayout.PropagConditionVector = ones(1, numLinks);
67
68     APpositions = round((rand(L,1) + 1i*rand(L,1)) * squareLength);
69     distanceAPstoUE_min = 20;
70     UEpositions = zeros(K, 1);
71     for k = 1:K
72         while true
73             UEposition_k = round((rand + 1i * rand) * squareLength);
74             distances = abs(APpositions - UEposition_k);
75             if min(distances) > distanceAPstoUE_min
76                 UEpositions(k) = UEposition_k;
77                 break;
78             end
79         end
80     end
81     for i = 1:L

```

```

82         cfgLayout.Stations(i).Pos = [real(APpositions(i)); imag(
83             APpositions(i)); 12.5];
84     end
85     for i = 1:K
86         cfgLayout.Stations(i+L).Pos = [real(UEpositions(i)); imag(
87             UEpositions(i)); 1.5];
88     end
89
90     %% Assign UE Velocities
91     for i = L + (1 : K)
92         MS_Speed_x(i - L) = rand * MS_Speed;
93         MS_Speed_y(i - L) = rand * MS_Speed;
94         cfgLayout.Stations(i).Velocity = [MS_Speed_x(i - L); MS_Speed_y(
95             i - L); 0];
96     end
97
98     %% Configure Pairing Between APs and UEs
99     cfgLayout.Pairing = [ repmat(1:L, 1, K); reshape(repmat((1:K), L, 1)
100         , K*L, 1).' + L];
101
102     %% WINNER II Channel Configuration
103     cfgWim = winner2.wimparset;
104     cfgWim.NumTimeSamples = frameLen;
105     cfgWim.IntraClusterDsUsed = 'yes';
106     cfgWim.CenterFrequency = fc;
107     cfgWim.UniformTimeSampling = 'yes';
108     cfgWim.ShadowingModelUsed = 'yes';
109     cfgWim.PathLossModelUsed = 'yes';
110     cfgWim.ManualPropCondition = 'no';
111     cfgWim.DelaySamplingInterval = 1 / bw;
112     cfgWim.RandomSeed = 31415926;
113     cfgWim.SampleDensity = TSDensity;

```

```

110
111     %% Generate Channel Coefficients
112     H = zeros(Nue, N, frameLen, Mf, numLinks);
113     [chanCoef, pathDelays, ~] = winner2.wim(cfgWim, cfgLayout);
114     for linkIdx = 1:numLinks
115         Alpha = permute(chanCoef{linkIdx}, [1, 2, 4, 3]);
116         Mp = size(Alpha, 4);
117         Alpha = reshape(Alpha(:,:,: ,1:Mp), Nue*N*frameLen, Mp);
118         Tau = pathDelays(linkIdx,1:Mp).';
119         H(:,:,: ,linkIdx) = reshape(Alpha * exp(-2*pi*1i*Tau*frequencies
120             ), Nue, N, frameLen, Mf);
121     end
122
123     %% Process Channel: PDP and Doppler
124     h = ifft(H, [], 4); % Time-domain channel (delay profile)
125     hd = fftshift(fft(h, [], 3), 3); % Doppler spectrum
126     Htau = permute(squeeze(mean(mean(abs(h).^2, 2), 1)), [2, 1, 3]); %
127         PDP
128     Hd = permute(squeeze(mean(mean(abs(hd).^2, 2), 1)), [2, 1, 3]); %
129         Doppler
130
131     %% Plot Frequency Response for First 10 Links
132     figure(1); hold on; grid on;
133     colors = lines(10);
134     for linkIdx = 1:10
135         plot(frequencies/1e9, 20*log10(abs(squeeze(H(1,1,1,: ,linkIdx))))),
136             'Color', colors(linkIdx,:), 'LineWidth', 1.5);
137     end
138     xlabel('Frequency (GHz)'); ylabel('Gain (dB)');
139     title('Channel Frequency Response');
140     legend('h1,1', 'h1,2', 'h1,3', 'h1,4', 'h1,5', 'h1,6', 'h1,7', 'h1,8', 'h1
141         ,9', 'h1,10');

```

```

137     set(gca, 'FontSize', 12);
138     hold off;
139
140     %% Plot Power Delay Profile (PDP)
141     figure(2); hold on; grid on;
142     for linkIdx = 1:10
143         plot(delay*1e9, 10*log10(abs(Htau(:,1,linkIdx))));
144     end
145     xlabel('Delay (ns)'); ylabel('Power (dB)');
146     title('Power Delay Profile');
147     hold off;
148
149     %% Plot Doppler Spectrum
150     figure(3); hold on; grid on;
151     for linkIdx = 1:10
152         plot(doppler, 10*log10(abs(Hd(:,1,linkIdx))));
153     end
154     xlabel('Doppler Frequency (Hz)'); ylabel('Power (dB)');
155     title('Doppler Spectrum');
156     hold off;
157
158     end
159 end
160 end

```

A.2 SUMO Vehicle Trajectory Extraction

The following script extracts vehicle positions and velocity components from a SUMO simulation after it has been run using TraCI. It logs the X/Y positions and decom-

posed speeds (X/Y) of each vehicle in the simulation over time and writes the results to a CSV file.

Code Listing A.2: *SUMO_CarPositionExtraction.py: Python script for extracting vehicle positions and velocities from SUMO simulation results via TraCI*

```
1 import traci
2 import os
3 import csv
4 import math
5
6 # Configuration
7 sumoBinary = "sumo-gui" # Use "sumo" for non-GUI version
8 sumoConfig = "osm.sumocfg" # Path to your SUMO configuration file
9
10 # Start SUMO with TraCI
11 traci.start([sumoBinary, "-c", sumoConfig])
12
13 # Simulation parameters
14 step = 0
15 max_steps = 4000 # Total number of simulation steps
16
17 # Prepare CSV output file for logging vehicle states
18 with open('vehicle_positions_xy_speeds.csv', mode='w', newline='') as file:
19     writer = csv.writer(file)
20     writer.writerow(['Step', 'Vehicle ID', 'X Position', 'Y Position', 'X
21                     Speed', 'Y Speed'])
22
23 # Main simulation loop
24 while step < max_steps and traci.simulation.getMinExpectedNumber() > 0:
25     traci.simulationStep() # Advance the simulation by one step
```

```

26     vehicle_ids = traci.vehicle.getIDList() # List of current vehicles in
        the simulation
27     for veh_id in vehicle_ids:
28         pos = traci.vehicle.getPosition(veh_id) # (x, y) position
29         speed = traci.vehicle.getSpeed(veh_id) # Speed magnitude
30         angle_deg = traci.vehicle.getAngle(veh_id) # Direction angle in
            degrees
31         angle_rad = math.radians(angle_deg) # Convert to radians
32
33         # Calculate velocity components
34         x_speed = speed * math.cos(angle_rad)
35         y_speed = speed * math.sin(angle_rad)
36
37         # Log data to CSV
38         writer.writerow([step, veh_id, pos[0], pos[1], x_speed, y_speed])
39
40     step += 1
41
42 # Close TraCI session
43 traci.close()
44 print("Simulation finished, data saved to vehicle_positions_xy_speeds.csv.")

```

A.3 Actor-Critic Agent for Deep Reinforcement Learning

The following MATLAB class implements an Actor-Critic agent for a Deep Deterministic Policy Gradient (DDPG) framework. It is tailored for resource allocation in UC-CFmMIMO systems using reinforcement learning. The code includes the actor and critic networks, experience replay, epsilon-greedy exploration, and target network updates.

Code Listing A.3: *ActorCriticAgent_DRL.m: MATLAB class defining the Actor-Critic reinforcement learning agent for dynamic frequency allocation*

```

1  % ActorCriticAgent class for Deep Deterministic Policy Gradient (DDPG)
2  % This class defines the actor and critic networks and their training logic
3  % using experience replay and soft target updates for stability.
4
5  classdef ActorCriticAgent < handle
6      properties
7          actorNetwork % Actor network (policy function)
8          criticNetwork % Critic network (Q-value estimator)
9          targetActor % Target actor network for stability
10         targetCritic % Target critic network for stability
11         learningRate % Learning rate for gradient updates
12         discountFactor % Gamma: future reward discount
13         tau % Soft update factor for target networks
14         buffer % Experience replay buffer object
15         bufferSize % Maximum size of replay buffer
16         batchSize % Number of samples per training step
17         epsilon % Exploration rate for epsilon-greedy policy
18         epsilonDecay % Decay rate for epsilon after each step
19         epsilonMin % Minimum epsilon value
20         K % Number of users (for action size)
21         S % Number of subbands (for action size)
22     end
23
24     methods
25         % Constructor: initializes networks and hyperparameters
26         function obj = ActorCriticAgent(stateSize, actionSize, K, S,
            learningRate, discountFactor, tau, bufferSize, batchSize, epsilon,
            epsilonDecay, epsilonMin)

```

```

27     obj.actorNetwork = obj.createNetwork(stateSize, actionSize, 'actor'
    );
28     obj.criticNetwork = obj.createNetwork(stateSize + actionSize, 1, '
    critic');
29     obj.targetActor = obj.createNetwork(stateSize, actionSize, 'actor')
    ;
30     obj.targetCritic = obj.createNetwork(stateSize + actionSize, 1, '
    critic');
31
32     obj.updateTargetNetworks(1); % Hard copy at initialization
33
34     obj.learningRate = learningRate;
35     obj.discountFactor = discountFactor;
36     obj.tau = tau;
37     obj.bufferSize = bufferSize;
38     obj.batchSize = batchSize;
39     obj.epsilon = epsilon;
40     obj.epsilonDecay = epsilonDecay;
41     obj.epsilonMin = epsilonMin;
42
43     obj.K = K;
44     obj.S = S;
45
46     obj.buffer = ReplayBuffer(bufferSize, actionSize);
47 end
48
49 % Network builder: creates a simple feedforward network
50 function net = createNetwork(obj, inputSize, outputSize, type)
51     layers = [
52         featureInputLayer(inputSize, 'Normalization', 'none', 'Name', '
            state')
53         fullyConnectedLayer(128, 'Name', 'fc1')

```

```

54         reluLayer('Name', 'relu1')
55         fullyConnectedLayer(128, 'Name', 'fc2')
56         reluLayer('Name', 'relu2')
57         fullyConnectedLayer(outputSize, 'Name', 'output')
58     ];
59     if strcmp(type, 'actor')
60         layers = [layers softmaxLayer('Name', 'softmax')]; % Output
61                 probabilities
62     end
63     net = dlnetwork(layerGraph(layers));
64 end
65 % Epsilon-greedy action selection: explores or exploits
66 function action = selectAction(obj, state)
67     if rand() < obj.epsilon
68         action = randi([1, obj.K * obj.S]); % Random action
69     else
70         % Deterministic policy from actor network
71         state = darray(state(:), 'CB');
72         probs = extractdata(forward(obj.actorNetwork, state));
73         probs = probs + 1e-8; % Prevent zero probability
74         probs = probs / sum(probs);
75         if any(isnan(probs))
76             action = randi([1, obj.K * obj.S]);
77         else
78             action = randsample(obj.K * obj.S, 1, true, probs);
79         end
80     end
81     obj.epsilon = max(obj.epsilonMin, obj.epsilon * obj.epsilonDecay);
82 end
83
84 % Store a new experience in the buffer

```

```

85     function storeExperience(obj, state, action, reward, nextState)
86         obj.buffer.store(state, action, reward, nextState);
87     end
88
89     % Train actor and critic networks using a batch of experiences
90     function [criticLoss, actorLoss] = train(obj)
91         if obj.buffer.count < obj.batchSize
92             criticLoss = [];
93             actorLoss = [];
94             return;
95         end
96
97         batch = obj.buffer.sample(obj.batchSize);
98         state = cell2mat(cellfun(@(s) s(:), {batch.state}, 'UniformOutput',
99             false));
100        nextState = cell2mat(cellfun(@(s) s(:), {batch.nextState}, '
101            UniformOutput', false));
102
103        actions = [batch.action];
104        rewards = [batch.reward];
105
106        state = dlarray(state, 'CB');
107        nextState = dlarray(nextState, 'CB');
108
109        % Predict next actions and target Q-values
110        nextActions = forward(obj.targetActor, nextState);
111        targetQ = forward(obj.targetCritic, [nextState; nextActions]);
112        targetQ = rewards + obj.discountFactor * extractdata(targetQ);
113        targetQ = dlarray(targetQ, 'CB');
114
115        % Update critic
116        [gCritic, criticLoss] = dlfeval(@obj.criticGradient, obj.
117            criticNetwork, state, actions, targetQ);

```

```

114     obj.criticNetwork = dlupdate(@(p, g) p - obj.learningRate * g, obj.
        criticNetwork, gCritic);
115
116     % Update actor
117     [gActor, actorLoss] = dlfeval(@obj.actorGradient, obj.actorNetwork,
        obj.criticNetwork, state);
118     obj.actorNetwork = dlupdate(@(p, g) p - obj.learningRate * g, obj.
        actorNetwork, gActor);
119
120     % Soft update target networks
121     obj.updateTargetNetworks(obj.tau);
122     end
123
124     % Compute critic gradients and loss
125     function [gradients, loss] = criticGradient(obj, criticNetwork, state,
        actions, targetQ)
126         batchSize = size(actions, 2);
127         oneHot = zeros(obj.K * obj.S, batchSize);
128         for i = 1:batchSize
129             oneHot(actions(i), i) = 1;
130         end
131         input = [state; dlarray(oneHot, 'CB')];
132         Q = forward(criticNetwork, input);
133         loss = mse(Q, targetQ);
134         gradients = dlgradient(loss, criticNetwork.Learnables);
135     end
136
137     % Compute actor gradients and loss
138     function [gradients, loss] = actorGradient(obj, actorNetwork,
        criticNetwork, state)
139         actions = forward(actorNetwork, state);
140         Q = forward(criticNetwork, [state; actions]);

```

```

141     loss = -mean(Q, 'all');
142     gradients = dlgradient(loss, actorNetwork.Learnables);
143 end
144
145 % Update target networks using soft updates
146 function updateTargetNetworks(obj, tau)
147     obj.targetActor.Learnables = obj.softUpdate(obj.actorNetwork.
148         Learnables, obj.targetActor.Learnables, tau);
149     obj.targetCritic.Learnables = obj.softUpdate(obj.criticNetwork.
150         Learnables, obj.targetCritic.Learnables, tau);
151 end
152 end
153
154 methods (Access = private)
155     % Soft update formula: new = tau * source + (1 - tau) * target
156     function updated = softUpdate(~, src, tgt, tau)
157         updated = src;
158         for i = 1:size(src, 1)
159             updated.Value{i} = tau * src.Value{i} + (1 - tau) * tgt.Value{i}
160         };
161     end
162 end
163 end
164 end

```